A cytoskeletal network maintains filament shape in the multicellular cyanobacterium *Anabaena* sp. PCC 7120

Benjamin L. Springstein[1]*, Dennis J. Nürnberg[2,†], Ann-Katrin Kieninger[3], Christian Woehle[1¥], Julia Weissenbach[1,‡], Marius L. Theune[1], Andreas O. Helbig[4], Andreas Tholey[4], Iris Maldener[3], Tal Dagan[1], Karina Stucken[5*+]

[1] Institute of General Microbiology, Christian-Albrechts-Universität zu Kiel, Kiel, Germany

[2] Department of Life Sciences, Imperial College, London SW7 2AZ, United Kingdom

[3] Department of Microbiology/Organismic Interactions, University of Tübingen, Tübingen, Germany

[4] AG Proteomics & Bioanalytics, Institute for Experimental Medicine, Christian-Albrechts-Universität zu Kiel, Kiel, Germany

[5] Department of Food Engineering, University of La Serena, La Serena, Chile.

[†] Present address: Institute of Experimental Physics, Free University of Berlin, Berlin, Germany

[¥] Present address: Max Planck Institute for Plant Breeding Research, Max Planck-Genome-center Cologne, Cologne, Germany

[‡] Present address: Faculty of Biology, Technion-Israel Institute of Technology, Haifa, 32000, Israel

* Corresponding authors: KS kstucken@userena.cl; BLS bspringstein@ifam.uni-kiel.de

Abstract

The determinants of bacterial cell shape are extensively studied in unicellular forms. Nonetheless, the mechanisms that shape bacterial multicellular forms remain understudied. Here we study coiled-coil rich proteins (CCRPs) in the multicellular cyanobacterium *Anabaena* sp. PCC 7120 (hereafter *Anabaena*). Our results reveal two CCPRs, termed LfiA and LfiB (for linear filament), which assemble into a heteropolymer that traverses the longitudinal cell axis. Two additional CCRPs, CypS (for cyanobacterial polar scaffold) and CeaR (for cyanobacterial elongasome activity regulator), form a polar proteinaceous scaffold and regulate MreB activity, respectively. Deletion mutants of these CCRPs are characterized by impaired filament shape and decreased viability. Our results indicate that the four CCRPs form a proteinaceous network that stabilizes the *Anabaena* multicellular filament. We propose that this cytoskeletal network is essential for the manifestation of the linear filament phenotype in *Anabaena*.

Introduction

Bacterial multicellularity ranges from transient associations, such as colonies and biofilms to permanent multicellular forms[1]. The basic characteristics of prokaryotic organisms that are considered as multicellular are mechanisms of cell-cell adhesion and intercellular communication[2]. Biofilms are considered as transient forms of prokaryotic multicellularity since they lack a reproducible multicellular shape[3]. The shape of the individual cell has been shown to have a strong impact on the spatial biofilm formation. Example is the different composition of cell morphologies within an *Escherichia coli* biofilm[4]. Studies of biofilm formation in *Rhodobacter sphaeroides* showed that wild type (WT) rod-shaped cells readily form biofilms on costal water surfaces, while coccoid-like cells that were treated with an inhibitor of MreB – a well-known cell shape determinant – lacked the ability to form biofilms and failed to attach to surfaces[5]. Hence, cytoskeletal structures that determine cell shape through the remodeling of the peptidoglycan (PG) sheet are key regulators of biofilm formation, specifically in environments that are subjected to constant changes[5–8]. MreB, together with the elongasome

(a multi-enzyme complex), is a regulator of longitudinal PG biogenesis, and thus it plays a crucial role in the adaption to different environments and prokaryotic multicellularity.

The key hallmarks of permanent bacterial multicellularity are morphological differentiation and a well-defined and reproducible shape, termed patterned multicellularity[3]. Unlike biofilms, patterned multicellular structures are the result of either coordinated swarming or developmental aggregation behavior as in myxobacteria[9]. Additional factors include cell division, proliferation and cell differentiation as in sporulating actinomycetes[10] and cyanobacterial filaments[11,12]. In myxobacteria as well as in actinomycetes, it has been shown that patterned multicellular traits are dependent on the coordinated function of different coiled-coil-rich proteins (CCRPs). Reminiscent of eukaryotic intermediate filaments (IFs)[13,14], many bacterial CCRPs were shown to perform analogous cytoskeletal functions through their ability to self-assemble into distinct filaments *in vitro* and *in vivo*[15–19]. Unlike FtsZ or MreB[20,21], bacterial IF-like CCRPs do not require any additional co-factors for polymerization *in vitro*[22]. For example, in *Myxococcus xanthus*, the coordinated swarming and aggregation into fruiting bodies is mediated by its gliding motility[23], which strictly depends on the filament-forming CCRP AglZ[24]. AglZ is organized in a large multi-protein complex that governs gliding motility in synergy with MreB, which still retained its PG synthesis function but was also co-opted for gliding motility in *M. xanthus*[25–28]. Actinobacteria, such as *Streptomyces* species, grow by building new cell wall (i.e. PG) only at the cell poles, independent of MreB[29,30], which is strikingly different from how most other bacteria grow[31]. This characteristic polar growth mode is organized by a cytoskeletal network of at least three CCRPs - DivIVA, Scy and FilP – that form the polarisome[16,17,32,33]. Similar to eukaryotic intermediate filaments (IFs), FilP and Scy self-assemble into filaments *in vitro*[17,32], thereby fulfilling a major criterium of cytoskeletal proteins[34]. Although of essential importance for growth and cell shape, the polarisome is not directly involved in the hallmark patterned multicellular trait of Actinobacteria. In contrast, patterned multicellularity in Actinobacteria is governed by a highly reproducible and coordinated cell division event during sporulation where up to 100 FtsZ-driven Z-rings are

formed. This then leads to the formation of evenly spaced septa, resulting in long chains of spores[3,35].

Cyanobacteria are characterized by a large phenotypic diversity, ranging from unicellular species to complex filamentous cyanobacteria of which some can undergo morphological differentiation[36]. Filamentous cyanobacteria that differentiate multiple cell types are considered the peak of prokaryotic complexity. The cell biology of multicellular cyanobacteria has been studied in the context of cytoplasmic continuity, intercellular communication, and cell differentiation[37]. Species of the Nostocaceae are characterized by the formation of linear filaments, where equally interspaced heterocysts (specialized cells for nitrogen fixation) are differentiated upon nitrogen starvation in a highly reproducible pattern[37]. Studies of multicellular growth in the model multicellular cyanobacterium *Anabaena* showed that FtsZ - the prokaryotic tubulin homolog - is an essential protein that localizes to future septum sites in a typical Z-ring structure, while MreB - the prokaryotic actin homolog - determines the cell shape of a single cell within an *Anabaena* filament but is dispensable for filament viability[38,39]. Deletion of MreB[39] or of a class B penicillin-binding-protein (PBP)[40] resulted in swollen and rounded cell morphotypes, a phenotype commonly associated with defects in PG biogenesis[41,42]. As a true-multicellular organism, *Anabaena* contains functional analogs to the eukaryotic gap-junctions, termed septal junctions, which facilitate intercellular communication[43] by direct cell connections[44]. These structures involve the septum localized proteins SepJ, FraC and FraD[37,45,46] and a nanopore array in the septal PG[47]. The importance of SepJ, FraC and FraD for multicellularity in *Anabaena* is highlighted by a defect in filament integrity and a resulting loss of multicellularity under diazotrophic growth conditions in strains lacking any of the three genes[46,48–50]. Besides the canonical cytoskeletal proteins FtsZ and MreB, no other cytoskeletal proteins have been described in *Anabaena.* Here we study the contribution of coiled-coil-rich filament-forming proteins to the *Anabaena* phenotype. For this purpose, we predicted *Anabaena* CCRPs with presumed IF-like functions and evaluated their cytoskeletal properties using *in vivo* and *in vitro* approaches.

Results

Prediction of CCRP candidates in *Anabaena*

Potential filament-forming proteins were predicted computationally by surveying the *Anabaena* genome for CCRPs, which putatively have IF-like function[15,24,32,51,52]. *Anabaena* CCRPs were filtered according to the presence of a central rod-domain, which is characteristic to eukaryotic IF and prokaryotic IF-like proteins[14,53,54]. Similar to Bagchi *et al*. (2008), who identified the filament-forming CCRP FilP in *Streptomyces coelicolor*[32], we defined the presence of a rod-domain as 80 amino acids in coiled-coil conformation. This analysis resulted in the identification of 186 rod-domain-containing CCRPs (Supplementary File 1). The 186 CCRPs were further filtered to include only hypothetical proteins of unknown function, yielding a set of 13 candidates for further analysis (Supplementary Fig. 1 and Supplementary Table 1). The distribution of homologs to these 13 candidates in cyanobacteria showed that eight *Anabaena* CCRPs have homologs in multicellular cyanobacteria as well as in unicellular cyanobacteria while five have homologs present only in multicellular cyanobacteria (Fig. 1a; Supplementary Table 1).

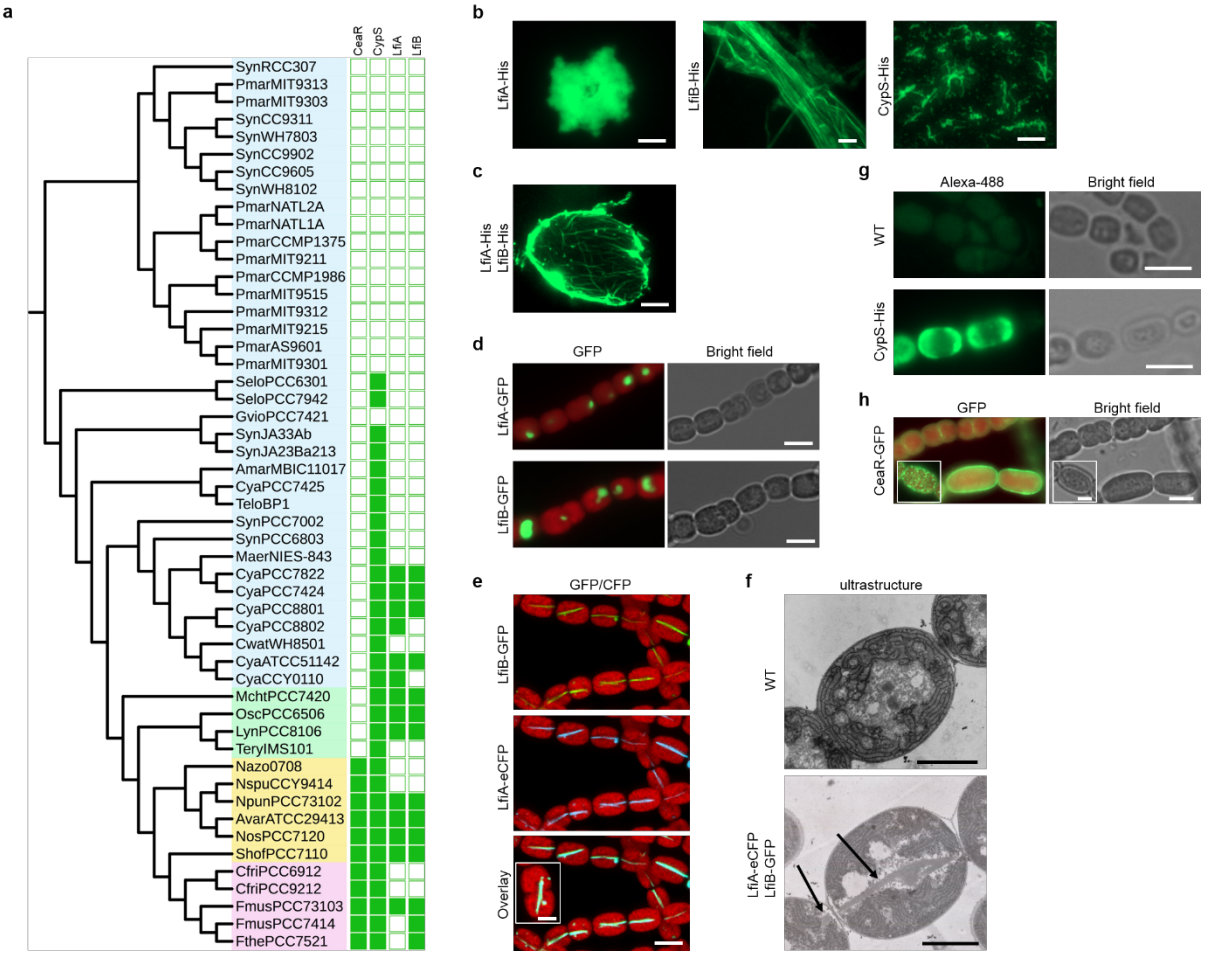

Fig. 1: Cyanobacterial CCRPs polymerize *in vitro* and *in vivo*

(**a**) Distribution of protein candidate homologs in cyanobacteria. Organism names include the genus first letter and species first three letters. The presence of homologous genes is marked by a green rectangle. Organism names are shaded according to cell or colony morphology; blue: unicellular, green: filamentous, yellow: filamentous and heterocyst forming, pink: heterocyst forming and true branching or multiseriate filaments. Homologs accession numbers are supplied in Supplementary File 2. (**b**-**c**) Epifluorescence micrographs of NHS-Fluorescein-stained *in vitro* filaments formed by purified and renatured (**b**) LfiA-His (1 mg ml^{-1}), LfiB-His (0.5 mg ml^{-1}) and CypS-His (0.5 mg ml^{-1}) or (**c**) co-renatured LfiA-His and LfiB-His (0.25 mg ml^{-1} each) in 25 mM HEPES, pH 7.4 (LfiB), HLB (LfiA and co-renatured LfiA/B) or PLB (CypS) renaturation buffer. (**d**) Merged GFP-fluorescence and chlorophyll autofluorescence (red) and bright field micrographs of *Anabaena* WT cells expressing LfiA-GFP or LfiB-GFP from P_{petE}. LfiA-GFP-expressing cells were grown in BG11 without copper and induced for 2 d with 1 µM $CuSO_4$. LfiB-GFP-expressing cells were grown in $BG11_0$. (**e**) Merged GFP and/or eCFP fluorescence and chlorophyll autofluorescence (red) micrographs of *Anabaena* WT cells co-expressing LfiA-eCFP and LfiB-GFP from P_{petE} and grown in $BG11_0$. Localization of LfiA/B grown in BG11 is depicted in Supplementary Fig. 7. (**f**) Electron micrographs of ultrathin sections of *Anabaena* WT and *Anabaena* cells co-expressing LfiA-eCFP and LfiB-GFP. Black arrows indicate electron-dense structures coinciding with the LfiA/B heteropolymer observed in Fig. 1e. Filaments appear to anchor or attach to the cell poles. (**g**) Alexa Fluor 488 and bright field micrographs of anti-His immunofluorescence staining of *Anabaena* WT and *Anabaena* cells expressing CypS-His from P_{petE} grown in liquid $BG11_0$ supplemented with 0.25 µM $CuSO_4$ for 2 d. Polar sites loaded with CypS-His plugs coincide with sites of retracted chlorophyll autofluorescence observed prior to immunofluorescence (Supplementary Fig. 6b). (**h**) Merged GFP fluorescence and chlorophyll autofluorescence and bright field micrographs of *Anabaena* WT cells expressing CeaR-GFP from P_{petE} grown on BG11. Notably, no enlarged cells were identified in the Δ*ceaR* mutant strain expressing CeaR-GFP from P_{ceaR} (Supplementary Fig. 8a), indicating that CeaR level in WT cells is tightly regulated. Inlay shows patchy and cell periphery-localized CeaR-GFP. N-terminal YFP translational fusion of CCRPs did not reveal coherent structures, suggesting that the N-terminus is essential for protein localization. Scale bars: 5 µm, (e) 1.25 µm, (f) 1.6 µm or (h inlay) 2.5 µm.

In vivo and in vitro filamentation of CCRP candidates

Out of the 13 candidates, four CCRPs showed self-association and filamentation properties, including LfiA together with LfiB, CypS and All4981 (that will be investigated in a separate report). The remaining nine candidates failed to form filamentous structures *in vivo* and *in vitro* and consequently were excluded from further analysis. An exception is CeaR whose computational structural prediction suggested similarity to the well-characterized prokaryotic IF-like protein crescentin from *Caulobacter crescentus*[15] (Supplementary Table 1). To evaluate the ability of candidate CCRPs to self-associate, we ectopically expressed C and N-terminally tagged (His_6, YFP, eCFP or GFP) recombinant proteins and investigated *in vitro* polymerization properties and *in vivo* localization pattern. The assembly of CCRPs into filaments *in vitro* was tested by fluorescence microscopy using the NHS-Fluorescein dye, which was previously successfully used to visualize FtsZ filaments[55]. For this, we purified His_6-tagged candidates by Ni-NTA affinity chromatography under denaturing conditions and renatured them by dialysis followed by NHS-fluorescein staining. As a positive control for our approach we used crescentin[15,56]. The NHS-fluorescein staining of crescentin revealed an extensive filamentous network in our *in vitro* assay (Supplementary Fig. 2). As negative controls, we included empty vector-carrying BL21 (DE3) cells, GroEL1.2 from *Chlorogloeopsis fritschii* PCC 6912 (known to self-interact[57]) and the maltose binding protein (MBP), all of which were tested negatively for filament formation *in vitro* using our approach (Supplementary Fig. 2).

LfiA and LfiB are interdependent for polymerization *in vitro* and *in vivo*

Since the candidate proteins were annotated as hypothetical proteins, we initially investigated and confirmed the transcription of all four genes under standard (BG11) and diazotrophic ($BG11_0$) growth conditions (Supplementary Fig. 3a,b). An additional inspection of the genomic loci suggested that *lfiA* and *lfiB* are encoded in an operon structure, however, RT-PCR data indicated that they are not co-transcribed (Supplementary Fig. 3a,c). Applying our *in vitro* polymerization assay to LfiA revealed amorphous non-filamentous aggregates while LfiB assembled into sheet-like filamentous structures (Fig. 1b). Nonetheless, most LfiB precipitated

upon renaturation, suggesting that LfiB has only a partial capacity to form filaments. Next, inspired by the close genomic localization of *lfiA* and *lfiB*, we tested for co-polymerization of both proteins. Upon co-renaturation, LfiA and LfiB assembled into a meshworks of heteropolymers (Fig. 1c). This demonstrates that LfiA and LfiB are interdependent for filamentous assembly *in vitro*. To examine the *in vivo* localization pattern of LfiA and LfiB, we expressed translational GFP fusions of both proteins from the replicative pRL25C plasmid, a derivate of the pDU1 plasmid[58], which is commonly used in experimental work in *Anabaena*[39,59,60]. The expression of LfiA-GFP and LfiB-GFP from their respective native promoters (as predicted using BPROM[61]) revealed no discernible expression of LfiB-GFP (Supplementary Fig. 4a). Consequently, we investigated the *in vivo* localization of both proteins from the frequently used copper-regulated *petE* promoter (P_{petE})[59,60,62,63], which has been previously used to study the localization of FtsZ and MreB in *Anabaena*[39,59,60]. We generally observed that the P_{petE}-driven gene expression does not always lead to expression of the translational fusion protein in every cell under standard growth conditions (BG11 medium). Notably, this was not observed under diazotrophic growth conditions (i.e. $BG11_0$) or upon supplementation with additional $CuSO_4$, where we saw more pronounced expression. The expression of LfiA-GFP and LfiB-GFP from P_{petE} in *Anabaena* independently did not reveal filamentous structures (Fig. 1d). However, upon co-expression of LfiA-eCFP and LfiB-GFP from P_{petE}, a distinct filamentous structure along the longitudinal cell axis could be observed (Fig. 1e). To confirm that the localization of LfiA-GFP and LfiB-GFP is not affected by the wildtype (WT) *lfiA* or *lfiB* alleles, we localized both proteins in a Δ*lfiA*Δ*lfiB* double mutant strain. This experiment revealed the same localization pattern as in the WT (Supplementary Fig. 4b), suggesting that co-polymerization is a dosage-dependent process. In support of this idea, we only observed pronounced *in vitro* co-polymerization with equal amounts of LfiA-His and LfiB-His (Supplementary Fig. 5). We further validated the co-polymerization of LfiA and LfiB by heterologous expression in the Δ*lfiA*Δ*lfiB* double mutant background and in *E. coli*; both experiments revealed the same interdependent polymerization pattern (Supplementary Fig. 4c and 7). The intracellular localization of the LfiA/LfiB heteropolymer in *Anabaena* suggests that

the polymer is either anchored at the cell poles or specifically broken up during cell division, as LfiA/LfiB filaments were never observed to cross cell-cell borders and only traversed through not yet fully divided cells (Figs. 1e inlay and 1f). Our results so far suggest that LfiA and LfiB form a heteropolymer *in vitro* and *in vivo* and that heteropolymer assembly may depend on LfiA and LfiB relative dosage.

CypS localizes to the cell poles in *Anabaena*

The *in vitro* polymerization assay of CypS revealed that CypS assembled into star-like structures of short filamentous strings (Fig. 1b). The expression of CypS-GFP in *Anabaena* WT cells from the predicted native promoter (P_{cypS}; using BPROM) did not reveal coherent fluorescence signals (Supplementary Fig. 6a). However, when expressed from P_{petE}, CypS-GFP was localized to the cytosol and the cell envelope (Supplementary Fig. 5a). The same localization to the cell envelope and the cytoplasm was also observed upon expression of CypS-GFP from P_{cypS} in a *ΔcypS* mutant background (Supplementary Fig. 5a). Notably, CypS-GFP only partially complemented the Δ*cypS* mutant swollen cell phenotype (Supplementary Fig. 6a). Consequently, we examined whether the addition of a C-terminal His-tag may reconstitute the CypS WT phenotype and found that CypS-His forms a functional protein fusion (Supplementary Fig 9a,c). Immunolocalization of CypS-His in *Anabaena* WT revealed that the protein forms large plugs at the cell poles (Fig. 1g) that appeared to displace the thylakoid membranes (Supplementary Fig. 6b). This suggests that the comparably large C-terminal GFP tag negatively affects CypS localization *in vivo*. However, upon additional induction of CypS-GFP expression, polar assemblies can also be seen (Supplementary Fig. 6a), suggesting that the GFP-tag only partially interferes with CypS localization. Further induction of CypS-His expression also resulted in the formation of swollen cells (Supplementary Fig. 6b), indicating that CypS has morphogenic properties. To test for a possible interplay between LfiA/LfiB and CypS we tested for the localization of LfiA/LfiB in the Δ*cypS* mutant strain. This revealed that in the absence of CypS, LfiA and LfiB co-localization in the form of a filamentous structure is

lost (Supplementary Fig. 7). Our results thus indicate that CypS forms polar plugs that are putative anchor sites for the LfiA/LfiB filament.

CeaR is morphogenic and is localized to the cell envelope and the Z-ring

Attempts to overexpress CeaR-His in *E. coli* for the *in vitro* polymerization assay were not successful, possibly due to the N-terminal transmembrane domains (TMDs; Supplementary Fig. 1). Removal of the CeaR N-terminal TMDs enabled overexpression in *E. coli,* but nonetheless no filamentous CeaR *in vitro* structures were observed. We note that genomes of unicellular cyanobacteria do not have a homologous gene to *ceaR* (Fig. 1a), and furthermore, unlike CypS, LfiA and LfiB, recombinant expression of CeaR-GFP in *Synechocystis* was unsuccessful. This suggests that CeaR function is specific to the multicellular cyanobacterial phenotype. Expression of a functional CeaR-GFP fusion protein (Supplementary Fig. 11b,d,e) from P_{ceaR} and from P_{petE} in *Anabaena* WT showed that the protein localized to the cell periphery in a patchy pattern (Fig. 1h, Supplementary Fig. 8a), yet it also accumulated at the septa or had localization at the Z-ring. Z-ring or septal localization was found in 25% of cells (589 out of 2301 counted cells) carrying P_{petE}::*ceaR-gfp* and in 17% of cells (206 out of 1237 counted cells) carrying P_{ceaR}::*ceaR-gfp*. In addition, we observed that the expression of CeaR-GFP from P_{petE} led to a swollen cell phenotype in a large proportion of cells (1754 (76%) of 2301 counted cells) and a similar proportion of swollen cells when CeaR-GFP was expressed from P_{ceaR} (789 (64%) of 1237 counted cells; Fig. 1h, Supplementary Fig. 8a). A similar swelling of cells was also identified in *Anabaena* WT cells expressing untagged CeaR from P_{ceaR} (435 (32%) of 1346 counted cells; Supplementary Fig. 8a). Strikingly, expression of both, CeaR-GFP or untagged CeaR in the Δ*ceaR* mutant strain did not induce cell swelling (Supplementary Figs. 8a and 9a). The localization pattern of CeaR indicates that CeaR is associated with the FtsZ-driven divisome. In agreement with our suggestion, CeaR-GFP localization to the Z-ring was lost upon deletion of the N-terminal TMDs from CeaR (Supplementary Fig. 8a). This indicates that membrane anchorage is key for proper CeaR function and localization.

Anabaena CCRP deletion strains show defects in filament shape and viability

To further study the function of the four CCRPs, we generated Δ*cypS,* Δ*ceaR* and a double Δ*lfiA*Δ*lfiB* mutant strain and examined their phenotype. Notably, single Δ*lfiA* or Δ*lfiB* mutant strains could not be generated, suggesting that the presence of only one of those proteins is lethal for *Anabaena*. Our results show that the Δ*cypS* and Δ*lfiA*Δ*lfiB* mutant strains were characterized by altered filament and cell shape phenotypes and reduced filament viability (Fig 2a, Supplementary Fig. 10a,b). Unlike the linear filament growth pattern of the *Anabaena* WT, both Δ*cypS* and Δ*lfiA*Δ*lfiB* mutant strains showed filaments with a zigzagged pattern (Fig. 2a, Supplementary Fig. 9d). Additionally, Δ*cypS* and Δ*lfiA*Δ*lfiB* cells were significantly larger and more rounded in comparison to the WT, reminiscent of Δ*mreB* mutant[39] (Fig. 2c). The defect phenotype of the Δ*cypS* and Δ*lfiA*Δ*lfiB* mutant strains could be complemented with pRL25C carrying P_{cypS}::*cypS* or $P_{lfiA/lfiB}$::*lfiA-lfiB*, respectively (Supplementary Fig. 9a,b). We also observed a slight decrease in cell volume in older Δ*ceaR* mutant cultures that also exhibited a shortened filament length phenotype (Fig. 2c, Supplementary Figs. 9d and 11c). This is in accordance with our observation of cell volume increase upon CeaR-GFP overexpression in *Anabaena* WT (Figs. 1h, Supplementary Fig. 8a). Our results thus show that CeaR expression level influences *Anabaena* cell shape and suggest a role of CeaR in PG biogenesis and cell-shape determination.

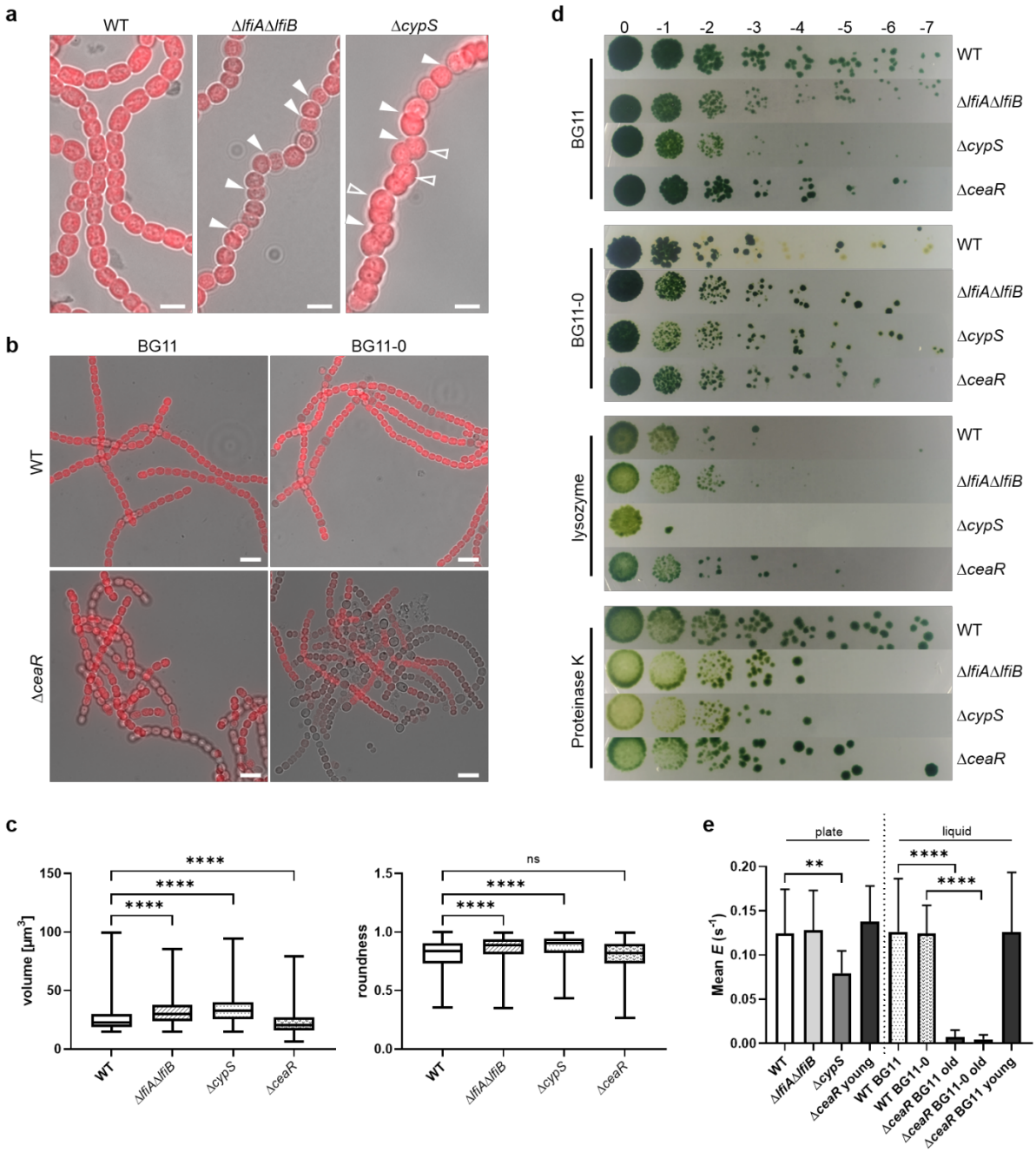

Fig. 2: *Anabaena* CCRP mutant strains reveal altered filament and cell shape phenotypes

(**a**-**b**) Merged chlorophyll autofluorescence and bright field micrographs of (**a**) *Anabaena* WT, Δ*lfiA*Δ*lfiB* and Δ*cypS* mutant strains grown on BG11 plates and (**b**) *Anabaena* WT and Δ*ceaR* mutant strain grown in BG11 and 5 d after transfer into $BG11_0$. Similar to what was observed upon transfer into $BG11_0$, reduced Δ*ceaR* filament length was also observed during prolonged cultivation on BG11 plates (Supplementary Figs. 9d and 11c). Unlike in the WT, we commonly observed bright red fluorescent filaments in the Δ*ceaR* mutant (Fig. 3d, Supplementary Fig. 9e). Ultrastructures revealed that those structures do not consist of thylakoid membranes (Supplementary Fig. 15), leaving the nature of those filaments unknown. White triangles indicate zigzagged growth and translucent triangles show swollen cells. Scale bars: (a) 5 μm and (b) 10 μm. (**c**) Cell roundness and volume of *Anabaena* WT, Δ*lfiA*Δ*lfiB*, Δ*cypS* and Δ*ceaR* mutant strains grown on BG11 plates measured with Fiji imaging software. *Anabaena* WT: n = 537; Δ*ceaR*: n = 796; Δ*lfiA*Δ*lfiB*: n = 404; Δ*ceaR*: n = 369. (**d**) *Anabaena* WT, Δ*lfiA*Δ*lfiB*, Δ*cypS* and Δ*ceaR* mutant strains were spotted onto BG11, $BG11_0$ or BG11 plates supplemented with lysozyme or Proteinase K in triplicates of serial dilutions of factor 10 and grown until no further colonies arose in the highest dilution (n = 2). (**e**) Mean exchange coefficients (*E*) of fluorescence recovery after photobleaching (FRAP) experiments from calcein-labelled *Anabaena* WT and CCRP mutant strains. Liquid *Anabaena* WT and Δ*ceaR* cultures were grown in BG11 and

partially transferred to $BG11_0$ 1 d prior labelling. Plate grown *Anabaena* WT, Δ*lfiA*Δ*lfiB* and Δ*cypS* mutant strains were grown on BG11 plates. Data present the number of recordings of bleached cells (n). *Anabaena* WT BG11 plate: n = 21; *Anabaena* WT liquid BG11: n = 10; *Anabaena* WT liquid $BG11_0$: n = 11; Δ*cypS*: n= 23; Δ*lfiA*Δ*lfiB*: n = 17; Δ*ceaR* liquid BG11: n = 16; Δ*ceaR* liquid $BG11_0$: n = 6. Representative FRAP micrographs are shown in Supplementary Fig. 12. Representative fluorescence recovery curves are shown in Supplementary Fig. 13. Values indicated with * are significantly different from the WT. *: $P < 0.05$, **: $P < 0.01$, ***: $P < 0.001$, ****: $P < 0.0001$. ns indicates no significant difference to the WT (using one-way ANOVA with Dunnett's multiple comparison test).

The round and swollen cell phenotypes of the Δ*cypS* and Δ*lfiA*Δ*lfiB* mutant strains are indicative of an impairment in cell wall integrity and/or defects in PG biogenesis as well as an elevated sensitivity to turgor pressure[41,42,64,65]. Similarly, the resemblance of the phenotypes of CeaR with MreB raised the hypothesis that the four investigated CCRPs could be involved in cell wall integrity or the PG biogenesis machinery. Consequently, we tested the sensitivity of the deletion strains to cell wall degrading enzymes and osmotic stressors. Our results show that the Δ*cypS* mutant had elevated sensitivity to lysozyme, and both, the Δ*cypS* and Δ*lfiA*Δ*lfiB* mutant strains, were slightly more sensitive to Proteinase K compared to the WT (Fig 2d). These results suggest that both mutants have a defect in cell wall integrity. An increased sensitivity to lysozyme has been previously been associated with a defect in elongasome function[39], suggesting that CypS could be associated with the *Anabaena* elongasome. Furthermore, Δ*cypS* and Δ*lfiA*Δ*lfiB* mutants were unable to grow in liquid culture (Supplementary Fig. 10a) with Δ*cypS* mutant cells readily bursting upon transfer to liquid culture (Supplementary Fig. 10b), hinting for an elevated sensitivity to fluid shear stress or turgor pressure. In contrast, the Δ*ceaR* mutant was unaffected by the presence of cell wall stressors (Fig. 2d) and grew well in BG11 growth medium (Fig. 2b). However, upon nitrogen stepdown (i.e., transfer into $BG11_0$), the Δ*ceaR* mutant strain readily fragmented into shorter filaments that aggregated into large-scale cell clumps (Fig. 2b, Supplementary Figs. 10a and 11d,e). Cells in those clumps also gradually lost their chlorophyll auto-fluorescence signal (an indicator for a decreased viability) and ultimately died within a few days (Fig 2b, Supplementary Fig. 11a,b,d). This shows that filament viability in the Δ*ceaR* mutant is impaired under diazotrophic conditions. The defect in filament viability could be complemented with pRL25C carrying P_{ceaR}::*ceaR* or P_{ceaR}::*ceaR-gfp* (Supplementary Fig. 11b,d,e).

316 Previous studies showed that mutants of genes involved in intercellular communication
317 in *Anabaena* show a similar, albeit more pronounced fragmentation phenotype (producing
318 unicellular forms) when transferred from BG11 to $BG11_0$ due to the loss of diazotrophy[46,48–50].
319 Proper nutrient exchange through septal junctions is essential for *Anabaena* viability,
320 especially under diazotrophic growth[37]. Consequently, we investigated the level of intercellular
321 communication using FRAP experiments of calcein stained *Anabaena* CCRP mutant strains.
322 Our results show that the Δ*lfiA*Δ*lfiB* mutant is not impaired in intercellular solute diffusion while
323 diffusion is reduced in the Δ*cypS* mutant and virtually absent in the Δ*ceaR* mutant grown in
324 liquid medium (Fig. 2e, Supplementary Figs. 12 and 13). Notably, solute diffusion was not
325 decreased in young Δ*ceaR* mutant cells (i.e. cultures up to 10 days; Fig. 2e), indicating the
326 effect of *ceaR* knockout on cell-cell communication depends on the culture age. This culture
327 age effect on cell-cell communication is also reflected by the different Δ*ceaR* mutant filament
328 length in younger and older (i.e. 3-4 weeks old) cultures. While young Δ*ceaR* mutant filaments
329 showed normal filament lengths, filaments from older Δ*ceaR* mutant cultures were shortened
330 (Supplementary Figs. 9d,e and 11c). To further investigate the underlying cause for the
331 impaired cell-cell communication, we isolated sacculi and observed that the Δ*ceaR* and the
332 Δ*cypS* mutant partially contained significantly larger septa with decreased nanopore counts
333 compared to the WT. We suggest that the larger septa may be responsible for the decrease in
334 solute diffusion (Supplementary Fig. 14). In addition, we observed that some nanopores in the
335 Δ*ceaR* mutant strain were large and irregular (Supplementary Fig. 14), which as well could
336 contribute to the decreased efficiency in solute diffusion.

337 **_Anabaena_ CCRPs are involved in MreB function and localization**

338 The swollen cell phenotype of *Anabaena* Δ*mreB* mutant strain has been previously reported
339 to have no effect on intracellular structures[39]. To assess whether the altered cell and filament
340 shape of *Anabaena* CCRP mutant strains has any effect on intracellular arrangements, we
341 compared ultrathin sections of *Anabaena* WT and CCRP mutant strains. Except for Δ*ceaR*
342 mutant cells that contain a red fluorescent filament (Fig. 3d; Supplementary Figs. 9e and 15),

intercellular ultrastructures of the mutant strains were largely unaffected regardless of their impact on filament viability and shape (Supplementary Fig. 15). The red fluorescent filaments are not assemblies of thylakoid membranes but appear to be void entities, whose nature is yet to be identified. However, the observed cell wall defects and altered cell shape phenotypes indicates that CypS, LfiA/LfiB and CeaR function is related to PG biogenesis, possibly through association with FtsZ or MreB. To test for a link with the FtsZ-driven divisome, we visualized Z-ring placement in *Anabaena* WT and in each of the mutant strains by immunofluorescence. No alterations in Z-ring placement were observed, indicating that Z-ring formation is unaffected in the mutant strains (Supplementary Fig. 16). To test for an association with the elongasome, we compared the MreB localization in cells ectopically expressing a functional GFP-MreB fusion[39] from P_{petE}. Notably, unlike in the previously reported P_{petE}::GFP-MreBCD overexpression strain[39], we never saw polar aggregate-like structures in our GFP-MreB-expressing strain (Fig. 3a). This suggests that the previously observed aggregations in the GFP-MreBCD strain[39] are specific to the *mre* operon overexpression rather than the overexpression of MreB only. In contrast, we observed short GFP-MreB filaments and occasionally GFP-MreB patches within the cells (Fig. 3a). When grown on $BG11_0$ plates, which we found to increase P_{petE}-driven expression levels, more pronounced GFP-MreB filaments were visible, readily spanning the whole cells (Supplementary Fig. 17). Expression of GFP-MreB in the mutant strains revealed considerable alterations of GFP-MreB localization (Fig 3a). Even though GFP-MreB filaments were present in the Δ*lfiA*Δ*lfiB* mutant strain, we only detected those in non-rounded cells that seemingly had a WT-like phenotype (Fig 3b inlay; 245 (24%) of 1040 cells counted), whereas in rounded cells of zigzagged filaments, the GFP-MreB signals were restricted to the cell poles (Fig. 3b; 795 (76%) of 1040 counted cells). These observations suggest that LfiA/LfiB are important for proper localization of MreB. Unlike LfiA/LfiB, CypS seems to have no direct influence on GFP-MreB localization, as indicated by the WT-like localization of GFP-MreB in the Δ*cypS* mutant strain (Fig. 3c). In contrast, in the Δ*ceaR* mutant, GFP-MreB only localized as aggregate-like patches and never formed filamentous strings as seen in the WT (Fig. 3d). This suggests that CeaR is important for proper

371 MreB polymerization. The negative effect of the absence of CeaR on GFP-MreB function and
372 localization became even more evident during growth in liquid culture. There, P_{petE}-driven
373 expression of GFP-MreB led to a prominent rounding of Δ*ceaR* mutant cells and a zigzagged
374 filament shape (Fig. 3d). Despite being expressed from the P_{petE}, GFP-MreB signal intensity
375 was strongly elevated in these cells, which suggests a role of CeaR in MreB turnover
376 regulation. The induced cell rounding of the Δ*ceaR* mutant upon GFP-MreB expression argues
377 for a defect in proper MreB function as the rounded phenotype resembles the previously
378 described Δ*mreB* mutant phenotype[39]. Similarly, the swollen cell phenotype of *Anabaena* cells
379 expressing CeaR-GFP (Fig. 1h, Supplementary Fig. 8a) is reminiscent of the enlarged cells
380 observed upon GFP-MreBCD overexpression[39]. An association of CeaR with MreB is further
381 reinforced by a banded and helical-like assembly of CeaR-GFP in *E. coli* (Supplementary Fig.
382 8b), resembling the localization of YFP-MreB in *E. coli*[66]. Thus, our observations suggest that
383 CeaR is involved in longitudinal PG synthesis by affecting MreB localization and function.

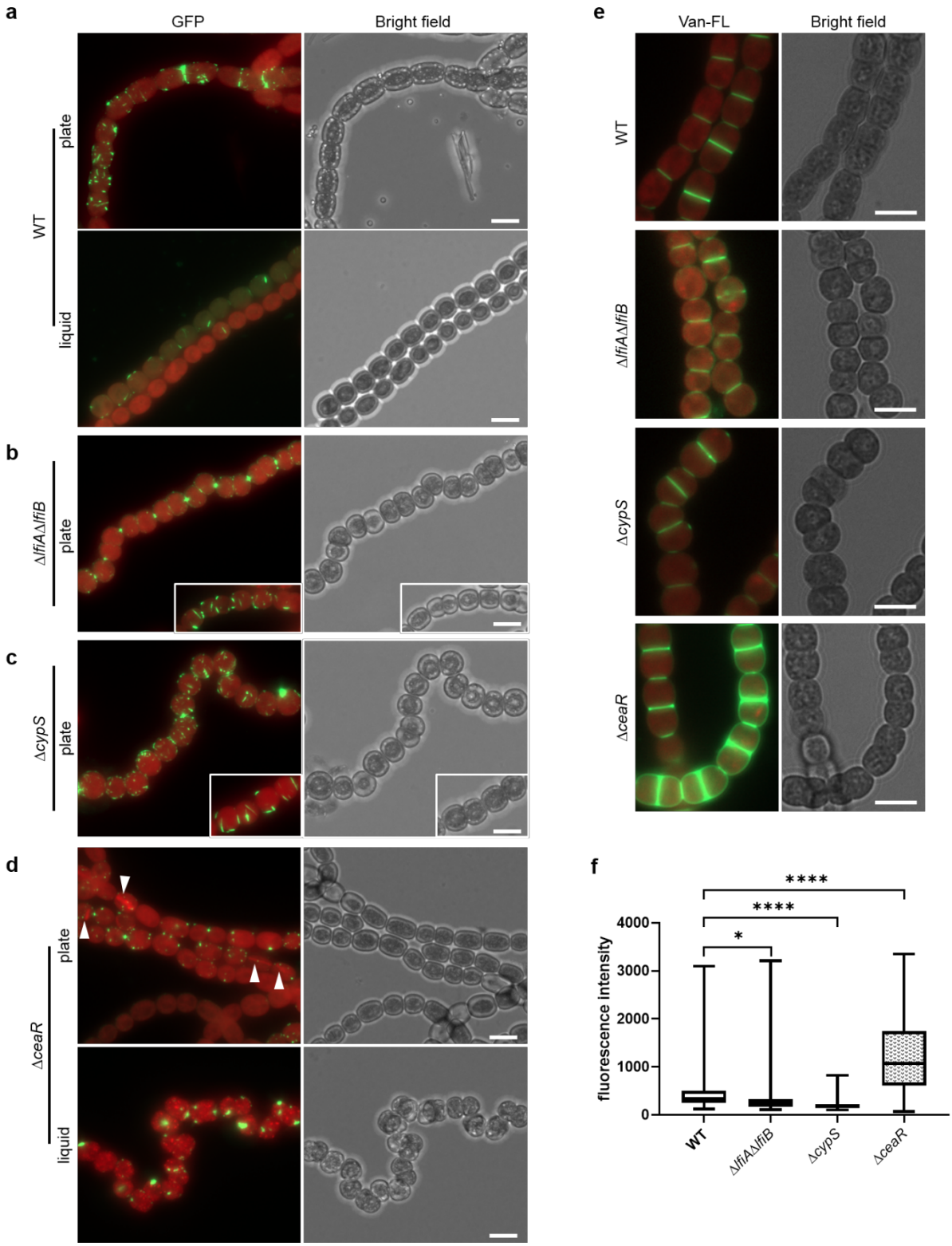

Fig. 3: CCRPs affect MreB localization and PG biogenesis

(**a**-**d**) Merged GFP fluorescence and chlorophyll autofluorescence and bright field micrographs of *Anabaena* WT, Δ*lfiA*Δ*lfiB*, Δ*cypS* and Δ*ceaR* mutant strains expressing GFP-MreB from P_{petE}. Cells were either grown on BG11 plates or in BG11 liquid medium prior visualization. White triangles indicate red fluorescent filaments within Δ*ceaR* mutant cells. Exposure time for GFP fluorescence excitation was 70 ms except for 14 ms in the Δ*ceaR* mutant grown in liquid BG11. Consequently, despite being expressed from the non-native P_{petE}, absence of CeaR detrimentally affects GFP-MreB localization and turnover. (**e**) Merged BODIPY™ FL Vancomycin (Van-FL) fluorescence and chlorophyll autofluorescence and bright field micrographs of *Anabaena* WT, Δ*lfiA*Δ*lfiB*, Δ*cypS* and

Δ*ceaR* mutant strains stained with 5 µg ml^{-1} Van-FL. As a result of the low Van-FL staining and for better visibility, Van-FL fluorescence intensity in Δ*lfiA*Δ*lfiB* and Δ*cypS* mutants was artificially increased about twofold after image acquisition. Unlike in the WT and the other two mutants, Δ*ceaR* mutant cells show longitudinal Van-FL staining, indicating an altered PG biogenesis activity or localization of enzymes involved in PG biogenesis. (**f**) Analysis of the arithmetic mean fluorescence intensities of cells from Fig. 3e. For all measurements, Van-FL fluorescence intensity from cell septa was recorded using 130 ms exposure time from an area of 3.52 µm^2. Sample size (n) was 200 stainings for each strain. Values indicated with * are significantly different from the WT. *: P < 0.05, **: P < 0.01, ***: P < 0.001, ****: P < 0.0001. ns indicates no significant different to the WT (using one-way ANOVA with Dunnett's multiple comparison test). Scale bars: 5 µm.

PG biogenesis is altered in *Anabaena* CCRP mutants

To further assess the function of *Anabaena* CCRPs in MreB and elongasome-driven PG turnover, we stained active sites of PG synthesis by fluorescently labeled vancomycin (Van-FL). This revealed alterations in the PG remodeling between WT and CCRP mutant strains (Fig. 3e,f). While Δ*lfiA*Δ*lfiB* and Δ*cypS* mutants showed a similar Van-FL staining pattern compared to the WT, both mutants revealed a significantly reduced staining intensity (Fig 3e,f). Hence, it is likely that CypS and LfiA/LfiB are linked to PG biogenesis. Unlike the other two mutants, the Δ*ceaR* mutant is characterized by an increased mean intensity of Van-FL staining that is observed not only in the septal wall, as in the WT, but also in the lateral cell wall (Fig. 3e). Consequently, we suggest that CeaR acts as a regulator PG biogenesis and/or localization of the PG biogenesis machinery. This is in agreement with the altered expression and localization pattern of GFP-MreB in the Δ*ceaR* mutant (Fig. 3d). The suggested role of the four CCRPs in PG turnover is furthermore in agreement with the observed swollen cell phenotype in the Δ*cypS* and Δ*lfiA*Δ*lfiB* mutant and with the altered MreB localization in the mutant strains. Since we observed that CCRP mutants affect cell wall integrity, we next examined the heterocyst-development in the CCRP mutants. Heterocysts contain an extra cell envelope with specific heterocyst glycolipids and envelope polysaccharides[37]. Therefore, we cultivated the CCRP mutant strains on BG11$_0$ plates and inspected heterocyst-formation and staining pattern with alcian blue, a dye that specifically binds to the heterocysts polysaccharide sheet. Our results so far did not reveal an observable defect in heterocyst-development in any of the mutants (Supplementary Fig. 18).

Anabaena CCRPs have the capacity to form an interconnected network and interact with SepJ and MreB

As our *Anabaena* CCRP mutant strains displayed similar phenotypes and the four *Anabaena* CCRPs were all linked to MreB function and localization as well PG biogenesis, we next investigated whether the four proteins interact with each other and with other known morphological determinants in *Anabaena*. Using bacterial two hybrid assays, we found that all of our four CCRPs were able to self-interact (Fig 4a). Additionally, all four CCRPs could cross-interact with each other (Fig. 4a) and we found that LfiA, LfiB and CeaR but not CypS, interacted with MreB. Additionally, CeaR weakly interacts with FtsZ (Fig. 4a, Supplementary Fig. 18), which is in agreement with the Z-ring-like *in vivo* localization of CeaR-GFP (Fig. 1h, Supplementary Fig. 8a). Furthermore, all proteins were identified as interaction partners of the septal protein SepJ, but not with FraC and FraD (Fig. 4a, Supplementary Fig. 19), two other septal junction proteins[45]. Since coiled-coil motifs are well-known protein-protein interaction domains[67–69], they are putatively prone for false-positive results in the interaction assays. Indeed, interactions of coiled-coil containing proteins are usually considered to be specific[67,70–76]; nonetheless, we further tested the interaction specificity of our four CCRPs – Cyps, LfiA, LfiB and CeaR – in the bacterial two-hybrid assay by including Alr3364, another *Anabaena* CCRP (Supplementary Fig. 1), as a negative control in our screening. Our results show that Alr3364 only weakly interacted (< 500 Miller Units/mg LacZ) with LfiA and LfiB and failed to interact with CypS and CeaR (Supplementary Fig. 20). This confirms that the strong interactions (all > 500 Miller Units/mg LacZ) observed between CypS, LfiA, LfiB and CeaR are indeed specific interactions. We attempted to further confirm our interaction results with affinity co-elution experiments. However, we found that Ni-NTA-bound *Anabaena* CCRPs readily precipitated upon transfer from denaturing to native buffer conditions, precluding further co-elution studies. Additionally, we observed that non-denaturing conditions failed to purify overexpressed CCRPs from *E. coli*, confirming their inherent insoluble nature, a property known to eukaryotic IFs[54,77]. Instead, we surveyed for further interaction partners in *Anabaena* WT cells expressing CeaR-GFP or LfiA-GFP by co-immunoprecipitation experiments

(Supplementary Fig. 21) and analyzed co-precipitated proteins by LC-MS/MS analytics (Supplementary File 3). This analysis confirmed that LfiA and LfiB interact with each other *in vivo* and validated the association of CeaR and LfiA with MreB in *Anabaena* (Supplementary Fig. 21c). Corroborating a role of CeaR in PG biogenesis and MreB function, CeaR was also found to be associated with three penicillin binding proteins (Supplementary Fig. 21c), which are known regulators of PG synthesis and are part of the elongasome[78,79]. Furthermore, both, CeaR and LfiA, co-precipitated ParA, and CeaR was additionally found to be associated with MinD (Supplementary Fig. 21c). Both ParA and MinD belong to a protein family of Walker-A-type ATPases and mediate plasmid and chromosome segregation[77,80,81]. To test for a similar function in our CCRPs, we compared the DNA distribution among the CCRP mutant cells as measured by distribution of 4′,6-Diamidin-2-phenylindol (DAPI) staining intensity. For that, we calculated the width of the DAPI focal area as the range of DAPI staining around the maximum intensity focus (±10 grey intensity in arbitrary units). This revealed that the staining focal area size was significantly different among the four tested strains ($P=3.14x10^{-41}$, using Kruskal-wallis). Post-hoc comparison showed that the focal area size in the *ΔceaR* mutant was larger than the others, and the area size in *Anabaena* WT was not significantly different than Δ*cypS*. The DAPI signal observed in the Δ*lfiA*Δ*lfiB* mutant appears as the most condensed, and indeed, the Δ*lfiA*Δ*lfiB* mutant focal DAPI area was smallest in comparison to the other strains (alpha=0.05, using Tukey test; Supplementary Fig. 22ab). Unlike the *ΔceaR* mutant and the WT, DAPI signals in the Δ*lfiA*Δ*lfiB* and Δ*cypS* mutant strains were also observed between two neighboring cells (Supplementary Fig 21a), indicating that DNA distribution is not properly executed during cell division in those strains.

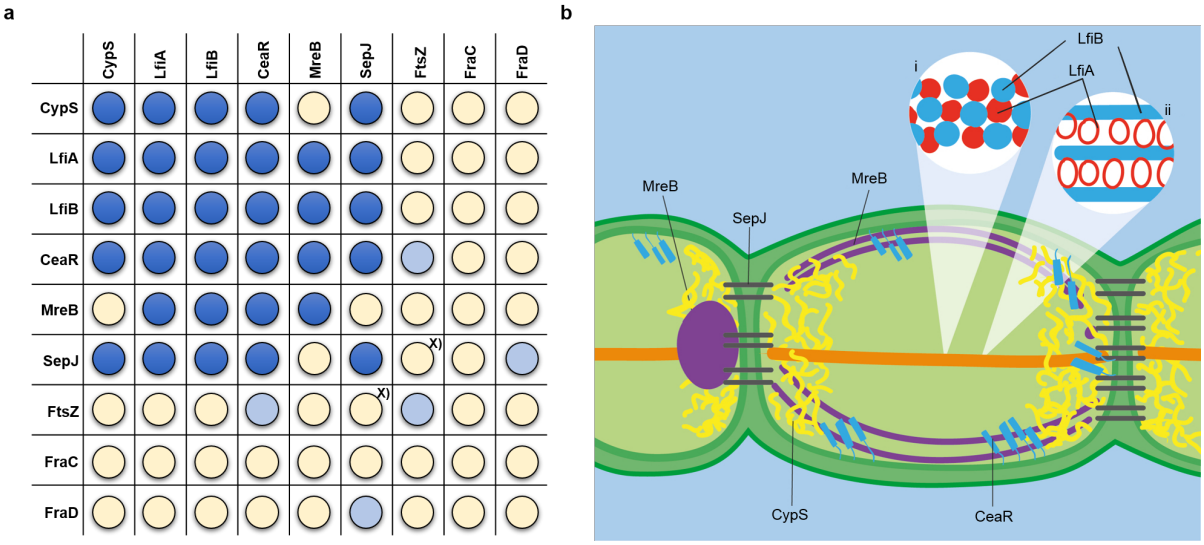

Fig. 4: *Anabaena* CCRPs form a putative cytoskeletal network that links the septal junction protein SepJ and the MreB cytoskeleton

(**a**) Graphical visualization of beta-galactosidase assay results of *E. coli* BTH101 cells co-expressing indicated translational fusion constructs of *Anabaena* proteins with the T18 and T25 subunit, investigating all possible pair-wise combinations. Corresponding data are shown in Supplementary Fig. 19. Blue spots indicate strong verified interactions (>500 Miller units mg^{-1}) while light blue dots mark moderate interactions (< 500 Miller units mg^{-1}) and no interactions are depicted with yellow-colored dots. Dots marked with "X" were previously reported by Ramos-León *et al.* (2015)[82]. (**b**) A model for an interconnected cytoskeletal network in *Anabaena*. Septal junctions, comprised of, among others, SepJ (grey), are directly connected to the CypS polar scaffold (yellow) that provides anchoring sites for the LfiA/B filament (orange). (i) Similar to α-tubulin and β-tubulin, the LfiA/B heteropolymer could be composed of alternating LfiA (red) and LfiB (blue) monomers. (ii) However, based on *in vivo* localizations, *in vitro* polymerization, domain predictions and structural similarities to eukaryotic plectin, it is more likely that LfiA acts as a cytolinker protein for LfiB, enabling proper polymerization. The LfiA/B filament spans through the cells, anchoring to CypS but never passes through the septal junctions. The identified *Anabaena* filament stabilizing effect of LfiA/B could then be relayed to the neighboring cells via interactions with CypS, CeaR (light blue), SepJ and MreB (purple). MreB localization is adapted from Hu *et al.* (2007)[39] in which MreB plugs accumulate at the septa (indicated in the dividing cell on the left) but also forms cell-traversing filaments (right cell). MreB activity and localization is dependent on CeaR. Furthermore, according to FRAP results, it is conceivable that CeaR regulates *Anabaena* filament viability through interaction with SepJ.

Discussion

Here we provide evidence for the capacity of three *Anabaena* CCRPs - CypS, LfiA together with LfiB - to form IF-like polymers *in vitro* and *in vivo*. The characterization of multiple CCRPs in our study was possible thanks to the easy to use and comparably high-throughput approach for the screening of novel filament-forming CCRPs using the NHS-Fluorescein dye. Our approach supplies an alternative for the examination of protein-filament formation by electron microscopy; instead it allows for a simplified protocol for the detection of protein filaments using fluorescence microscopy. In accordance with previous studies of eukaryotic IF proteins[83,84], *Anabaena* CCRPs N-terminally tagged with a YFP-tag failed to produce a discernible

structures/fluorescence signal. This suggests that the N-terminus is essential for localization or function of the *Anabaena* CCRPs and supports our observations of CypS and LfiA/LfiB as *bona fide* prokaryotic CCRPs with IF-like function. While the previously described prokaryotic IF-like proteins form homopolymers[15,24,32,52,85], LfiA and LfiB assemble into a heteropolymer comprising the two proteins. Furthermore, LfiA and LfiB have the capacity to co-polymerize in a heterologous *E. coli* system, similarly to other known CCRPs such as Scc from *Leptospira biflexa*[85] or crescentin[86,87]. We note, however, that the results from our *in vivo* experiments of LfiA/LfiB co-polymerization are based on artificial expression of the two CCRPs. We hypothesize that the absence of a LfiA/LfiB heteropolymer in strains expressing LfiA-GFP or LfiB-GFP alone (with the WT alleles still present) may be due to a dosage-dependent effect, where the presence of unequal concentration of LfiA and LfiB in the cell leads to protein aggregates. Our observation of LfiA-GFP or LfiB-GFP aggregates when they were expressed alone in the Δ*lfiA*Δ*lfiB* mutant strain supports the dosage effect hypothesis. Also, in our *in vitro* polymerization assay, LfiA and LfiB only formed clear filamentous structures when both proteins are present in equal concentrations. Furthermore, the genomic neighbourhood of LfiA and LfiB suggests that the LfiA/LfiB heteropolymer formation is relying on co-translational assembly (e.g., as observed for LuxA/LuxB[88]). Co-translational assembly of the WT LfiA/LfiB would lead to an efficient binding of the two subunits such that the expression of one unit only in excess (i.e., LfiA-GFP or LfiB-GFP) would lead to the formation of aggregates.

Our results demonstrate that the four CCRPs described here form an interconnected cytoskeletal network in *Anabaena*. The network is likely anchored to the cell poles through the interaction with the septal junction protein SepJ. Together with the cell shape-determining protein MreB[89], *Anabaena* CCRPs possibly contribute to the cell shape and relay filament shape-stabilizing properties to neighboring cells, thereby maintaining the linear *Anabaena* filament phenotype (Fig. 4b). The interaction of *Anabaena* CCRPs with SepJ suggests that not only filament integrity[46,48] but also filament shape is strongly dependent on proper septal junction function and stability. Hence the four CCRPs are likely involved in filament integrity, similarly to the integral membrane proteins SepJ and FraC/FraD. The *Anabaena* CCRPs might

constitute stabilizing platforms or scaffolds for other proteinaceous structures, similarly to the stabilizing function of the eukaryotic cytoskeleton for cell-cell contacts (i.e. desmosomes)[90]. Notably, LfiA shares structural similarities with the spectrin repeats of plectin (Supplementary Table 1), a well-described eukaryotic cytolinker protein. Plectins link the three eukaryotic cytoskeletal systems (actin filaments, microtubules and IFs), thereby contributing to the resistance to deformation of vertebrate cells[90,91]. They furthermore stabilize desmosomes and are hence directly involved in cell-cell connection integrity[92]. An analogous cytolinker function of LfiA could explain why LfiB alone did not form filaments and suggests that LfiB requires LfiA as the linking protein for polymerization. Based on the structural similarity to spectrin, it is also conceivable that LfiA and LfiB possess similar functions as α and β-spectrin. Together, spectrin α/β-heteropolymers produce a cell shape-maintaining interconnected cytoskeletal network (the so called spectre) below the plasma membrane of erythrocytes[93]. Furthermore, similar to LfiA/LfiB, spectrins are directly linked to the actin cytoskeleton[90]. This link of LfiA/LfiB to the actin-like MreB cytoskeleton is evident in the altered localization of GFP-MreB in the Δ*lfiA*Δ*lfiB* mutant strain. The observed-PG staining pattern where PG staining was strongly elevated in the Δ*ceaR* mutant strain suggests that in *Anabaena* WT, CeaR acts to (down)regulate MreB or elongasome function (hence its name: cyanobacterial elongasome regulator). Although less pronounced, PG staining was decreased in both *ΔcypS* and Δ*lfiA*Δ*lfiB* mutants, suggesting that CypS and LfiA/LfiB could act as positive regulators of elongasome function. These observations further imply an association of CypS with the elongasome, despite the failure of CypS to directly interact with MreB (Fig. 4a). MreB and the elongasome are the main determinants of the PG exoskeleton, which provides the cell with structural integrity and resistance to turgor pressure[79,94]. Notably, both Δ*cypS* and Δ*lfiA*Δ*lfiB* mutant strains were unable to grow in liquid culture, hinting for a defect in the resistance to turgor pressure. The growth defect in liquid culture of the Δ*cypS* and Δ*lfiA*Δ*lfiB* mutant strains may result from altered elongasome functionality due to the absence of CypS and LfiA/LfiB. The association of *Anabaena* CCRPs with proper elongasome function is further supported by the elevated sensitivity of the Δ*cypS* mutant strain to lysozyme, similar to the Δ*mreB* mutant strain[39]. An

558 interaction of prokaryotic IF-like proteins with MreB and PG synthesis has been previously
559 described in other bacteria. Examples are the gliding motility in *M. xanthus,* where a multi-
560 protein complex, including the IF-like CCRP AglZ and MreB was found to coordinate type A-
561 motility[25]. Similarly, the curved morphotype of *C. crescentus* is induced by crescentin, which
562 modulates PG biogenesis by exuding local mechanical forces to the cell membrane[22,56]. Thus,
563 our results are in agreement with a functional link between IF-like CCRPs and the MreB
564 cytoskeleton in bacteria.

565 The conserved combination of all four CCRPs in heterocystous cyanobacteria that form
566 linear filaments (or false branching; Fig. 1a) suggests that the linear filament formation has a
567 selective advantage. Both Δ*cypS* and Δ*lfiA*Δ*lfiB* mutants had a zigzagged phenotype and were
568 unable to grow in liquid culture. The zigzagged mutants provide more accessible surface for
569 the acting mechanical forces in liquid[95], including fluid shear stress[96], ultimately resulting in
570 forces that cannot be endured by the abnormal mutant filaments. Notably, while the selective
571 advantage of cell shape is considered to be mostly a manifestation of biotic and abiotic
572 selective factors in the cell environment[97], the selective advantage of multicellular shapes is
573 likely related to the efficiency of intercellular communication and transport[95]. Indeed, the results
574 of our FRAP experiments show that the efficiency of flow in the zigzagged Δ*cypS* mutant
575 filament is reduced. Furthermore, the Δ*ceaR* mutant failed to grow in diazotrophic conditions
576 where transport of metabolites in the filament is considered essential for *Anabaena* viability. A
577 similar observation has been made for knockout mutant strains of SepJ, FraC and FraD that
578 are essential for *Anabaena* multicellularity[46,49,50]. Additionally, the decrease in solute diffusion
579 in the Δ*ceaR* mutant strain suggests that CeaR is involved in the buildup or stabilization of the
580 septal junctions. This notion is further supported by the abnormal nanopore formation observed
581 in some Δ*ceaR* mutant septa. Our results thus suggest that CeaR is important for *Anabaena*
582 multicellularity while CypS, LfiA and LfiB serve as regulators of *Anabaena* patterned
583 multicellularity. The evolution of patterned multicellularity is considered an important step
584 towards a sustainable division of labor and the development of cell differentiation[3]. Our study

reveals the role of cytoskeletal proteins in the evolution and maintenance of bacterial multicellular form.

Acknowledgments

We thank Katrin Schumann, Myriam Barz, Lisa Stuckenschneider, Lisa-Marie Philipp and Claudia Menzel for their assistance in the experimental work. We thank Tanita Wein for critical comments on the manuscript. FRAP experiments were done at the Facility for Imaging by Light Microscopy (FILM) at Imperial College London. We thank Tine Pape for assistance with graphic illustrations (funded by the cluster of excellence ‘‘The Future Ocean’’ at Kiel University). The study was supported by the German science foundation (DFG) (Grant No. STU513/2-1 awarded to KS). DJN was supported by the BBSRC as part of the joint NSF Ideas Lab grant on ‘Nitrogen: improving on nature’ (grant BB/L011506/1). IM and AK were supported by German science foundation (DFG) (Grant SFB766).

Author contribution

BLS and KS designed the study. BLS established and performed the experimental work with contributions from MT and JW. CW and TD performed comparative genomics analysis. DJN and AKK performed FRAP assays and AKK and IM carried out ultrathin structures and nanopore analyses. AOH and AT analyzed protein samples by mass spectrometry. BLS, TD and KS drafted the manuscript with contributions from all coauthors.

Competing interests

The authors declare no competing interests.

Supplementary information

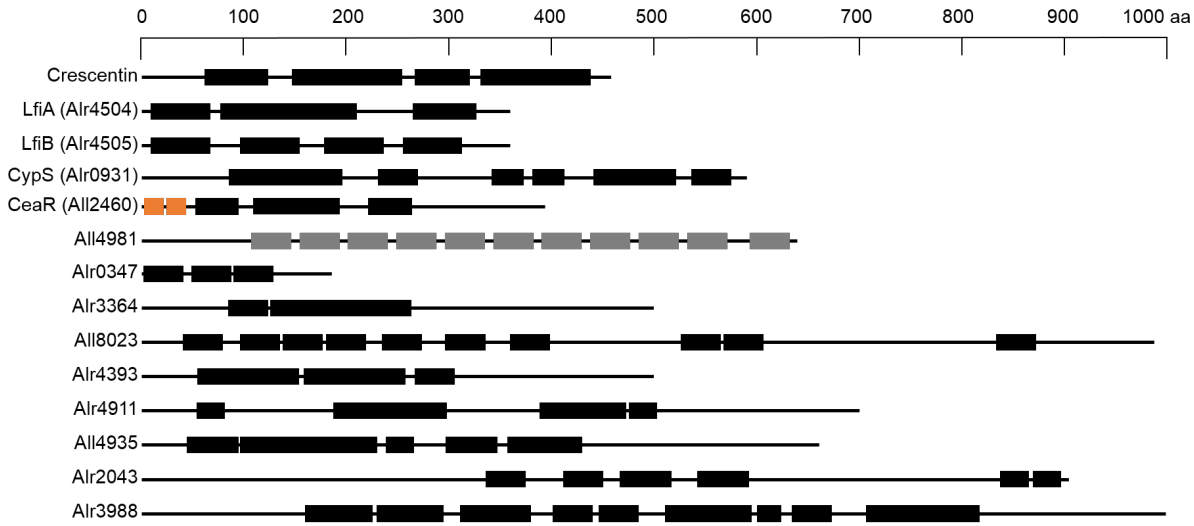

Supplementary Fig. 1:Domain architecture of IF-like protein candidates

Depiction of coiled-coil domains of protein candidates and Crescentin from *Caulobacter crescentus* based on the COILS algorithm[98] with a window width of 21. The scale on top is given in amino acid residues (aa) and amino acid sequences in coiled-coil conformation are depicted by black bars, transmembrane domains are shown in orange bars, while non-coiled-coil sequences are represented by black lines. Tetratricopeptide repeats (TRPs) are shown as grey bars. Cyanobacterial proteins are given as cyanobase locus tags.

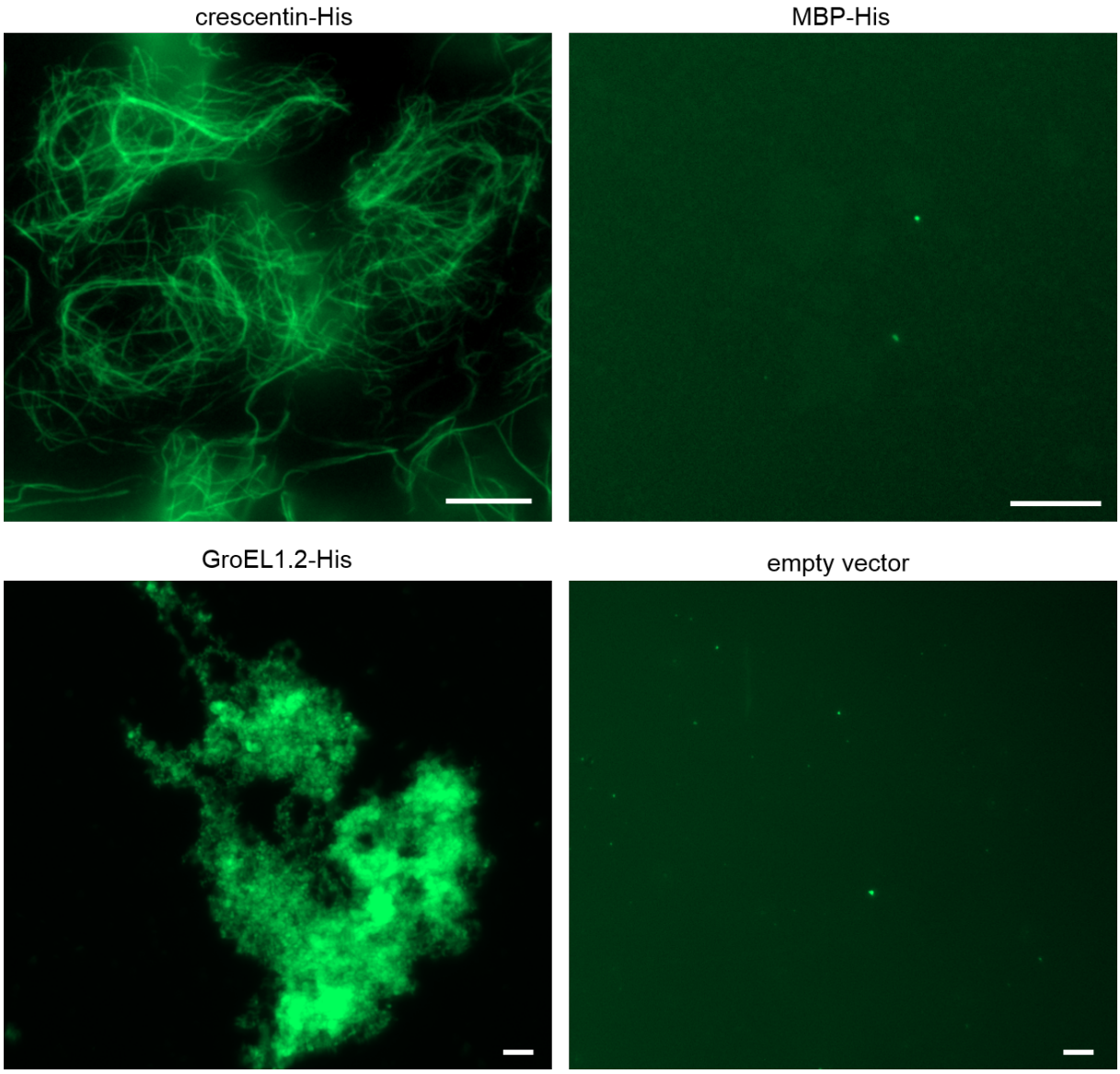

Supplementary Fig. 2: *In vitro* polymerization assay controls

NHS-fluorescein fluorescence micrographs of purified and renatured Crescentin-His, MBP-His and GroEL1.2 from *Chlorogloeopsis fritschii* PCC 6912 (0.5 mg ml^{-1} each) as well as purified cell-free extracts of *E. coli* BL21 (DE3) carrying empty vector (pET21a(+)) in HLB. Notably, GroEL1.2, able to self-interact[57], collapses into indistinct aggregates, showing that oligomerizing proteins do not form filaments in our assay. Proteins and cell-free extracts (empty vector) were dialyzed in a step-wise urea-decreasing manner and stained with an excess of NHS-Fluorescein. Scale bars: 10 µm.

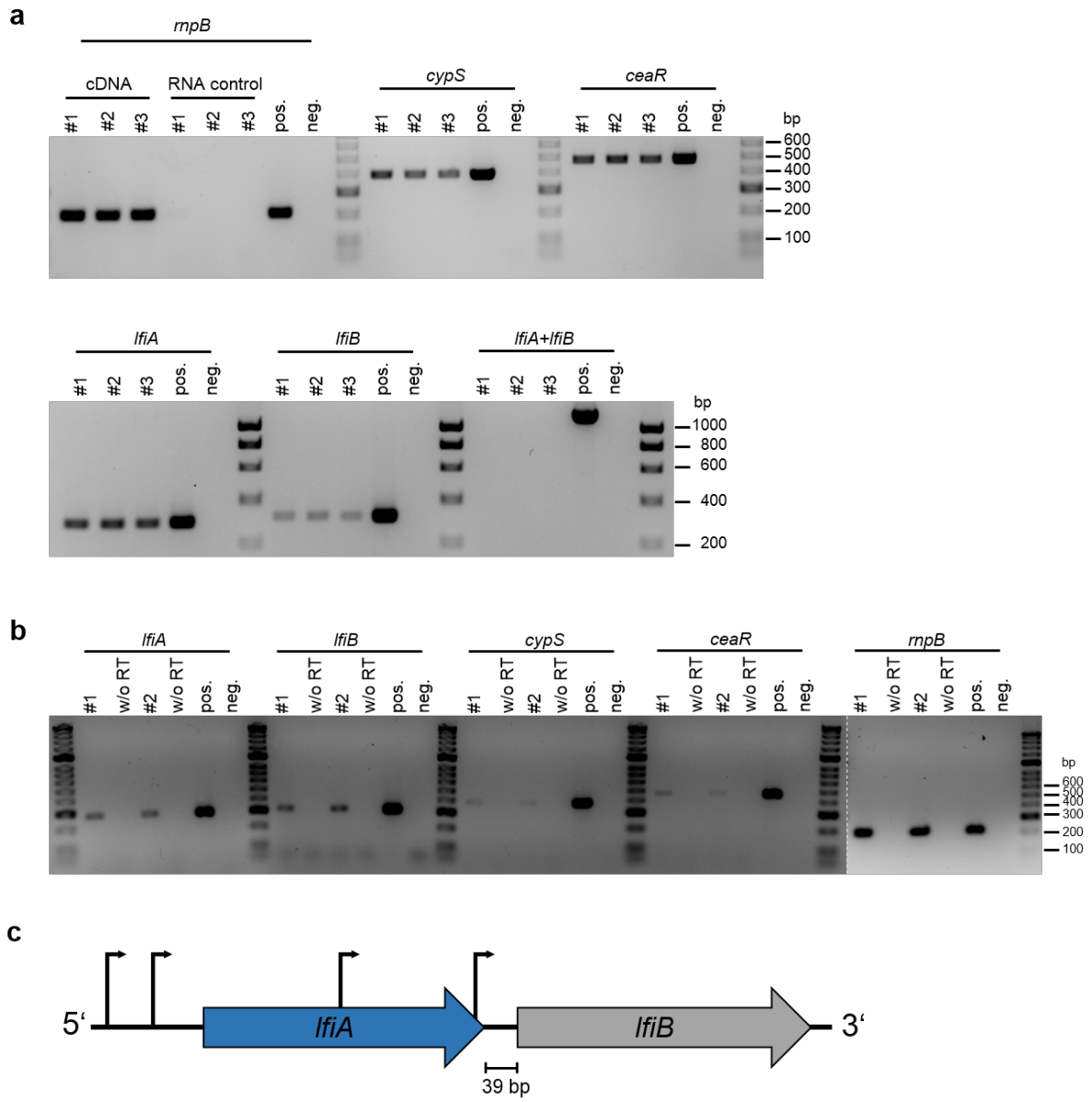

Supplementary Fig. 3: *Anabaena* CCRPs are expressed at standard growth conditions

(a,b) RT-PCR of whole RNA from *Anabaena* WT cultures grown in (a) BG11 or (b) $BG11_0$ liquid medium from (a) three or (b) two independent biological replicates. Gene transcripts were verified using internal gene primers (*rnpB*: #1/#2; *cypS*: #3/#4; *ceaR*: #5/#6; *IfiA*: #7/#8; *IfiB*: #9/#10; *IfiA* and *IfiB*: #7/#10). As negative control (neg), PCR reactions were performed with water instead of cDNA or RNA and as a positive control (pos) *Anabaena* gDNA was included. PCR fragments were resolved on a 2% agarose gel in TAE buffer. For each RT-PCR reaction, 100 ng cDNA was used. Absence of residual genomic DNA in DNase I-treated samples was verified with (a) 100 ng DNase I-treated RNA (RNA control) or (b) 100 ng DNase I-treated RNA that was subjected to cDNA synthesis reaction lacking reverse transcriptase (w/o RT). No common transcript for *IfiA* with *IfiB* was detected, suggesting that both proteins are not encoded in an operon.

(c) Depiction of the genomic environment of *IfiA* (blue) and *IfiB* (grey) within the *Anabaena* genome and their respective *in silico* predicted promoters depicted by black arrows (as predicted by BPROM[61]). Promoters of *IfiA* are predicted to reside 204 bp and 543 bp upstream of the open reading frame (ORF) and promoters of *IfiB* are located 22 bp and 450 bp upstream of the ORF, thereby residing within the *IfiA* ORF.

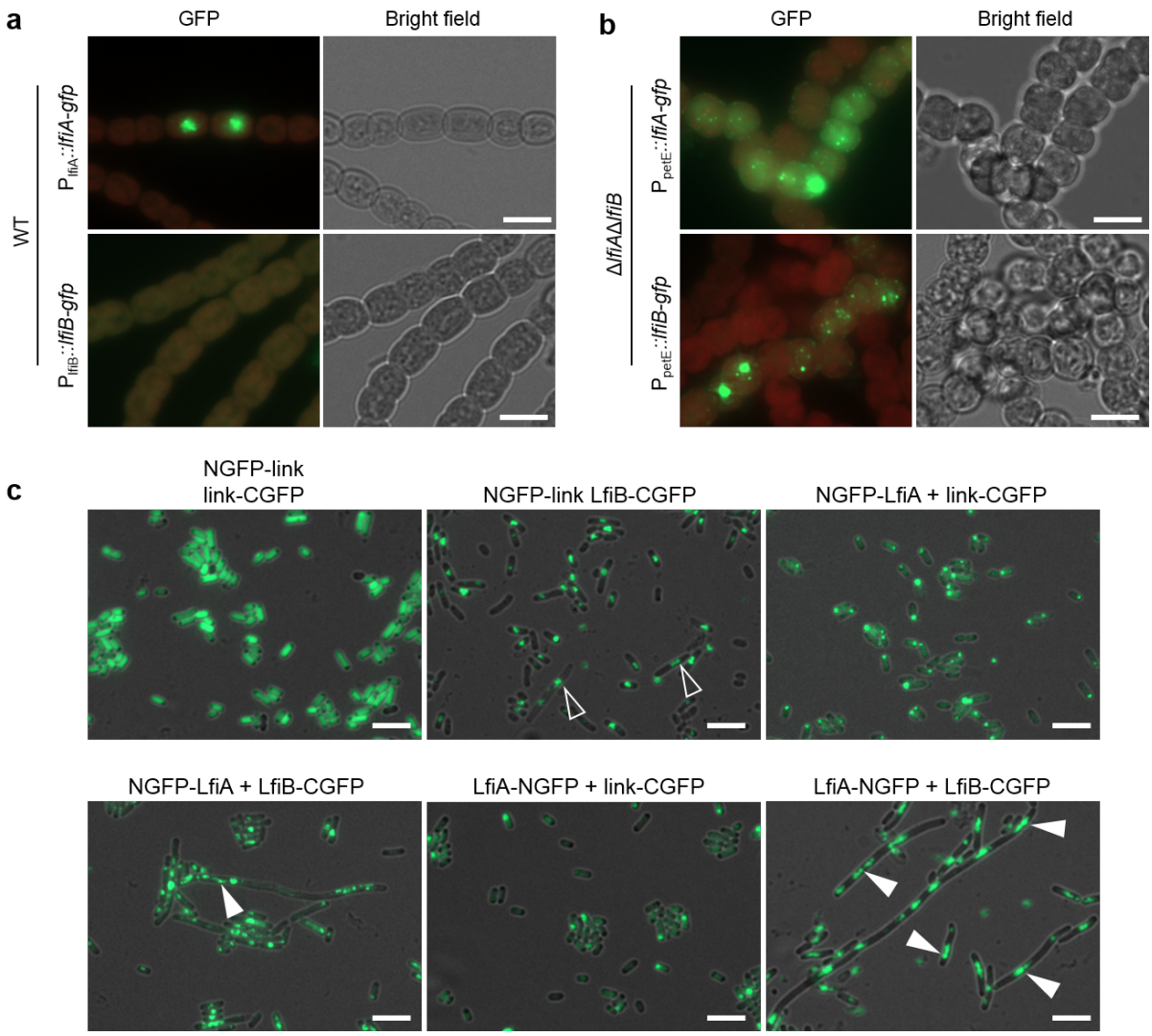

Supplementary Fig. 4: Heterologous expression of LfiA and LfiB

(a) Merged GFP fluorescence and chlorophyll autofluorescence (red) and bright field micrographs of *Anabaena* WT cells expressing LfiA-GFP or LfiB-GFP from P_{lfiA} and P_{lfiB}. No expression of LfiB-GFP is detectable from P_{lfiB} while expression of LfiA-GFP from P_{lfiA} leads to similar patchy clumps within the cells as observed from P_{petE} in Fig. 1d. Scale bars: 5 µm.

(b) Merged GFP fluorescence and chlorophyll autofluorescence and bright field micrographs of Δ*lfiA*Δ*lfiB* mutant strain expressing LfiA-GFP or LfiB-GFP from P_{petE}. Cells were grown on BG11 growth plates. For expression of LfiA-GFP, BG11 plates were supplemented with 1 µM $CuSO_4$. This experiment shows that LfiA-GFP and LfiB-GFP from P_{petE} (Fig. 1d) expression and localization in *Anabaena* WT is not affected by native LfiA or LfiB present in the WT background. Scale bars: 5 µm.

(c) Detection of protein-protein interactions with the GFP-fragment reassembly assay[99]. Merged GFP fluorescence and bright field micrographs of *E. coli* BL21(DE3) cells co-expressing NGFP-link (empty pET11a-link-NGFP) and -link-CGFP (empty pMRBAD-link-CGFP), NGFP-link and LfiB-CGFP, NGFP-LfiA and link-CGFP, NGFP-LfiA and LfiB-CGFP, LfiA-NGFP and link-CGFP or LfiA-NGFP and LfiB-CGFP. Cells were grown to an OD_{600} of 0.5, induced with 0.2% L-arabinose and 0.05 mM IPTG and incubated for 48 h at 20 °C. Transparent triangles point to structures resembling LfiB-His *in vitro* polymers. White triangles indicate FilP-GFP-like[32] filamentous structures that resemble structures indicated with translucent triangles but span longer distances. Co-expression of both, LfiA and LfiB leads to an elongated cell phenotype. FilP-like structures and elongated cells can already be seen upon co-expression of NGFP-LfiA with LfiB-CGFP but only upon co-expression of LfiA and LfiB with C-terminal GFP-fragments leads to a clear filamentous cell phenotype and abundant intracellular filamentous structures. This suggests that the N-terminus is important for heteropolymerization. Scale bars: 5 µm.

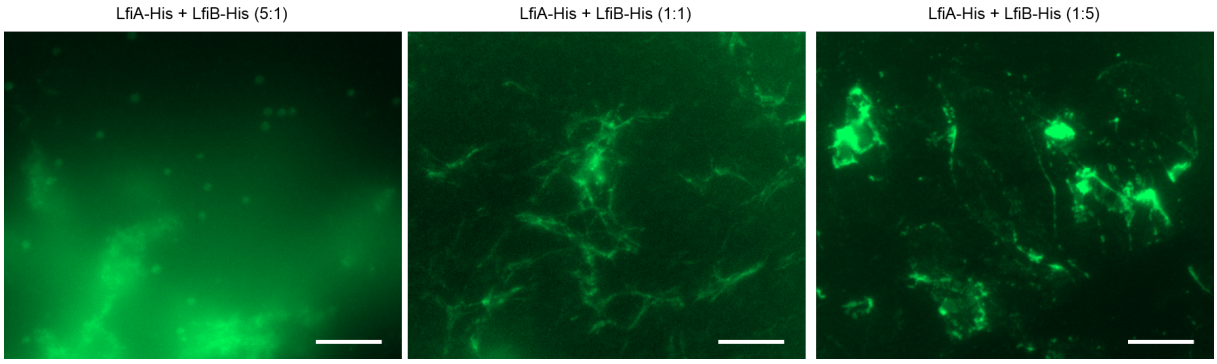

Supplementary Fig. 5: Co-polymerization of LfiA and LfiB is dosage-dependent

NHS-fluorescein micrographs of purified and co-renatured LfiA-His and LfiB-His in HLB. LfiA-His and LfiB-His were combined in different ratios, either with a fivefold excess of LfiA-His (left image; corresponding to 0.25 mg ml^{-1} LfiA-His and 0.05 mg ml^{-1} LfiB-His), a fivefold excess of LfiB-His (right image; corresponding to 0.25 mg ml^{-1} LfiB-His and 0.05 mg ml^{-1} LfiA-His) or an equal concentration of LfiA-His and LfiB-His (central image; 0.25 mg ml^{-1} each). Proteins were dialyzed in a stepwise urea-decreasing manner and stained with an excess of NHS-Fluorescein. Fine heteropolymers only form when equal concentrations of LfiA-His and LfiB-His are present. In concert with the partial self-polymerization capacity of LfiB-His (Fig. 1b), certain filamentous structures are also detected in the LfiB-His excess samples. However, most protein still precipitated under those conditions. Scale bars: 10 µm.

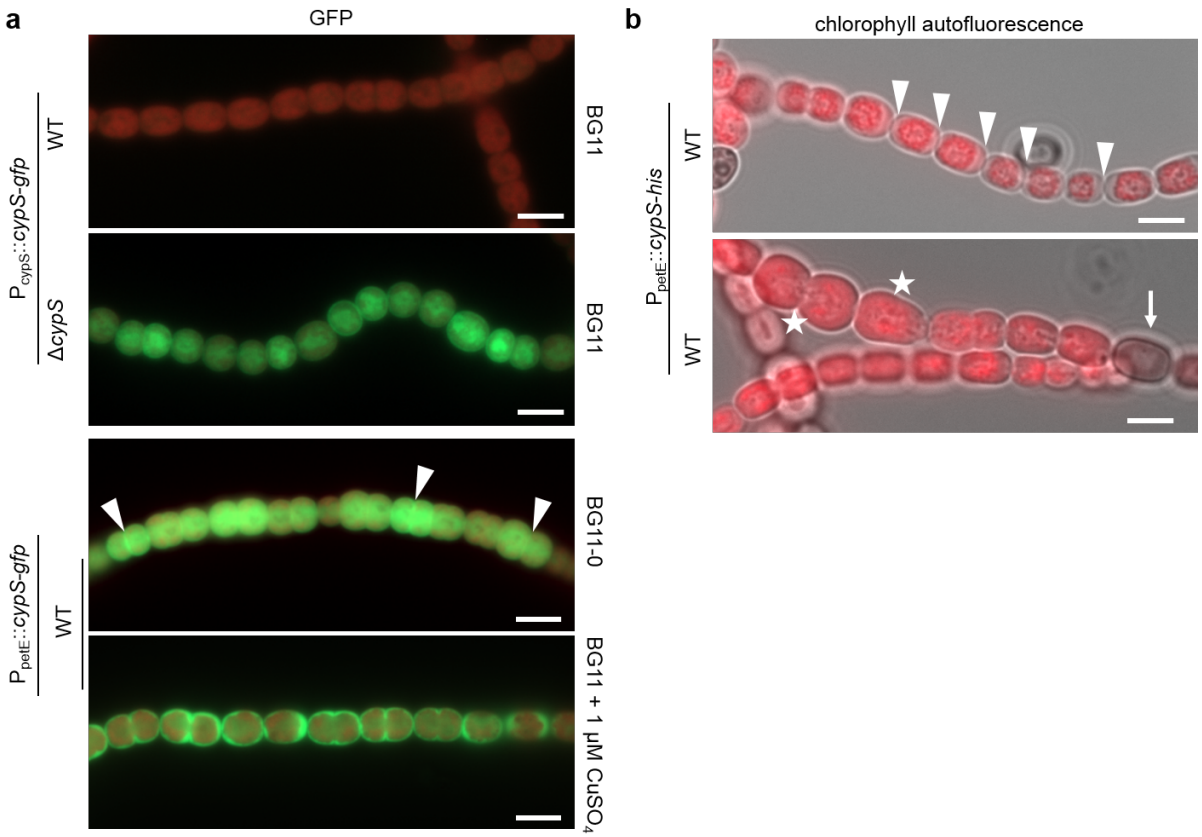

Supplementary Fig. 6: CypS *in vivo* localization is tag orientation-dependent

(a) Merged GFP fluorescence and chlorophyll autofluorescence micrographs of *Anabaena* WT and Δ*cypS* mutant strain expressing CypS-GFP from P_{petE} or P_{cypS}. Strains carrying P_{cypS}::*cypS-gfp* were grown in BG11, while the strains carrying P_{petE}::*cyps-gfp* are grown in indicated media with or without $CuSO_4$ supplementation. White triangles indicate membrane localization, which is most pronounced in dividing cells. Further induction of protein expression shows polar localization of CypS-GFP, similar to CypS-His. In the presence of native *cypS* (i.e. *Anabaena* WT), no CypS-GFP expression was detected from P_{cyps}, indicating that CypS dosage is tightly controlled in the WT. Control is likely exerted at the transcriptional level as overexpression from P_{petE} still produces detectable protein in the WT background. Scale bars: 5 µm.

(b) Merged bright field and chlorophyll autofluorescence micrographs of *Anabaena* WT cells expressing CypS-His from P_{petE} grown in $BG11_0$ supplemented with 0.25 µM $CuSO_4$ (upper image) or with 2.5 µM $CuSO_4$ for 2 d (lower image). White triangles mark cell septa with the most prominent retraction of chlorophyll signal away from the poles. White stars indicate swollen cells. White arrow points to a heterocyst. Note that the areas devoid of chlorophyll signal are occupied by CypS-His plugs (Fig. 1g), suggesting that CypS forms a dense proteinaceous meshwork at the cell poles. Scale bars: 5 µm.

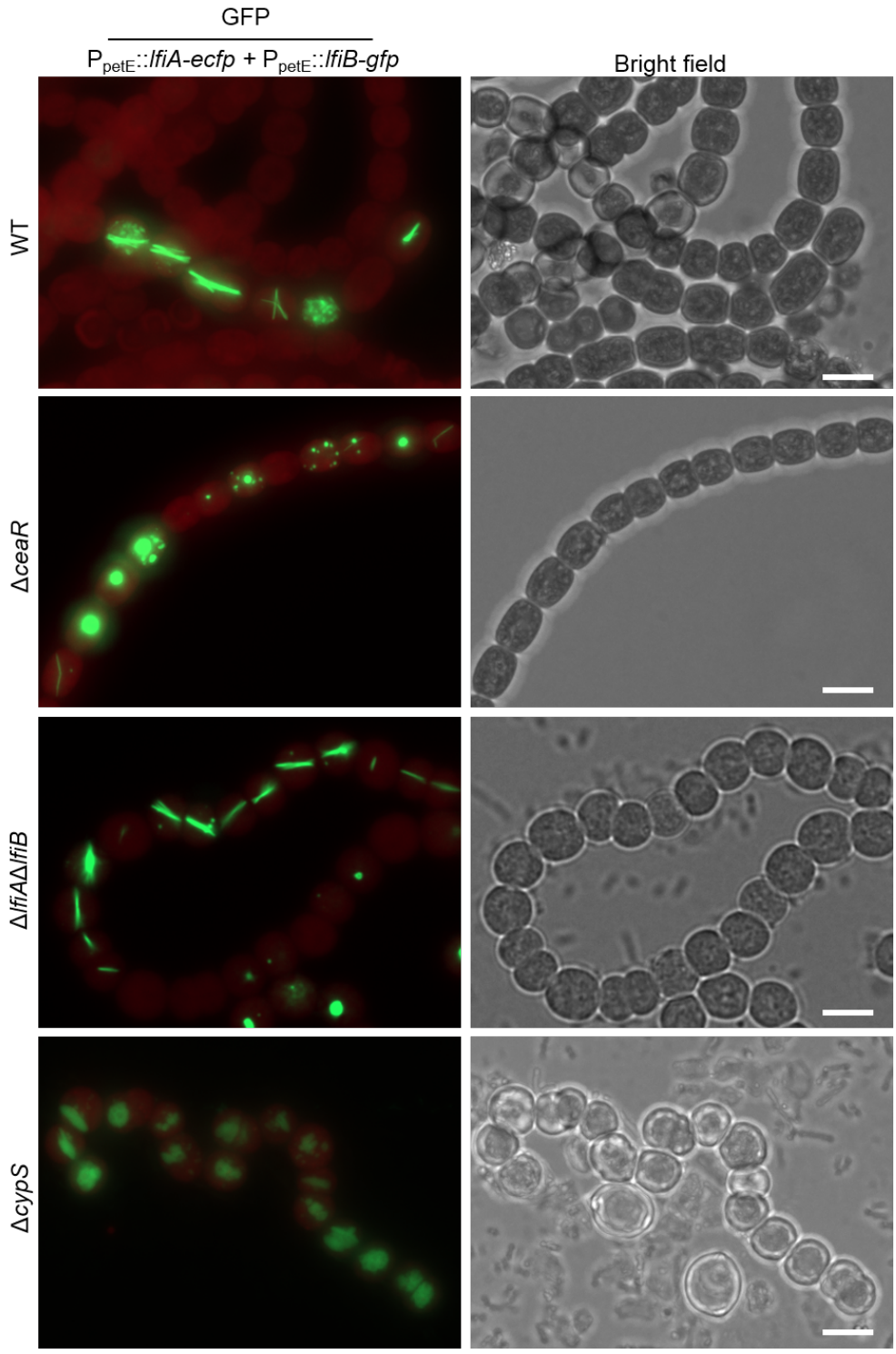

685

686 **Supplementary Fig. 7: *Anabaena* CCRPs affect LfiA/B *in vivo* localization**

687 Mergend GFP-fluorescence and chlorophyll autofluorescence and bright field micrographs of *Anabaena* WT and
688 *Anabaena* mutant strains co-expressing LfiA-eCFP and LfiB-GFP from P_{petE}. First, second and fourth images are
689 maximum intensity projections of a Z-stack. Localization of the LfiA/B filament is slightly altered in the Δ*ceaR* mutant
690 strain and fully deranged in the Δ*cypS* mutant strain. This suggests that CypS is involved in LfiA/B polar attachment,
691 possibly by providing a proteinaceous scaffold for LfiA/B anchorage. Also, Δ*cypS* mutant strain expressing LfiA/B
692 showed a decrease in filament viability. Colonies arose upon transformation with the LfiA/B-expressing construct
693 but did not grow upon re-streaking on fresh plates. Lack of fluorescence signal in some of the depicted cells is likely
694 due to the phenotypic variation of copy numbers of the pRL25C plasmid in different cells within an *Anabaena*
695 filament[100]. Scale bars: 5 µm.

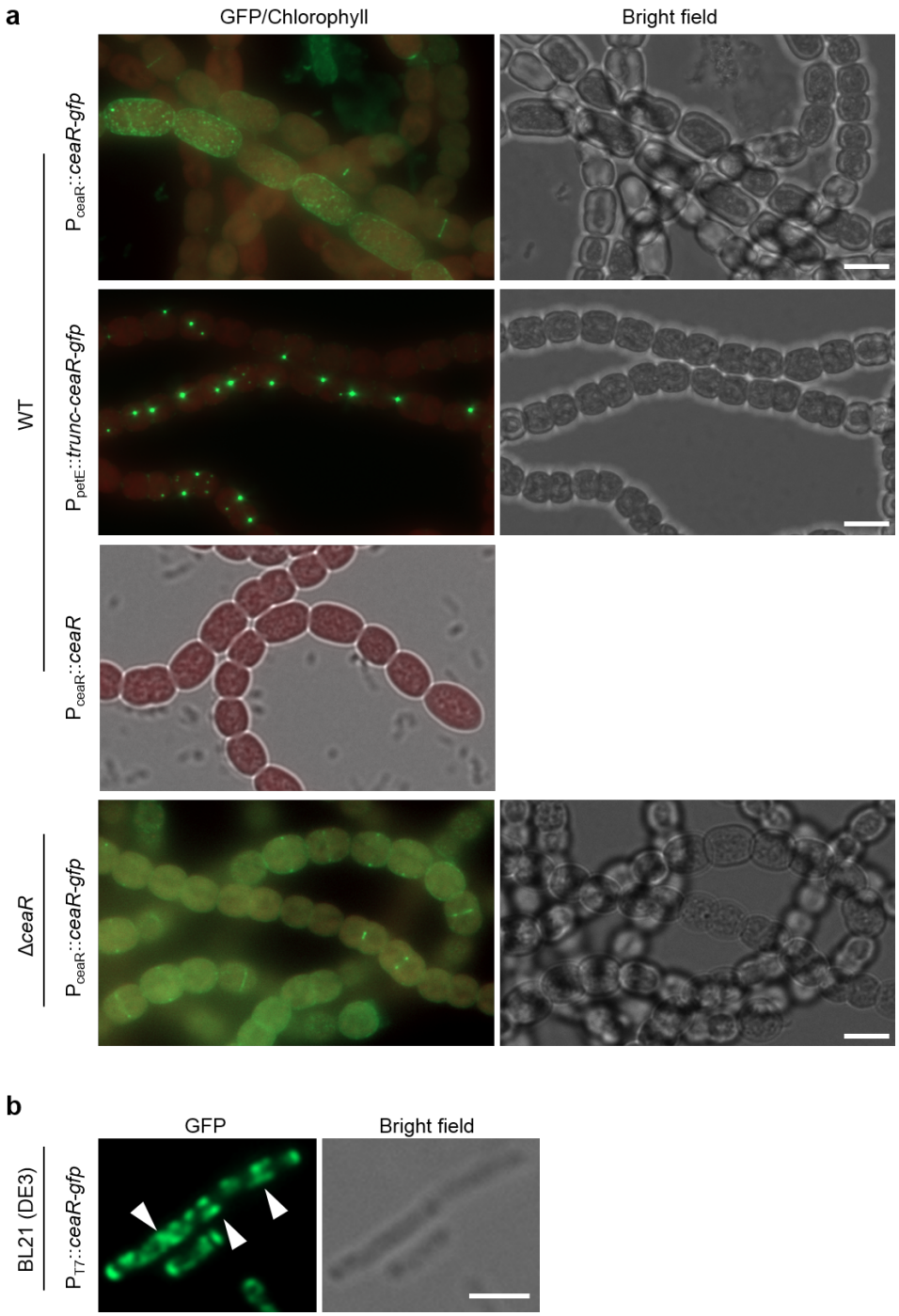

Supplementary Fig. 8: *In vivo* localization of CeaR-GFP in *Anabaena* and *E. coli*

(a) Merged GFP-fluorescence and chlorophyll autofluorescence and bright field micrographs of *Anabaena* WT or Δ*ceaR* mutant strain expressing CeaR-GFP, CeaR-GFP without the N-terminal transmembrane domain (first 52 aa removed; *trunc-ceaR*) or CeaR form P_{petE} or P_{ceaR}. Additional expression of CeaR-GFP from P_{ceaR} or P_{petE} and CeaR from P_{ceaR} induces a swollen cell phenotype. This phenomenon is not present upon expression of CeaR-GFP or CeaR (Supplementary Fig. 9a) from P_{ceaR} in the Δ*ceaR* mutant strain, indicating that *ceaR* expression or protein level is tightly regulated in *Anabaena* WT. Expression of truncated CeaR-GFP in *Anabaena* WT cells was induced for 1 d with 0.2 µM $CuSO_4$. Scale bars: 5 µm.

(b) GFP-fluorescence and bright field micrographs of *E. coli* BL21 (DE3) cells expressing CeaR-GFP. Cells were grown till an OD_{600} of 0.5 and induced for 48 h at 20 °C with 0.05 mM IPTG. White triangles indicate banded and helical localization of CeaR-GFP. Scale bar: 5 µm.

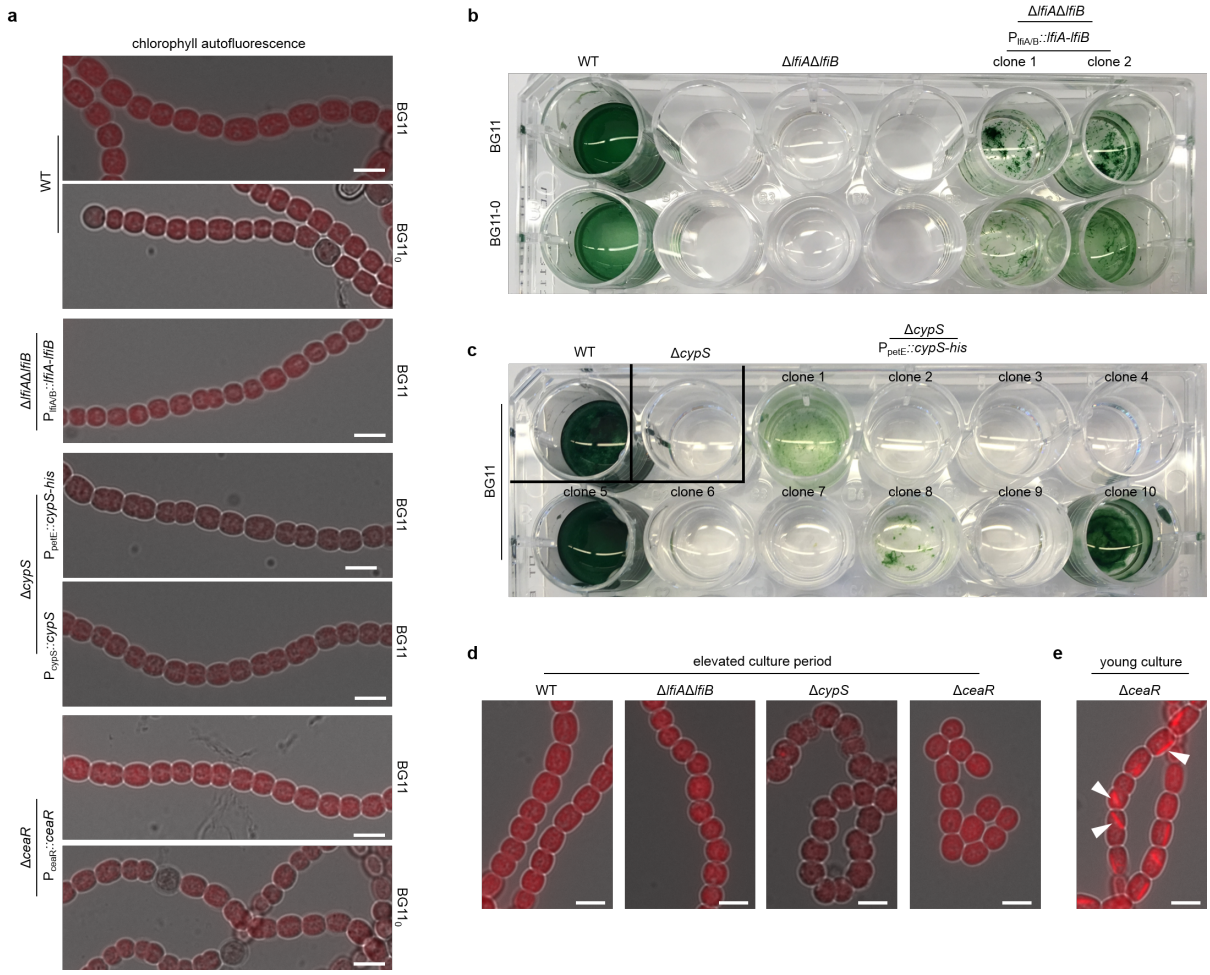

Supplementary Fig. 9: Mutant phenotype complementation and culture age-dependency of *Anabaena* mutant phenotypes

(a) Morphological complementation of *Anabaena* CCRP mutant strains as a result of native expression of *lfiA-lfiB*, *cypS* and *ceaR* from pRL25C. Notably, CypS-His expressed from P_{petE} also complemented the morphological defect of the Δ*cypS* mutant strain and rescues the linear *Anabaena* filament shape. The ability to complement the mutant phenotypes using the pRL25C plasmid shows that pDU1-based plasmids can be successfully employed to rescue WT phenotypes despite their variation in the relative copy number[100]. Scale bars: 5 µm.

(b,c) Complementation of (b) Δ*lfiA*Δ*lfiB* and (c) Δ*cypS* mutant strains by expressing *lfiA-lfiB* from $P_{lfiA/B}$ or *cypS-his* from P_{petE} from the replicative pRL25C plasmid. Note, not all tested clones successfully complemented the mutant growth defects in liquid culture, likely due to the phenotypic variation caused by the copy number variation of pRL25C[100,101].

(d) Merged bright field and chlorophyll autofluorescence micrographs of (a) *Anabaena* WT and Δ*lfiA*Δ*lfiB*, Δ*cypS* and Δ*ceaR* mutant strains grown on BG11 plates for an elevated time period (about 3 weeks) or (d) Δ*ceaR* mutant strain grown on BG11 plates for about one week. White triangles indicate red fluorescent filaments. Note: a decreased viability of the Δ*cypS* mutant strain is evident by a decreased chlorophyll autofluorescence signal. Scale bars: 5 µm.

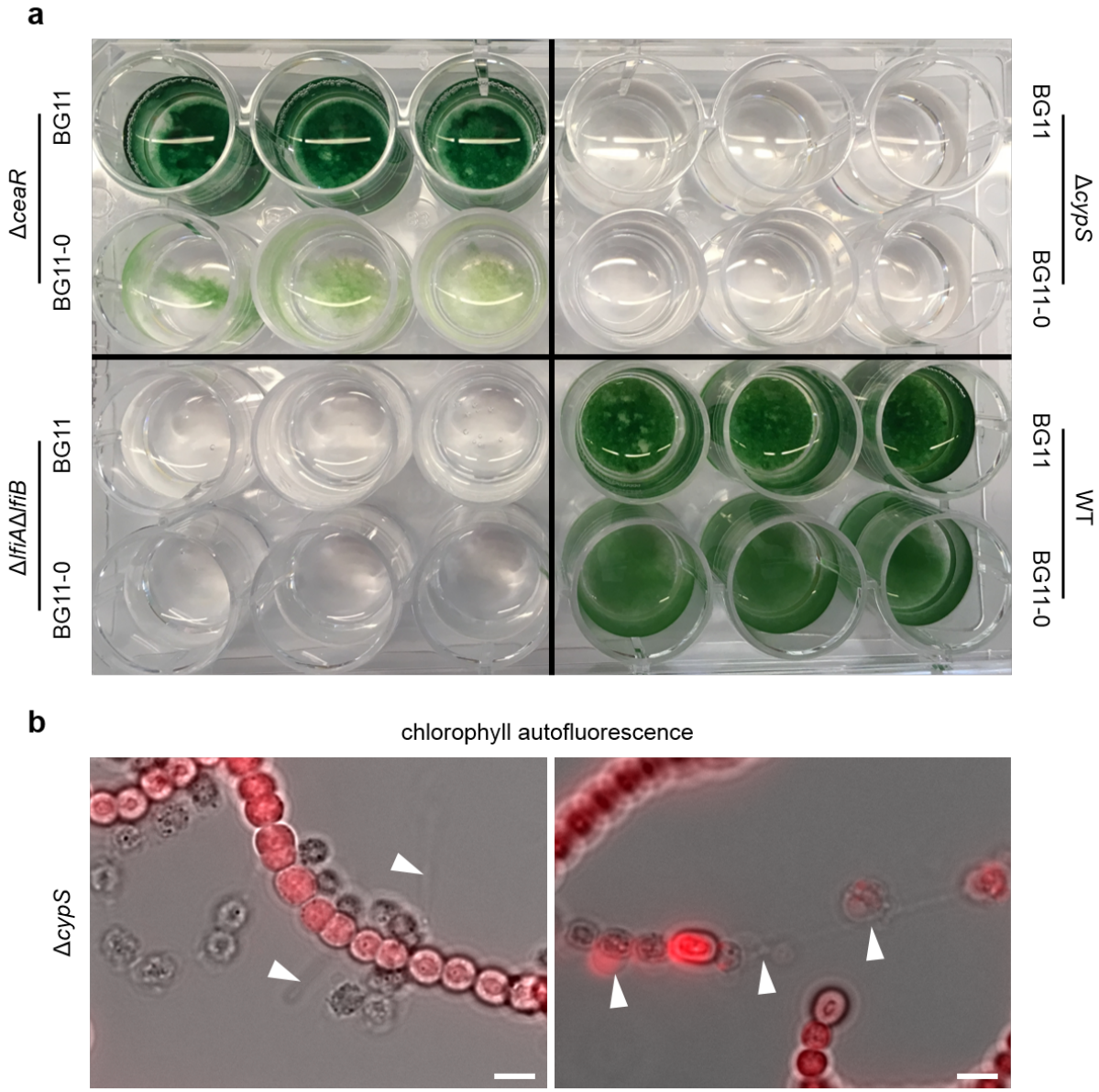

725

726 **Supplementary Fig. 10: *Anabaena* CCRP mutant strains show growth defects in liquid culture**

727 (a) *Anabaena* WT, Δ*cypS,* Δ*lfiA*Δ*lfiB* and Δ*ceaR* mutant strains were grown on BG11 plates, transferred to liquid
728 BG11 and $BG11_0$ medium and incubated for 12 d at standard growth conditions without shaking. The Δ*ceaR* mutant
729 strain can somewhat manage to survive in $BG11_0$ liquid medium without agitation. Nevertheless, prolonged
730 incubation usually led to cell death. On the contrary, Δ*ceaR* mutant cells are not viable when grown in liquid media
731 with agitation.

732 (b) Merged bright field and chlorophyll autofluorescence micrographs of Δ*cypS* mutant strain resuspended in BG11
733 liquid medium from BG11 plates. Cells were visualized immediately after transfer. White triangles indicate material
734 released from cells upon cell rupture. Scale bars: 5 µm.

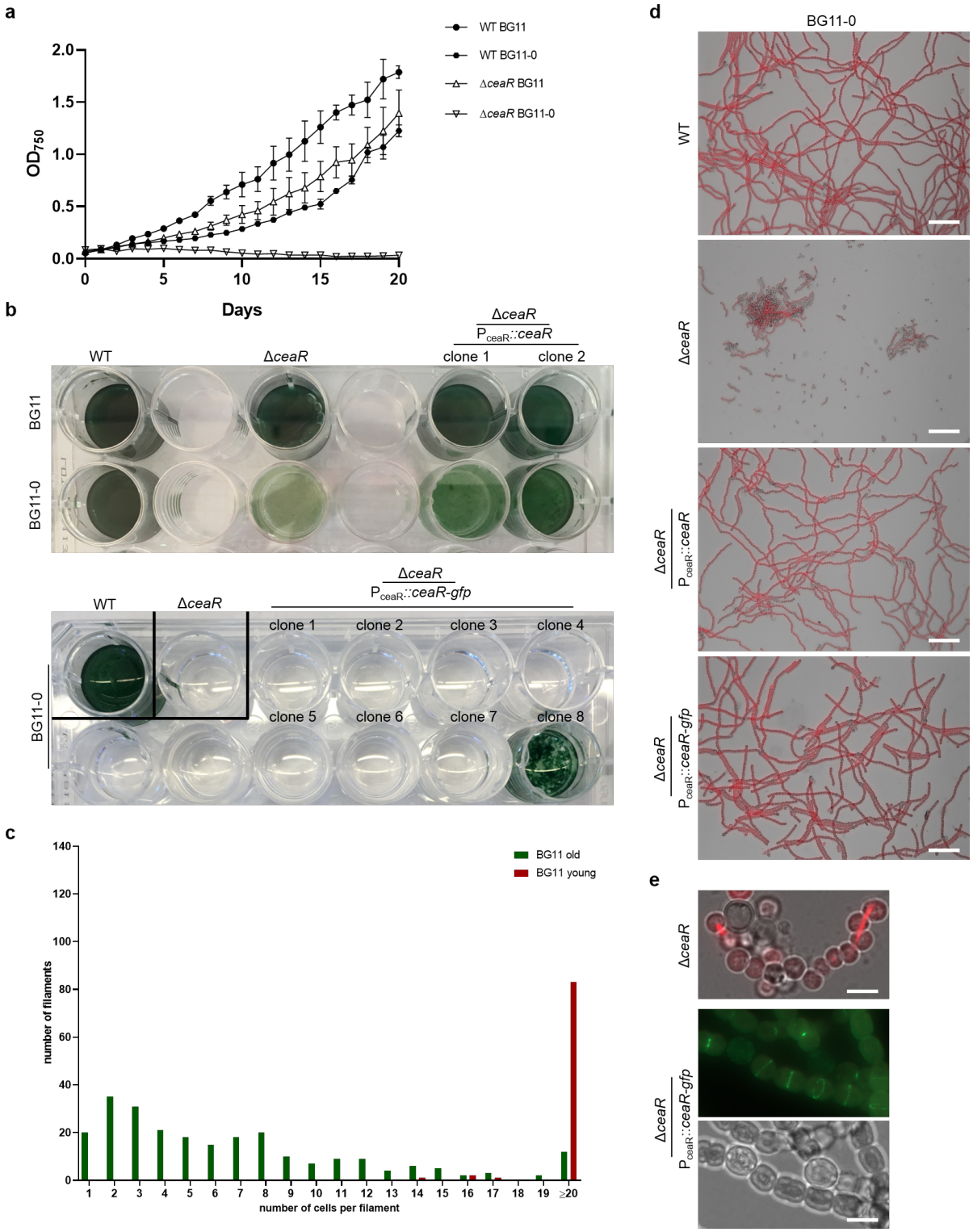

Supplementary Fig. 11: Fragmentation and decreased viability of the *ΔceaR* mutant strain

(a) *Anabaena* WT and Δ*ceaR* mutant strain were grown in BG11, washed three times in BG11 or $BG11_0$, adjusted to an OD_{750} of 0.1 and then grown in triplicates at standard growth conditions. OD_{750} values were recorded once a day for 20 d. Error bars show the standard deviation (n = 3).

(b) *Anabaena* WT grows in BG11 and $BG11_0$ while the Δ*ceaR* mutant strain only grows in BG11. Growth in $BG11_0$ can, however, be rescued using the pRL25C plasmid bearing P_{ceaR}::*ceaR* or P_{ceaR}::*ceaR-gfp*, showing that the CeaR-GFP fusion protein is active.

(c) Filament length (number of cells per filament) of Δ*ceaR* mutant strain from young and older cultures grown in BG11 liquid medium. Filament length of filaments with up to 19 cells were individually counted while filaments with with more than 20 cells are listed with ≥20.

(d) Merged bright field and chlorophyll autofluorescence micrographs of *Anabaena* WT, Δ*ceaR* mutant and the Δ*ceaR* mutant carrying a pRL25C plasmid bearing P_{ceaR}::*ceaR* or P_{ceaR}::*ceaR-gfp*. Micrographs show cells from Supplementary Fig. 11b 48 h after transfer to $BG11_0$. The Δ*ceaR* mutant fragments into short filaments that clump together with cells losing their chlorophyll auto-fluorescence signal. However, the Δ*ceaR* mutant fragmentation/aggregation can be fully complemented with a pRL25C plasmid bearing P_{ceaR}::*ceaR* or P_{ceaR}::*ceaR-gfp*.

(e) Micrographs of Δ*ceaR* mutant and Δ*ceaR* mutant expressing CeaR-GFP from P_{ceaR} on the pRL25C plasmid 48 h after transfer to $BG11_0$

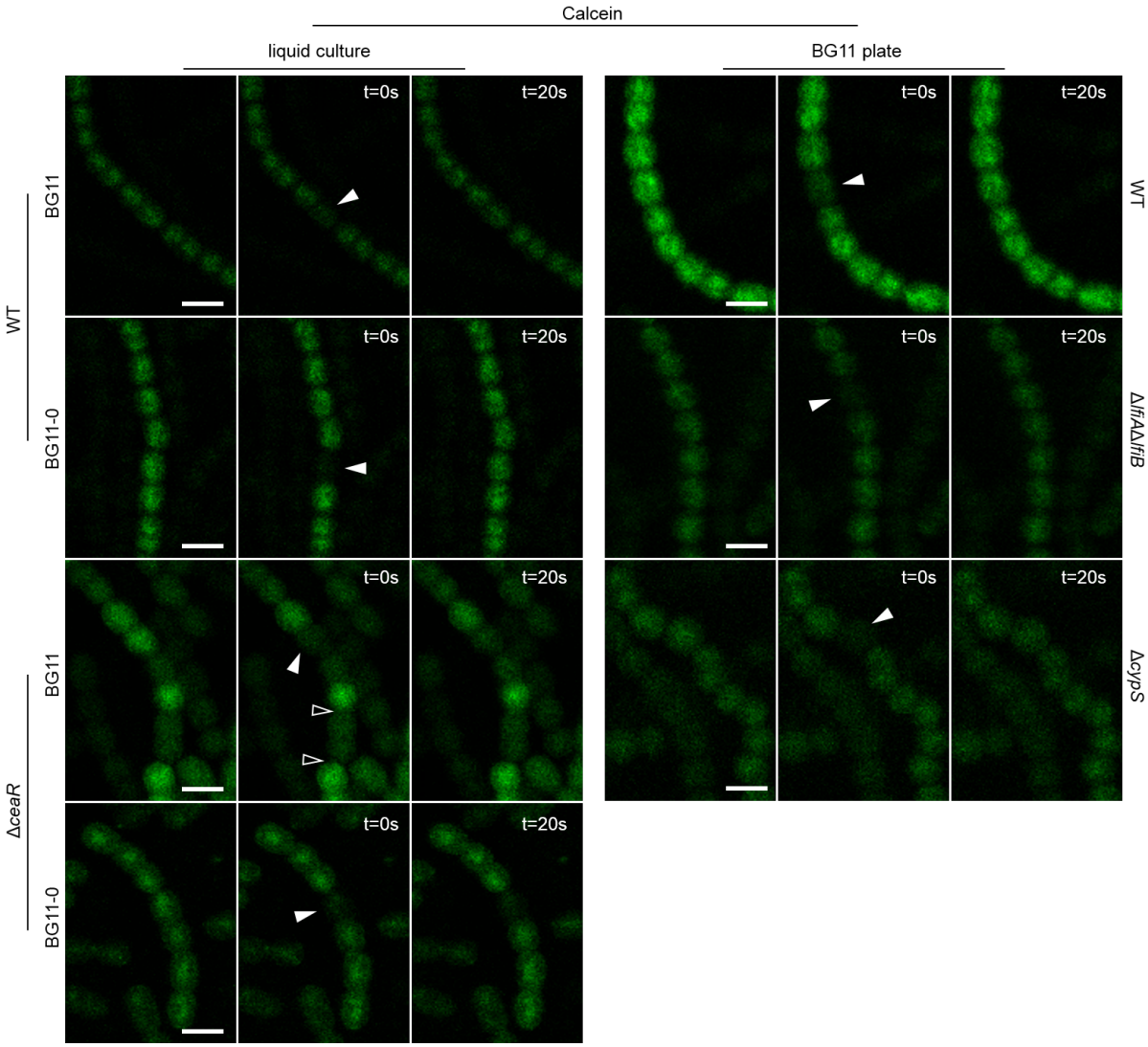

Supplementary Fig. 12: *Anabaena* CCRP mutant strains display defects in cell-cell solute diffusion

Representative calcein fluorescence micrographs depicting intercellular molecular exchange following laser-based bleaching of calcein fluorescence in *Anabaena* WT or Δ*ceaR* mutant strain grown in liquid BG11 and liquid $BG11_0$ as well as in *Anabaena* WT and Δ*lfiA*Δ*lfiB* and Δ*cypS* mutant strains grown on BG11 plates. White triangles indicate bleached cells. Translucent triangles show diffusion barriers present in the Δ*ceaR* mutant strain. Fluorescence images show respective cells prior bleaching, immediately after bleaching (t = 0) and after 20 seconds after bleaching (t = 20s). Images show representative examples. Scale bars: 5 µm.

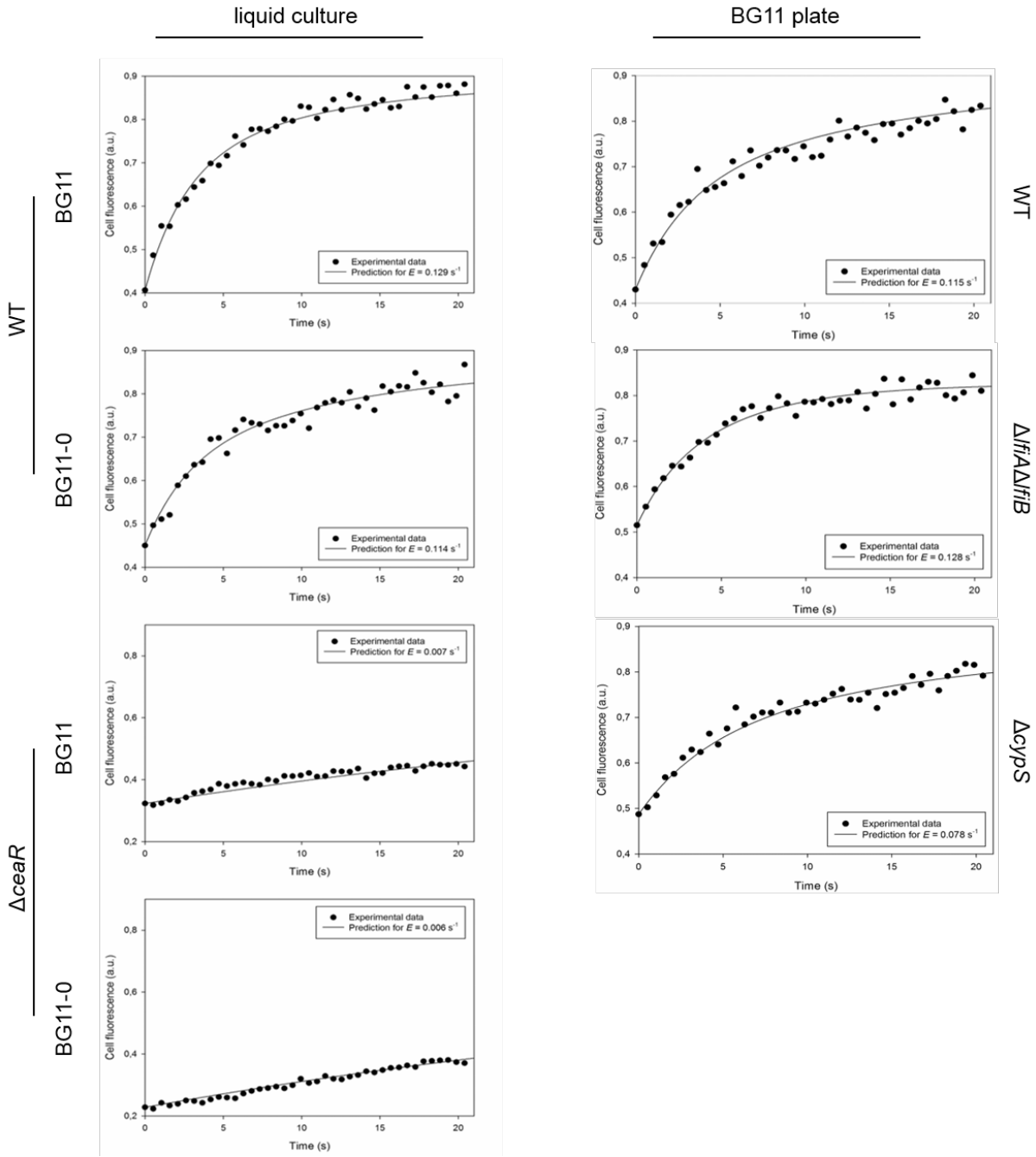

Supplementary Fig. 13: Exchange coefficients of FRAP assays

Fluorescence recovery curves with their predicted exchange coefficient values (*E*)[43] for selected bleached cells of *Anabaena* WT or Δ*ceaR* mutant strain grown in liquid BG11 and liquid $BG11_0$ as well as in *Anabaena* WT and Δ*lfiA*Δ*lfiB* and Δ*cypS* mutant strains grown on BG11 plates. Fluorescence values are given in arbitrary units (a.u.)[43] over a time course of 20 s post bleaching.

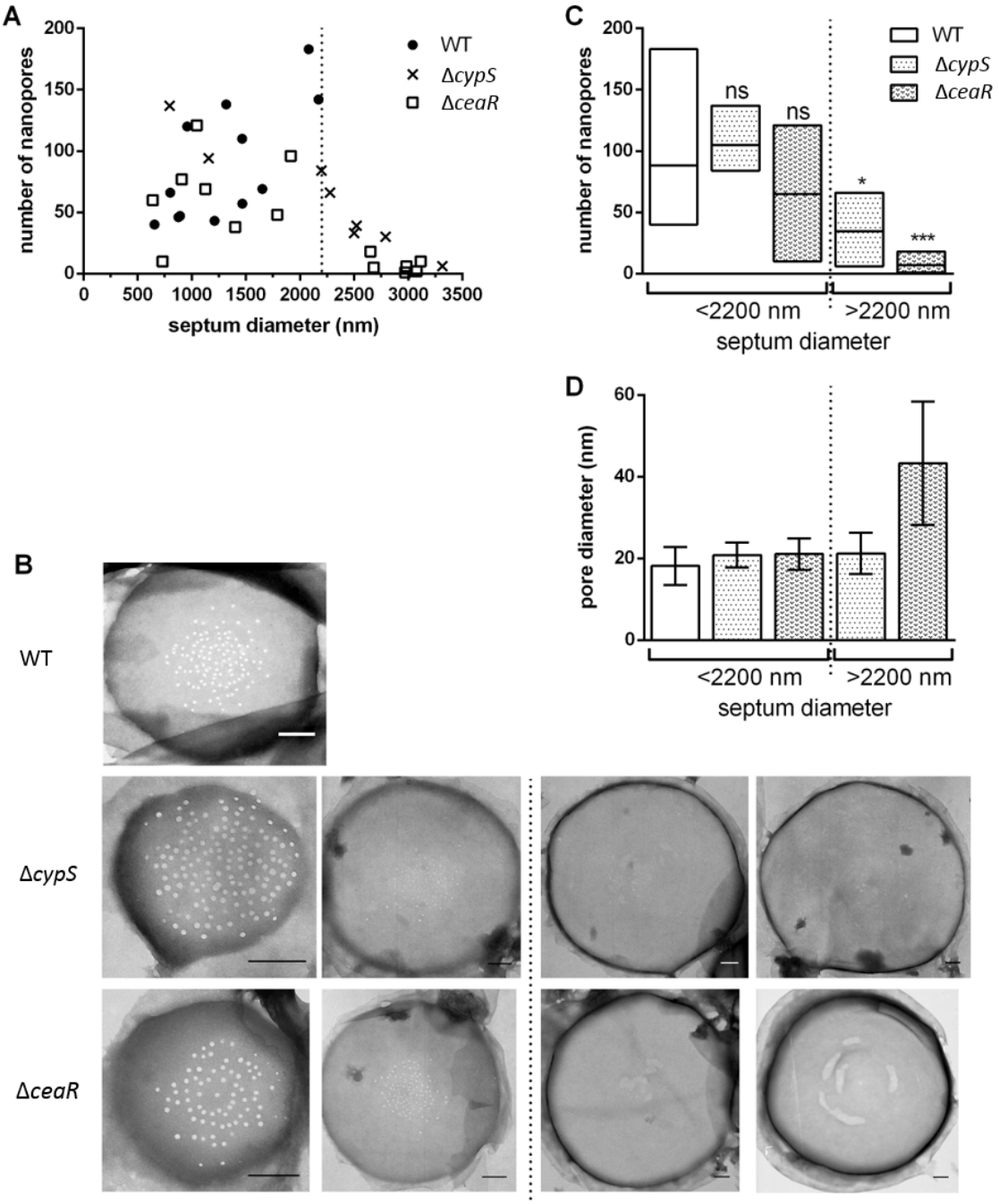

Supplementary Fig. 14: Septal nanopore array

(a) The number of nanopores is shown correlated to the septum size. In contrast to the WT, *Anabaena* CCRP mutants show a subset of large septa (>2200 nm) with few nanopores.

(b) Representative transmission electron microscopy images of indicated strains are shown. The dotted line divides the septa into a diameter of <2200 nm (left) and >2200 nm (right) derived from (a). Scale bars: 250 nm.

(c) Number of pores per septum (</> 2200 nm). Student's t-test (mutants vs. WT). P-values are indicated (ns: not significant, *P<0.05, ***P<0.001). P-values were calculated from the following number of septa: n (WT) = 12; n (Δ*cypS* <2200 nm) = 3; n (Δ*ceaR* <2200 nm) = 8; n (Δ*cypS* >2200 nm) = 5; n (Δ*ceaR* >2200 nm) = 6. WT data were derived from Bornikoel, *et al*[102].

(d) Nanopore diameter. Floating bars show the mean value from the number of analyzed nanopores. Sample size was n (WT) = 1061; n (Δ*cypS* <2200 nm) = 315; n (Δ*ceaR* <2200 nm) = 371; n (Δ*cypS* >2200 nm) = 174; n (Δ*ceaR* >2200 nm) = 42.

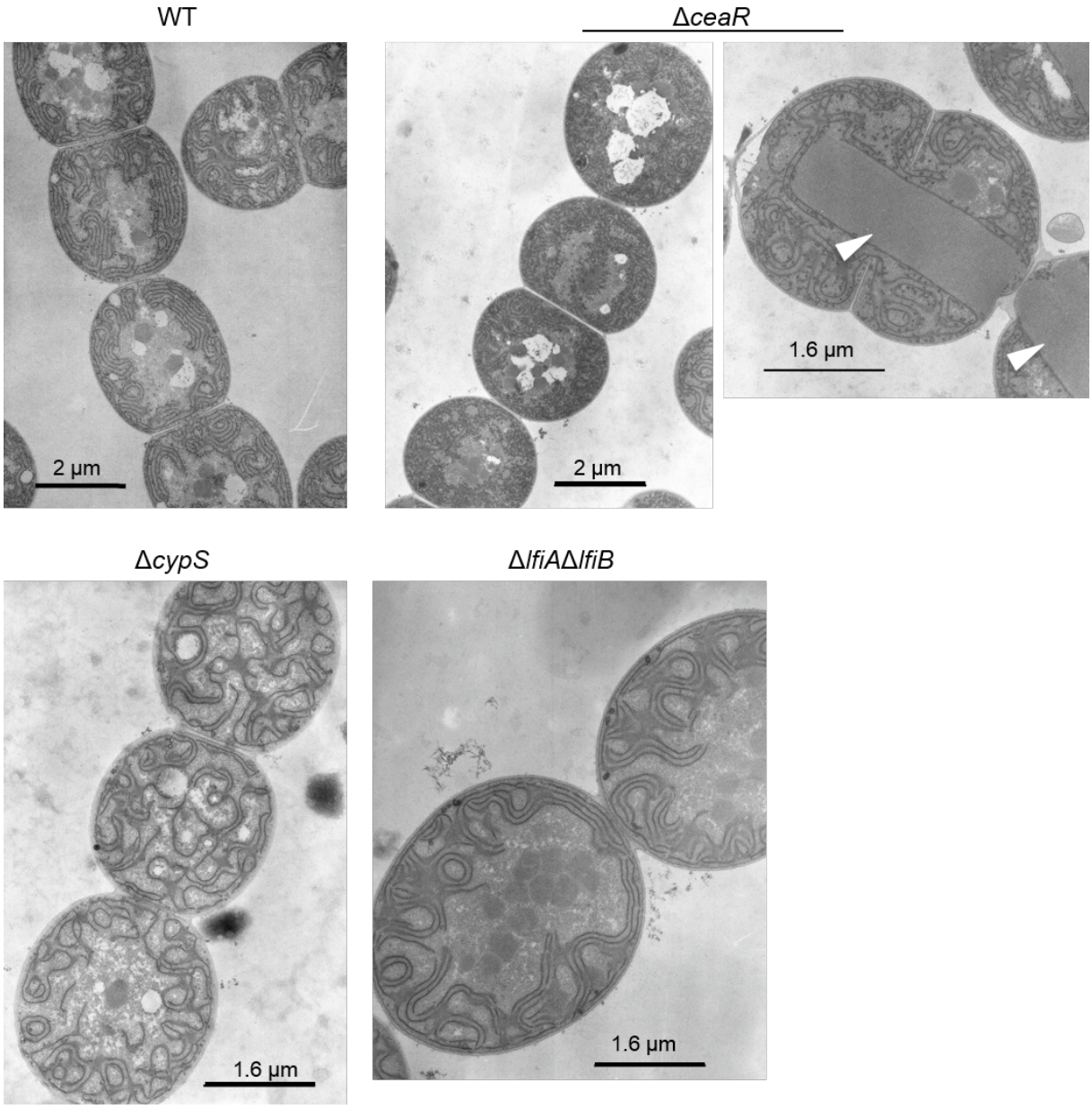

781

782 **Supplementary Fig. 15: Ultrastructure of *Anabaena* WT and CCRP mutant strains**

783 Ultrathin sections of *Anabaena* WT and *Anabaena* CCRP mutant strains grown on BG11 plates. White triangles indicate
784 unusual structures in the Δ*ceaR* mutant that coincide with the observed red fluorescent filaments in the Δ*ceaR* mutant
785 visualized by live cell fluorescence microscopy (Fig. 3d, Supplementary Fig. 9e).

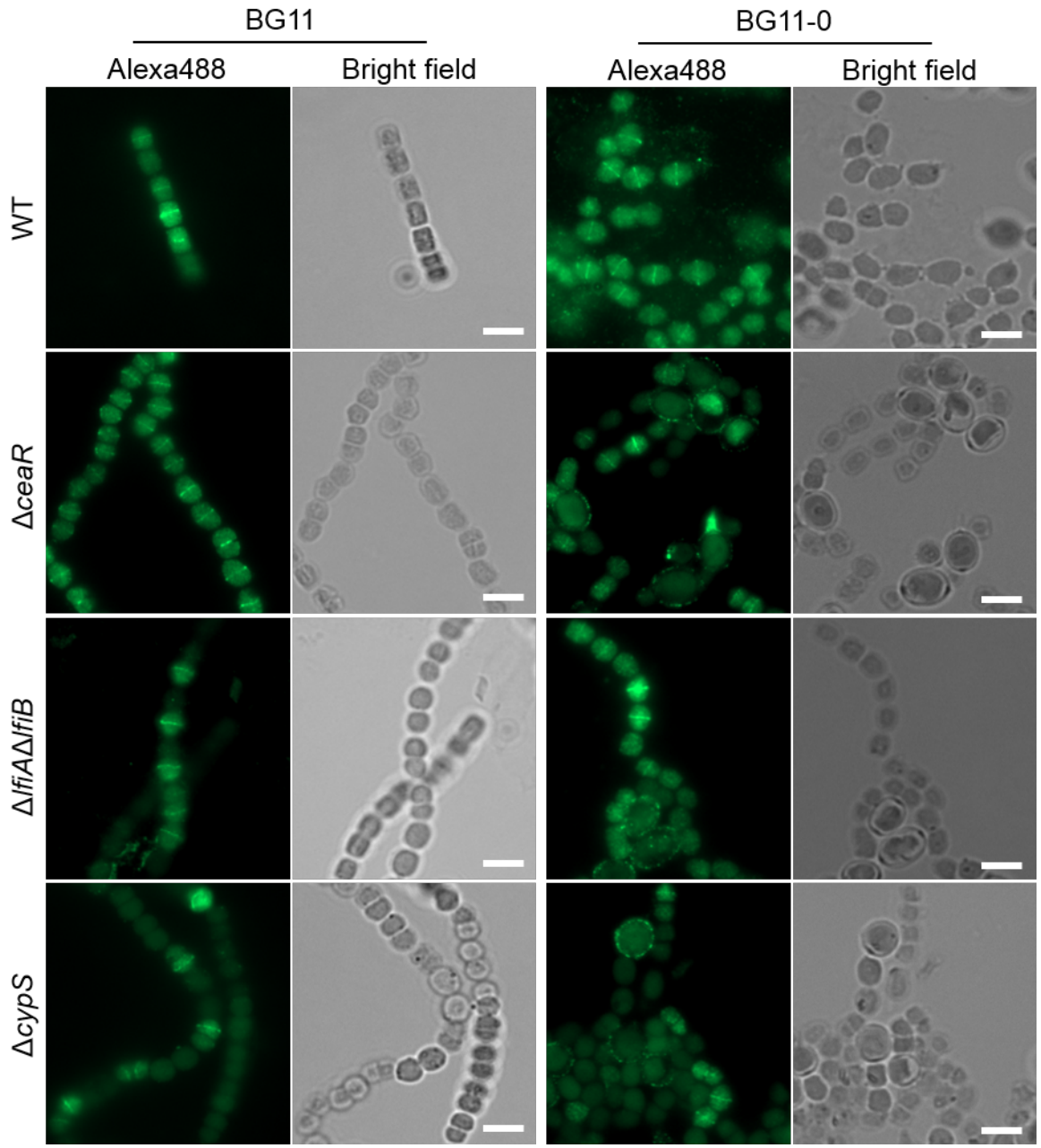

786

787 **Supplementary Fig. 16: FtsZ localization is unaffected in *Anabaena* CCRP mutant strains**

788 Alexa Flour-488 fluorescence and bright field micrographs of *Anabaena* WT and Δ*ceaR*, Δ*lfiA*Δ*lfiB* and Δ*cypS*
789 mutant strains grown on BG11 or $BG11_0$ growth plates. Cells were subjected to immunofluorescence staining using
790 anti-FtsZ primary antibody and Alexa Fluor-488 coated secondary antibody essentially as described by Ramos-
791 León *et al.*[82]. Cells were mounted in ProLong Diamond antifade mountant (Thermo Fischer Scientific). Scale bars:
792 5 µm.

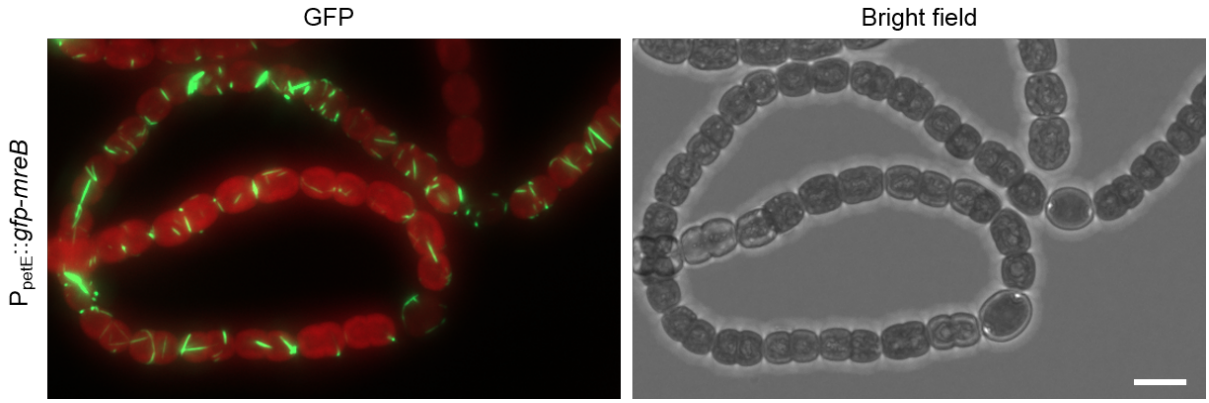

Supplementary Fig. 17: GFP-MreB forms extensive filaments in *Anabaena* WT

Merged GFP fluorescence and chlorophyll autofluorescence and bright field micrographs of *Anabaena* WT expressing GFP-MreB from P_{petE}. Cells were grown on $BG11_0$ growth plates. Maximum intensity projections of a Z-stack. Scale bar: 5 µm.

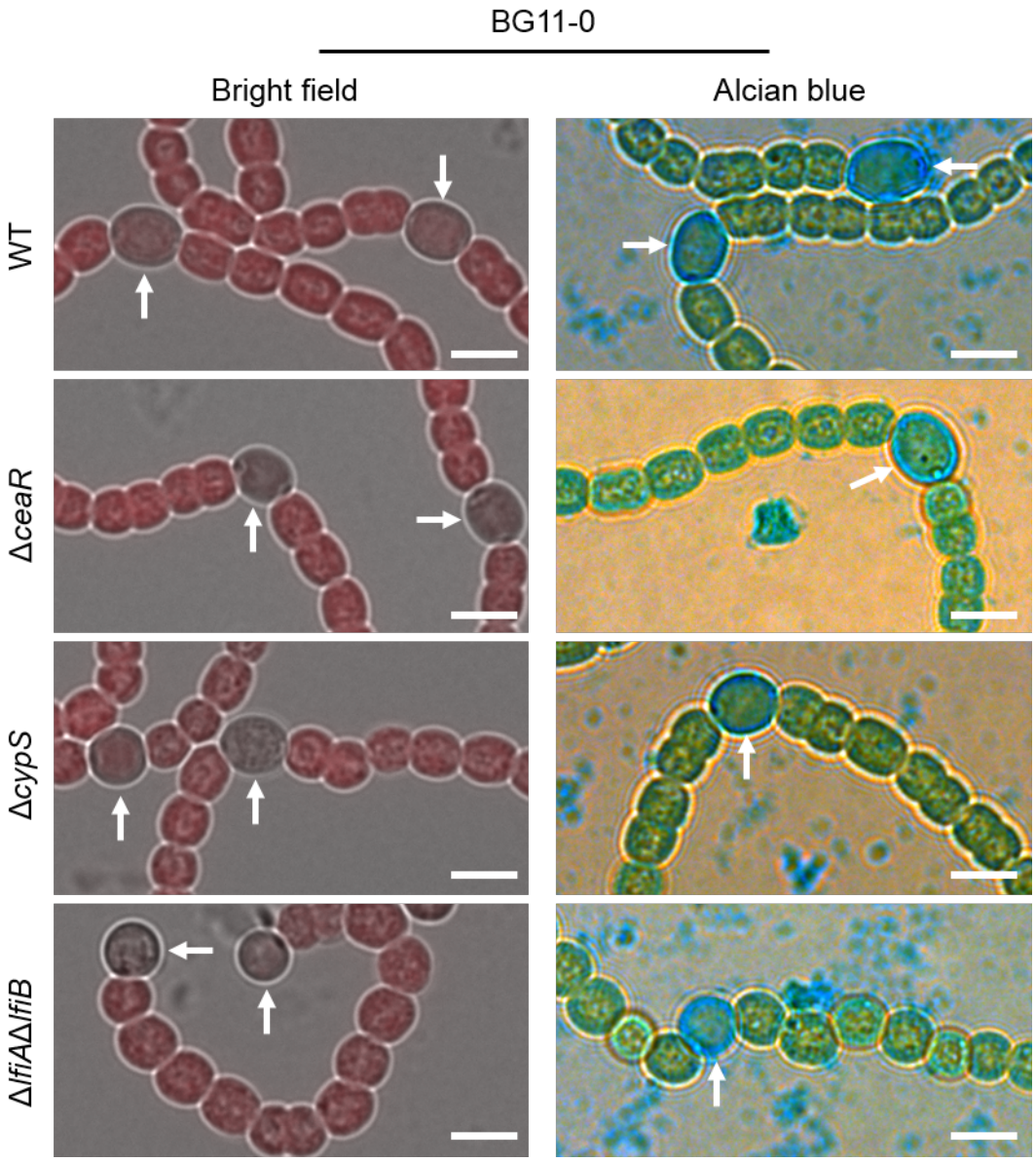

Supplementary Fig. 18: Alcian blue staining is unaltered in *Anabaena* CCRP mutant strains

Bright field micrographs of *Anabaena* WT and Δ*ceaR*, Δ*lfiA*Δ*lfiB* and Δ*cypS* mutant strains grown on $BG11_0$ plates. Cells were either observed directly by bright field microscopy or previously stained with 0.5% alcian blue (final concentration). Heterocysts are indicated by white arrows. Scale bars: 5 µm.

803

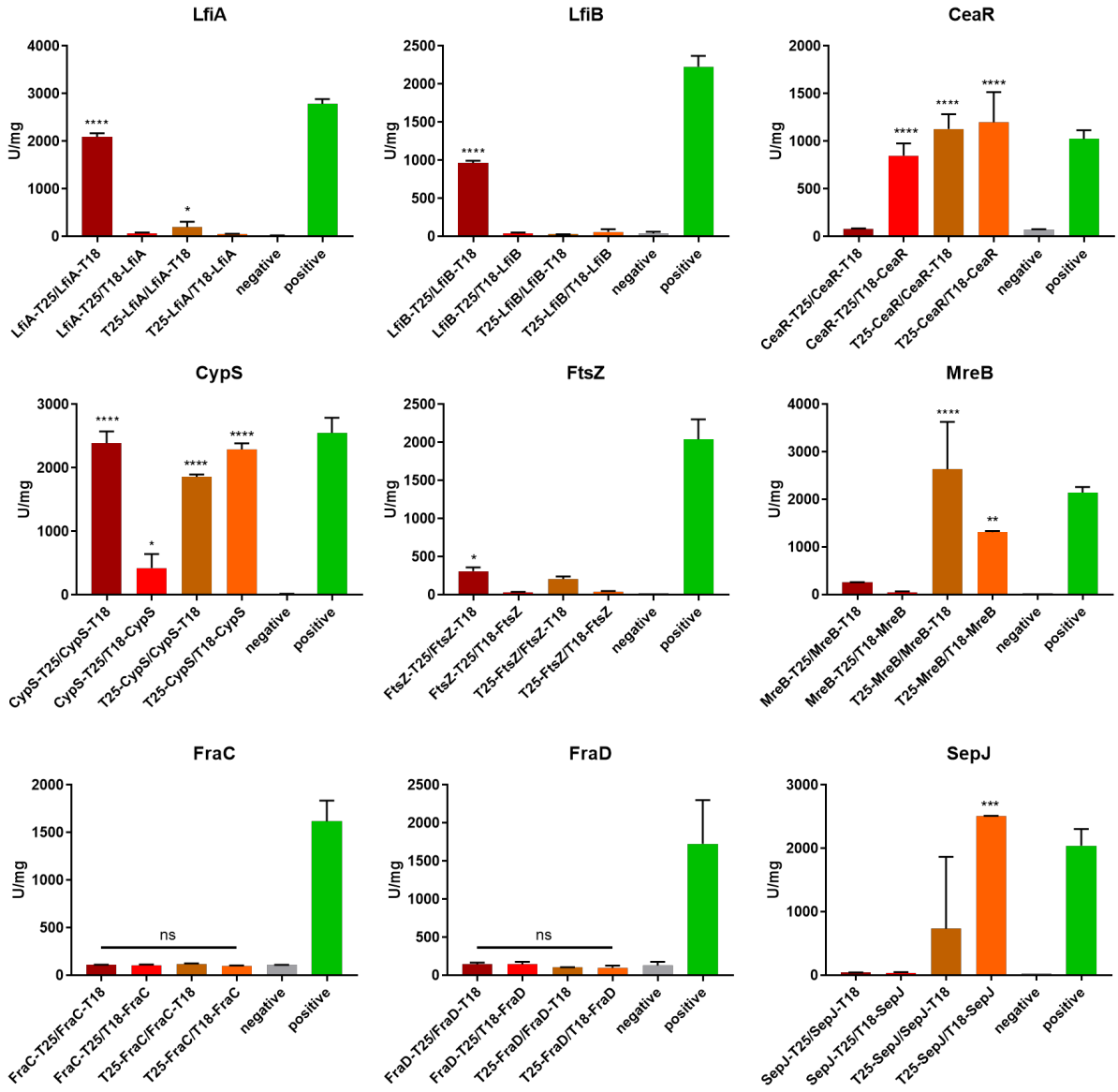

804

805 Figure description follows on page 47.

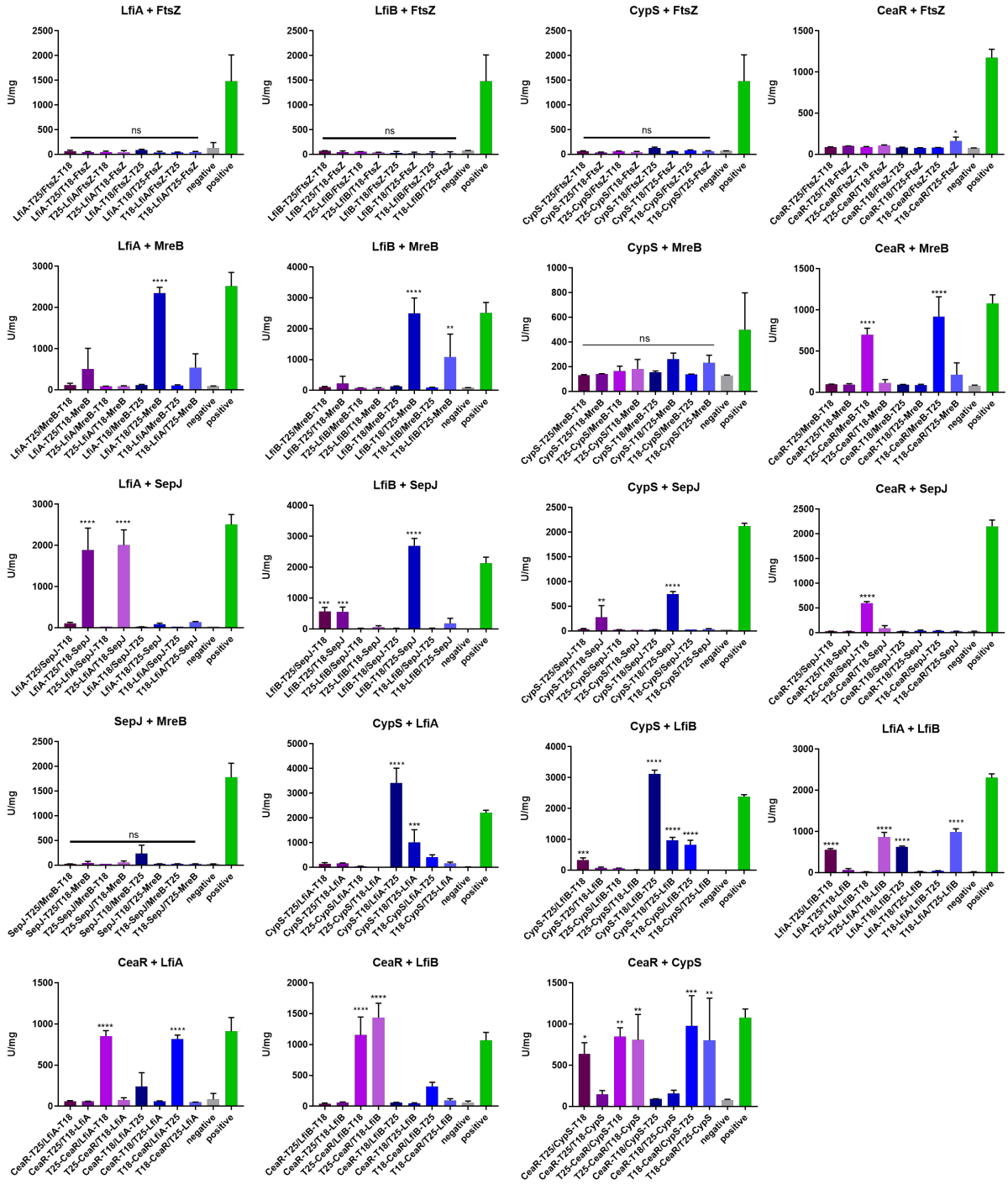

Figure description follows on page 47.

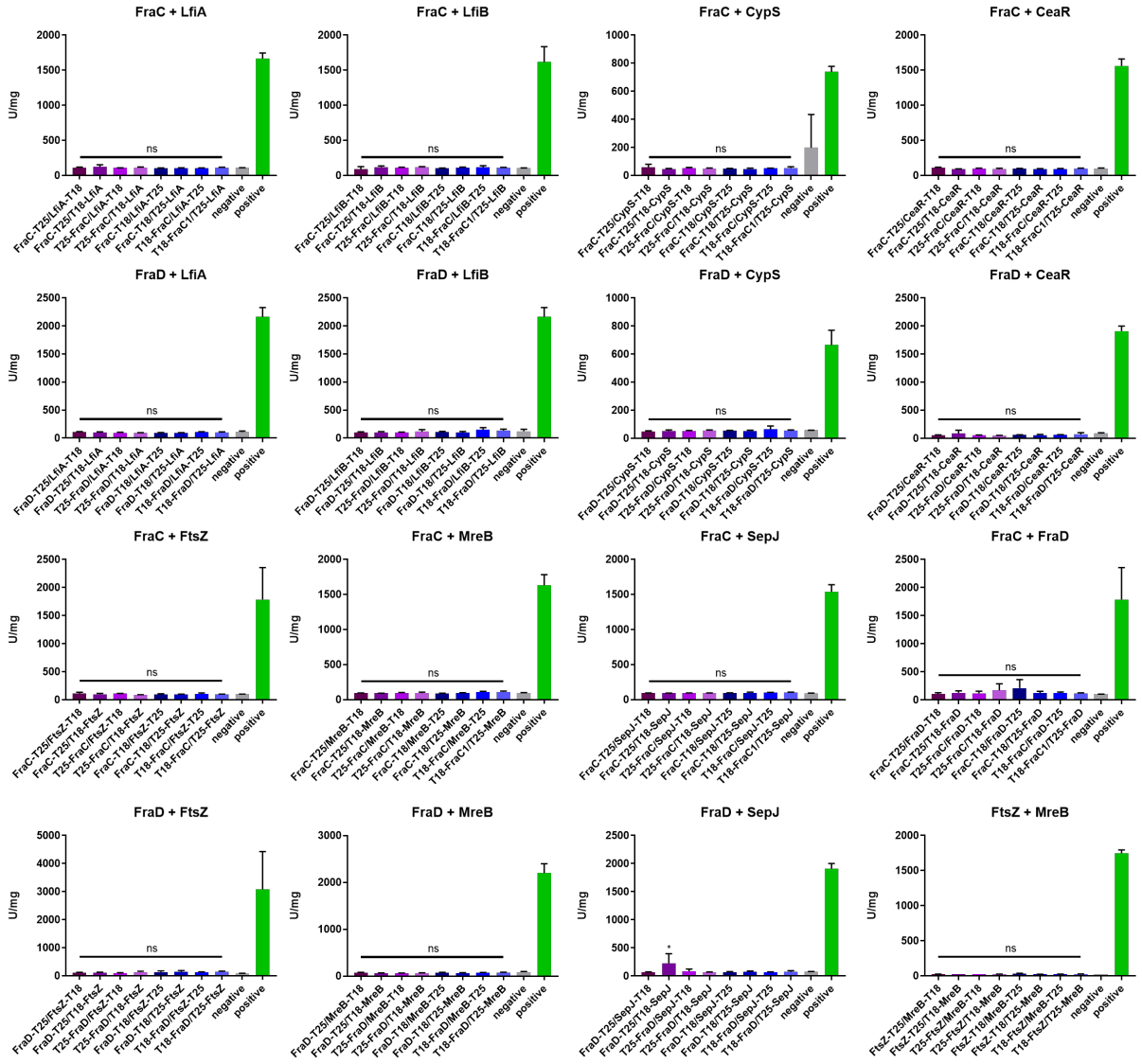

Supplementary Fig. 19: *Anabaena* possess a complex cytoskeletal network that is linked to a septal junction protein

Beta-galactosidase assays of *E. coli* BTH101 cells co-expressing indicated T25 and T18 translational fusions of all possible pair-wise combinations. *E. coli* cells carrying the respective plasmids were subjected to beta-galactosidase assay as described by Karimova *et al.*[103] in triplicates from three independent colonies grown for 2 d at 20 °C. Quantity values are given in Miller Units per milligram LacZ of the mean results from three independent colonies. Negative: N-terminal T25 fusion construct of the respective protein co-transformed with empty pUT18C. Positive: Zip/Zip control. Error bars indicate standard deviations (n = 3). *: P < 0.05, **: P < 0.01, ***: P < 0.001, ****: P < 0.0001 (Dunnett's multiple comparison test and one-way ANOVA).

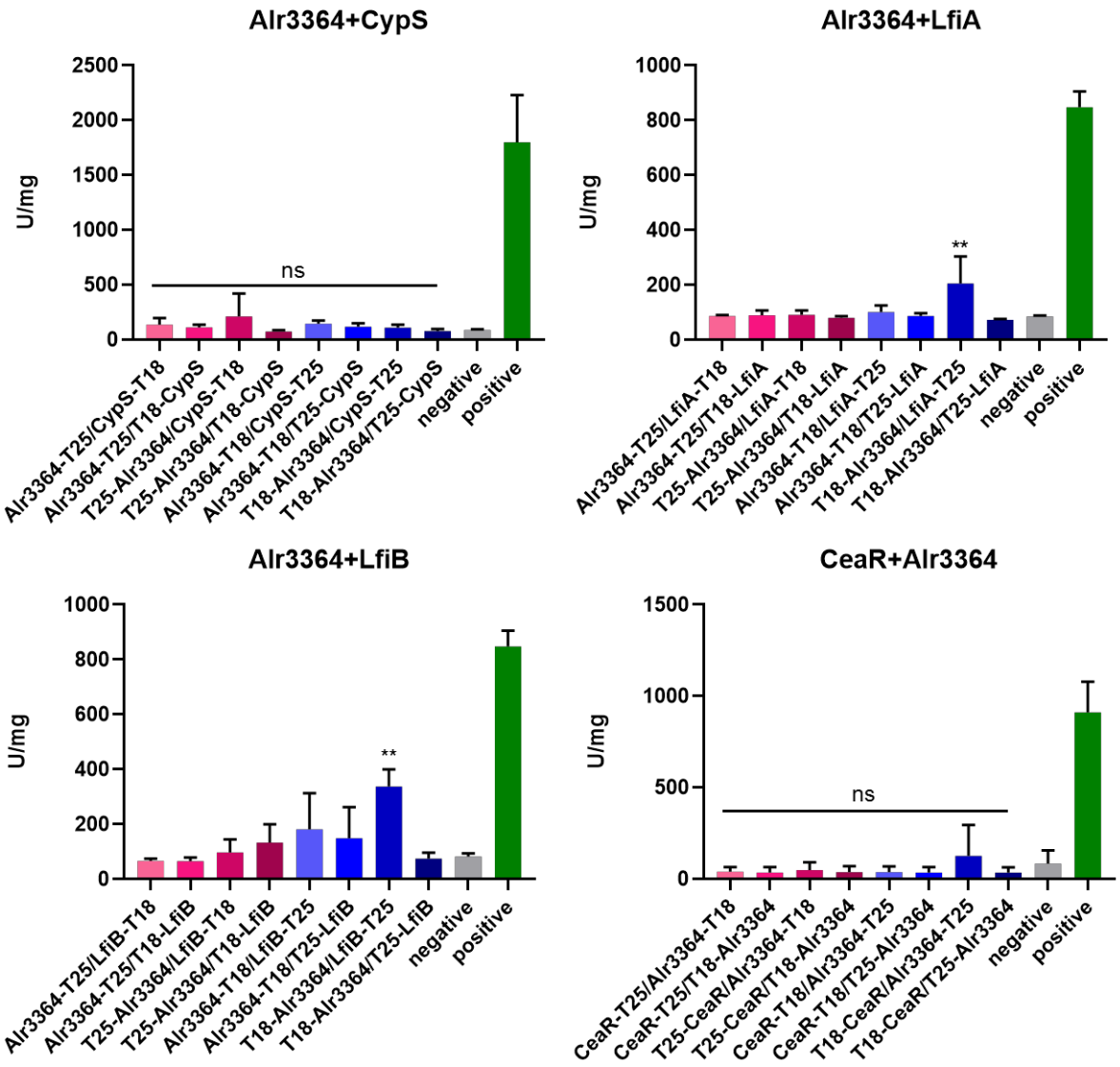

Supplementary Fig. 20: Interaction of *Anabaena* IF-like CCRPs is specific in a bacterial two hybrid system

Beta-galactosidase assays of *E. coli* BTH101 cells co-expressing indicated T25 and T18 translational fusions of all possible pair-wise combinations. *E. coli* cells carrying the respective plasmids were subjected to beta-galactosidase assay as described by Karimova *et al.*[103] in triplicates from three independent colonies grown for 2 d at 20 °C. Quantity values are given in Miller Units per milligram LacZ of the mean results from three independent colonies. Negative: N-terminal T25 fusion construct of the respective protein co-transformed with empty pUT18C. Positive: Zip/Zip control. Error bars indicate standard deviations (n = 3). Values indicated with * are significantly different from the WT. **: $P < 0.01$ (Dunnett's multiple comparison test and one-way ANOVA).

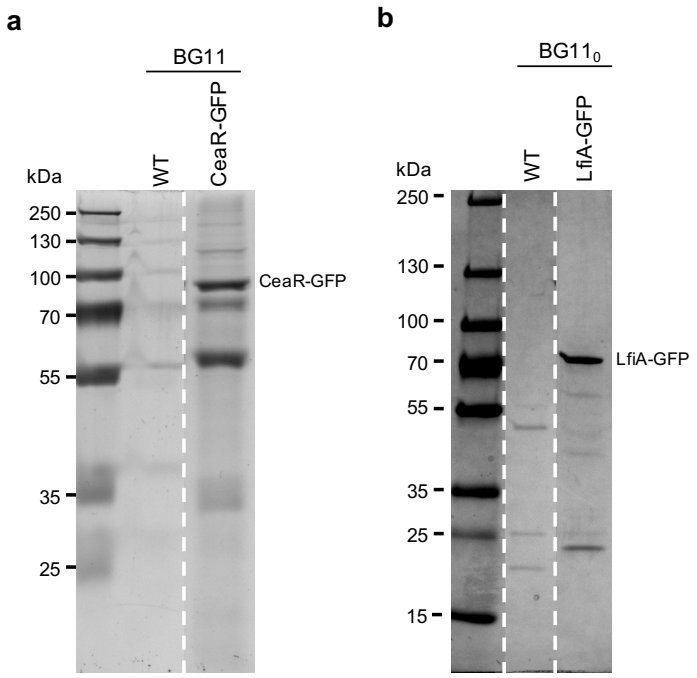

c

CeaR-GFP	LfiA-GFP
All4981	LfiB
MreB	MreB
ParA	ParA
MinD	
SepJ	
All2981 (PBP1a)	
All2952 (PBP1a)	
Alr0718 (PBP2)	
Alr3365	
Alr4550 (S-layer protein)	

PBP: Penicillin-binding protein

827

828 **Supplementary Fig. 21: Identification of proteins interacting with *Anabaena* CCRPs**

829 (a,b) Cell-free extracts of *Anabaena* WT expressing (a) CeaR-GFP or (b) LfiA-GFP from P_{petE} were subjected to co-
830 immunoprecipitation using anti-GFP magnetic beads (μMACS GFP isolation Kit; Miltenyi Biotec). CeaR-GFP-
831 expressing cells were grown in BG11 without copper and protein expression was induced for 1 d with 0.5 μM $CuSO_4$.
832 LfiA-GFP expressing cells were grown in $BG11_0$ without copper and protein expression was induced for 5 d with
833 0.5 μM $CuSO_4$. *Anabaena* WT cells were grown in BG11 and $BG11_0$ supplemented with 0.5 μM $CuSO_4$ for 1 or
834 5 d, respectively. Cells were lysed in PBS-N and pooled duplicates of precipitated proteins of two independent
835 experiments were analyzed by mass spectrometry and 25 μl of the co-precipitate were resolved in a (a) 10% SDS-
836 polyacrylamide gel or in a (b) 4-15% TGX precast gel (Bio-Rad) and detected by Quick Coomassie stain (Serva).

837 (c) Excerpt of the identified specific interactors of CeaR-GFP and LfiA-GFP. The full list is listed in Supplementary
838 File 3. Notably, CeaR directly interacts with All4981, another filament forming protein in *Anabaena* (covered in a
839 separate report) as well as Alr3365 that lies directly downstream of *alr3364* in the *Anabaena* genome, which we
840 also identified in our screening for CCRPs in *Anabaena* (Supplementary Fig. 1). Both, CeaR and LfiA, interact with
841 ParA, hinting for a putative role in chromosome or plasmid segregation in *Anabaena*.

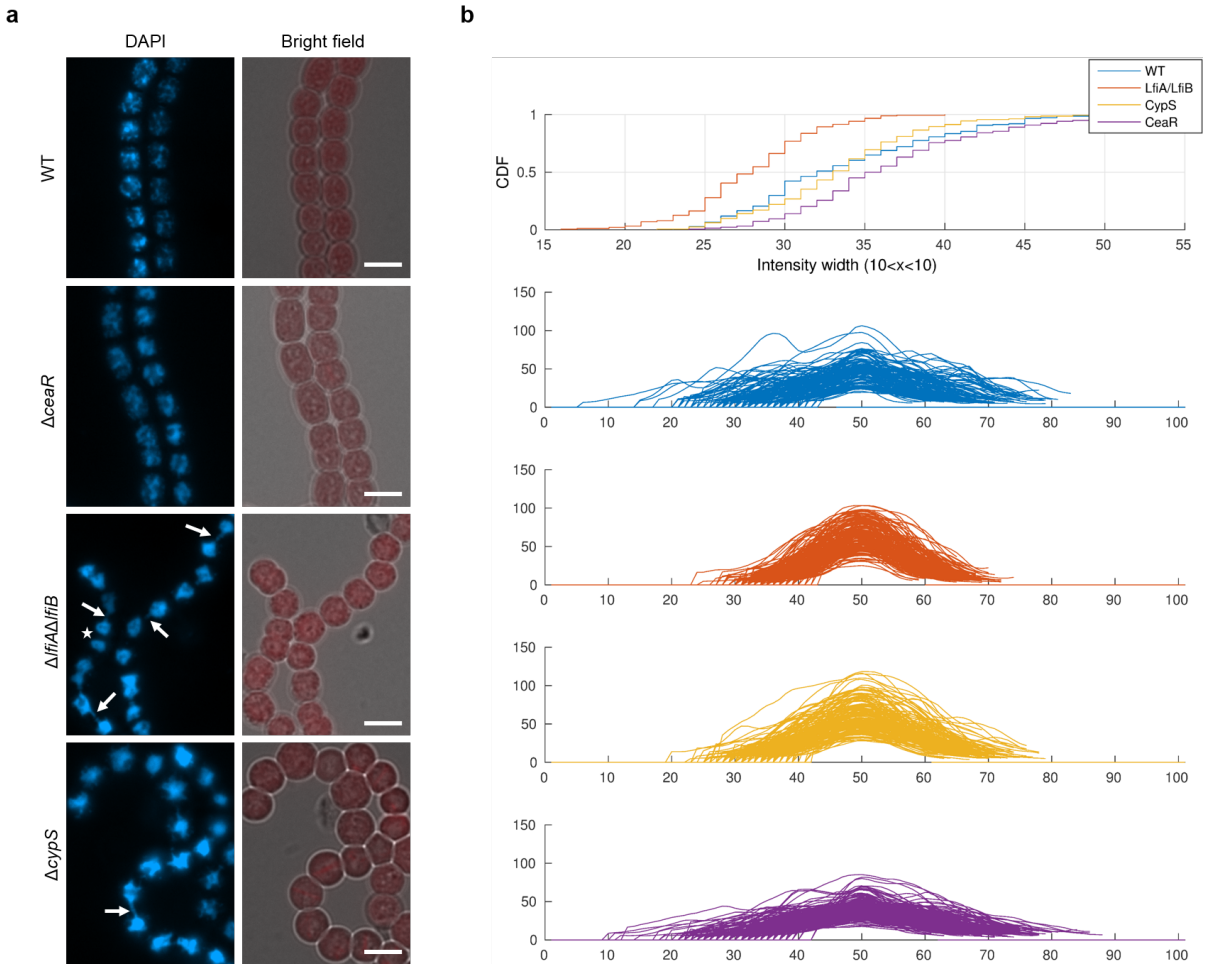

842

843 **Supplementary Fig. 22: Condensation of intracellular DNA in Anabaena CCRPs**

844 (a) DAPI fluorescence and merged bright field and chlorophyll autofluorescence micrographs of *Anabaena* WT and
845 Δ*ceaR*, Δ*lfiA*Δ*lfiB* and Δ*cypS* mutant strains grown on BG11 growth plates. Cells were resuspended in BG11 and
846 incubated with 10 µg ml^{-1} DAPI (final concentration). White arrows indicate strings of DNA that traverse from one
847 cell to the other. Notably, no such strings are observed in dividing cells (white star), suggesting that it is an effect
848 that occurs after complete cell division. Scale bars: 5 µm.

849 (b) Plot profile showing the DAPI signal intensities of pixels (grey value) along *Anabaena* WT and *Anabaena* mutant
850 cells (n =151 for each strain) in arbitrary units (a.u.) and arranged to the respective peak maxima. The focal area
851 size in the Δ*lfiA*Δ*lfiB* mutant was smallest in comparison to the other strains, Δ*ceaR* was larger than the others, and
852 the area size in WT was not significantly different than Δ*cypS* (alpha=0.05, using Tukey test). Notably, the
853 comparison of cell size among the strains reveals a similar result: the Δ*lfiA*Δ*lfiB* mutant cell size was smallest in
854 comparison to the other strains, Δ*ceaR* was larger than the others, and the area size in WT was not significantly
855 different than the Δ*cypS* mutant ($P=1.75x10^{-54}$, using Kruskal-wallis; alpha=0.05, using Tukey test). Consequently,
856 we compared the area of the focal DAPI staining decided by the cell size among the strains. This reveals that this
857 ratio is smallest in Δ*ceaR*, largest in Δ*cypS* and not significantly different between Δ*lfiA*Δ*lfiB* and the WT.

Supplementary Table 1: Characteristics of protein candidates

Locus tag	Genus	Subsection	Homolog distribution	Predicted proteins of similar structure (I-TASSER)	Conserved domains	Others
crescentin	*C. crescentus*	n/a	n/a	Cytoplasmic domain of bacterial cell division protein EzrA	SMC_N, CCDC158	Validated IF-like protein[86,107–109]
cypS (*alr0931*)	*Anabaena*	IV	I, II, III, IV, V	Cytoplasmic domain of bacterial cell division protein EzrA	SMC_N, CCDC158 DUF3084, Neuromodulin_N	
all4981	*Anabaena*	IV	III, IV, V	TTC7B/Hyccin Complex or Clathrin coat	TPR	4 bp overlap to *all4982*
lfiA (*alr4504*)	*Anabaena*	IV	I, II, III, IV, V	Spectrin repeats 7, 8, and 9 of the plakin domain of plectin	SMC_N	*lfiB* localized downstream of *lfiA*
lfiB (*alr4505*)	*Anabaena*	IV	I, II, III, IV, V	Cytoplasmic domain of bacterial cell division protein EzrA	SMC_N, DUF3552	
ceaR (*all2460*)	*Anabaena*	IV	III, IV, V	Cytoplasmic domain of bacterial cell division protein EzrA	SMC_N, TerB_C, CALCOCO1, Spc7	Two N-terminal TMHs
alr0347	*Anabaena*	IV	I, II, III, IV, V	*Bacillus subtilis* Smc coiled-coil middle fragment	Filament superfamily	
alr3364	*Anabaena*	IV	II, III, IV, V	Cytoplasmic domain of bacterial cell division protein EzrA	SMC_N, FtsK, DUF4696	
all8023	*Anabaena*	IV	IV	Human ATR-ATRIP complex	SMC_N, Pentapeptide, Yjbl	
alr4393	*Anabaena*	IV	I, II, III, IV, V	Cytoplasmic domain of bacterial cell division protein EzrA	SMC_N, DUF3084	
alr4911	*Anabaena*	IV	I, II, III, IV, V	Structure of the Smc head domain with a coiled coil and joint derived from *Pyrococcus yayanosii*	SMC_N, P-loop_NTPase DNA_S_dndD, Spc7, SbcC	
all4935	*Anabaena*	IV	IV	Cytoplasmic domain of bacterial cell division protein EzrA	DUF4114, DUF3084	
alr2043	*Anabaena*	IV	IV, V	Human ATR-ATRIP complex (replication stress response)	SMC_N, Tubulin_2	
alr3988	*Anabaena*	IV	I, II, III, IV, V	Two dynein tail domains bound to dynactin and BICDR1	SMC_N, SbcC	

The first column indicates the respective locus tags of protein candidates and Crescentin. The second and third column indicate the respective subsection of the corresponding genus according to Rippka *et al.* (1979)[36]. Column four lists the subsections that contain homologous proteins to the respective candidate. Column five contains proteins predicted to be structurally similar to the protein candidates in the PDB (Protein Data Bank) based on I-TASSER[104–106]. The sixth column indicates predicted sub-domains of protein candidates identified by BLAST CDS. Column seven states other features of interest. Abbreviations: (TMH) Transmembrane helix; (DUF) Domain of unknown function; (CCDC158) Coiled-coil domain-containing protein 158; (SMC) Structural maintenance of chromosomes; (SbcC) DNA repair exonuclease SbcCD ATPase; (CALCOCO1) Calcium binding and coiled-coil domain; (TRP): Tetratricopeptide repeat; (Spc7) Spc7 kinetochore protein; (TerB_C) TerB-C occurs C-terminal of TerB in TerB-N containing proteins, putative metal chelating; (Filament superfamily) Intermediate filament protein; (FtsK) DNA segregation ATPase FtsK; (Pentapeptide) Pentapeptide repeats often found in many cyanobacterial proteins with unknown function (predicted to be a β-helix); (Yjbl) Uncharacterized protein containing pentapeptide repeats; (DNA_S_dndD) DNA sulfur modification protein DndD; (Tubulin_2 superfamily) Tubulin like; Many of the residues conserved in Tubulin (pfam00091) are also conserved in this family; (P-loop_NTPase) P-loop containing Nucleoside Triphosphate Hydrolases superfamily. n/a: not applicable.

Material and methods

Bacterial strains and growth conditions

Anabaena WT was obtained from the Pasteur Culture Collection (PCC) of cyanobacteria (France). Cells were grown photoautotropically in BG11 or without combined nitrogen ($BG11_0$) at constant light with a light intensity of 30 µmol m^{-2} s^{-1}. When appropriate, 5 µg ml^{-1} spectinomycin (Sp), 5 µg ml^{-1} streptomycin (Sm) or 30 µg ml^{-1} neomycin (Nm) was added to strains carrying respective plasmids or chromosomal insertions. In some cases, basal copper-regulated *petE*-driven expression of gene candidates in *Anabaena* cells was lethal or growth inhibiting, therefore these strains were grown in BG11 without copper and protein expression was later induced by the addition of $CuSO_4$ at indicated concentrations to the culture. *E. coli* strains DH5α, DH5αMCR, XL1-blue and HB101 were used for cloning and conjugation by triparental mating. BTH101 was used for BACTH system and BL21 (DE3) was used for expression of His_6- and GFP-tagged proteins in *E. coli*. All strains were grown in LB medium containing the appropriate antibiotics at standard concentrations. Supplementary Tables 2-5 list all used bacterial strains, plasmids and oligonucleotides.

Prediction of coiled-coil rich proteins

Genome sequence of *Anabaena* (GCA_000009705.1) was analyzed by the COILS algorithm[98] as described by Bagchi *et al*.[32]. The algorithm was run with a window width of 21 and the cut-off for amino acids in coiled-coil conformation was set to ≥ 80 amino acid residues. The resulting set of protein candidates was further manually examined with online available bioinformatic tools (NCBI Conserved Domain Search, NCBI BLAST, TMHMM Server, PSORTb, I-TASSER). Protein candidates exhibiting BLAST hits involved in cytoskeletal processes or similar domain architectures as known IF proteins like CreS, FilP, vimentin, desmin or keratin were selected, and enzymatic proteins as well as proteins predicted to be involved in other cellular processes were excluded.

Distribution of homologs in cyanobacteria

Cyanobacteria species tree is according to Dagan *et al.*[110] with the root of the tree as recently inferred by Tria, Landan and Dagan[111]. Homologs to the *Anabaena* proteins were detected by amino acid sequence similarity using stand-alone BLAST[112] ver. 2.2.26. Protein sequences that were found as BLAST hits with a threshold of E-value ≤ $1x10^{-5}$ were further compared to the *Anabaena* protein by global alignment using needle[113]. Hits having ≥30% identical amino

acids in the global alignment were considered as homologs. The phylogenetic tree was visualized with iTOL[114].

Genomic DNA and RNA isolation and cDNA synthesis

Genomic DNA (gDNA) from *Anabaena* was isolated using the GeneJET Plant Genomic DNA Purification Kit (Thermo Fischer Scientific) and the DNeasy Plant Mini Kit (QIAGEN) according to the manufacturer's instructions from 10 ml cyanobacterial cultures.

RNA from *Anabaena* WT was isolated using the Direct-zol™ RNA MiniPrep Kit (Zymo Research) according to the manufacturer's instructions. RNA was isolated in technical triplicates from 10 ml cultures. Isolated RNA was treated with DNA-free™ Kit (2 units rDNAs/reaction; Thermo Fischer Scientific) and 200 ng RNA was reverse transcribed using the qScript™ cDNA Synthesis Kit (Quanta Biosciences). RT-PCR of cDNA samples for *mpB*, *cypS*, *ceaR*, *lfiA*, *lfiB* and *lfiA+lfiB* was done using primer pairs #1/#2, #3/#4, #5/#6, #7/#8, #9/#10, #7/#10, respectively.

Transformation

Transformation of chemically competent *E. coli* was performed by the standard heat shock procedure[115]. *Anabaena* was transformed by triparental mating according to Ungerer and Pakrasi[116]. Briefly, 100 µl of overnight cultures of DH5α carrying the conjugal plasmid pRL443 and DH5αMCR carrying the cargo plasmid and the helper plasmid pRL623, encoding for three methylases, were mixed with 200 µl *Anabaena* culture (for transformation into *Anabaena* mutant strains, cells were scraped from the plate and resuspended in 200 µl BG11). This mixture was directly applied onto sterilized nitrocellulose membranes placed on top of BG11 plates supplemented with 5% LB medium. Cells were incubated in the dark at 30 °C for 6-8 h with subsequent transfer of the membranes to BG11 plates. After another 24 h, membranes were transferred to BG11 plates supplemented with appropriate antibiotics.

Plasmid construction

Ectopic expression of *Anabaena* protein candidates was achieved from a self-replicating plasmid (pRL25C[117]) under the control of the copper-inducible *petE* promoter (P_{petE}) or the native promoter (predicted by BPROM[61]) of the respective gene. All constructs were verified by Sanger sequencing (Eurofins Genomics).

Initially, we generated pTHS1 (pRL25C, P_{petE}::*lfiA-gfp)*, which served as template for many other pRL25C-based plasmids employed in this study. For this, P_{petE} and *lfiA* were amplified from *Anabaena* gDNA using primers #11/#12 and #13/#14, respectively. *gfpmut3.1* was amplified from pJET1.2 containing P_{petE}-*gfp*[118] using primers #15/#16. This *gfpmut3.1* (hereafter *gfp*) is deprived of its internal NdeI site and contains a 5' linker sequence of 12 alternating codons encoding for alanine and serine. The PCR fragments were next ligated into PCR-amplified pRL25C (using primers #17/#18) by Gibson assembly.

For pTHS2 (pRL25C, P_{petE}::*lfiB-gfp*) and pTHS3 (pRL25C, P_{petE}::*ceaR-gfp*), *lfiB* and *ceaR* were amplified from *Anabaena* gDNA using primers #19/#20 or #21/#22, respectively and ligated into PCR-linearized pTHS1 (using primers #23/#24; thereby removing only *lfiA* and leaving P_{petE} and *gfp* in the vector) by Gibson assembly.

For pTHS4 (pRL25C, P_{petE}::*cypS-gfp*), *cypS* was amplified by PCR from *Anabaena* gDNA using primers #36/#38, introducing NdeI and SacI sites, and then ligated into pJET1.2-P_{petE}::*gfp*, thereby generating P_{petE}::*cypS-gfp* which is flanked by a 5' BamHI site and a 3' EcoRI site. The P_{petE}::*cypS-gfp* fragment was excised by BamHI and EcoRI and ligated into BamHI and EcoRI-digested pRL25C.

For pTSH5 (pRL25C, P_{petE}::*trunc-ceaR-gfp*), pTHS3 was amplified using primers #148/#148 and re-ligated using Quick Ligase (NEB). Thereby, the first 153 bp from *ceaR* were removed

For pTHS6 (P_{petE}::*cypS-his*), *cypS-his* was amplified from pTHS8 using primers #25/#26 and ligated into PCR-linearized pRL25C (using primers #24/#27) by Gibson assembly.

For pTHS7 (pRL25C, P_{petE}-*lfiA*-ec*fp,* P_{petE}-*lfiB-gfp*), P_{petE}-*lfiA* was amplified from pTHS1 using primers #28/#29 and ligated into ClaI-digested pRL25C by Gibson assembly together with *myc-link-ecfp* (initially amplified with primers #30/#31, purified and then again amplified with primers #32/#33). This construct was digested by BamHI and ligated by Gibson assembly with PCR-amplified P_{petE}::*lfiB-gfp* from pTHS2 (using primers #34/#35).

pET21a(+) plasmids bearing C-terminal His-tag translational fusions of CCRPs were generated by restriction-based cloning techniques. For this, *cypS*, *lfiA*, *lfiB* or *ceaR* were amplified by PCR from *Anabaena* gDNA using primers #36/#37, #39/#40, #41/#42 or #43/#44, respectively, introducing NdeI and XhoI sites. NdeI and XhoI-digested fragments were then ligated into pET21a(+) using Quick Ligase (NEB). This procedure yielded plasmids pTHS8, pTHS9, pTHS10 and pTSH11, respectively.

pET21a(+) bearing C-terminal *gfp* translational fusions were generated based on pTHS12 (pET21a(+), P_{T7}::*cypS-gfp*). For this, *cypS* was amplified by PCR from *Anabaena* gDNA with primers 36#/#38, introducing NdeI and SacI sites, and ligated into NdeI and SacI-digested

pJET1.2 bearing P_{petE}-*gfp*. *cypS-gfp* was excised by NdeI and EcoRI and ligated into NdeI and EcoRI-digested pET21a(+), generating pTHS12. For pTHS13 (pET21a(+), P_{T7}::*ceaR-gfp*), *ceaR-gfp* was amplified by PCR from pTHS3 using primers #47/#48 and ligated into PCR-linearized pTHS12 (primers #49/#50) by Gibson assembly.

GFP-fragment reassembly plasmids were generated by Gibson assembly. For this aim, *lfiA* was amplified by PCR from *Anabaena* gDNA with primer 51/52 or 53/54 and ligated into XhoI and BamHI or NheI digested pET11a-link-NGFP, generating pTHS15 or pTHS16. *lfiB* was amplified by PCR from *Anabaena* gDNA with primers 55/56 and ligated into NcoI and AatII digested pMRBAD-link-CGFP, generating pTHS17.

Clonings for bacterial two-hybrid plasmids were done using Gibson assembly of PCR-linearized pKNT25, pKT25, pUT18 or pUT18C plasmids, using primers #57/#58 for pKNT25 and pUT18, primers #59/#60 for pKT25 and primers 61/62 for pUT18C. For each gene, three primer combinations were used for amplification from *Anabaena* gDNA. The first primer pair was always used for cloning of the respective gene into pKNT25 and pUT18 while the second and third primer pairs were used for cloning into pKT25 or pUT18C, respectively: *cypS* (primers #63/#64, #65/#66 or #67/#68), *lfiA* (primers #69/#70, #71/#72 or #73/#74), *lfiB* (primers #75/#76, #77/#78 or #79/#80), *ceaR* (primers #81/#82, #83/#84 or #85/#86), *sepJ* (primers #87/#88, #89/#90 or #91/#92), *ftsZ* (primers #93/#94, #95/#96 or #97/#98), *mreB* (primers #99/#100, #101/#102 or #103/#104), *fraC* (primers #105/#106, #107/#108 or #109/#110) and *fraD* (primers #111/#112, #113/#114 or #115/#116). This yielded plasmids pTHS17-pTHS52, respectively.

Like for P_{petE}-driven expression, native expression of *Anabaena* CCRPs was mediated from the pRL25C plasmid. For pTHS56 (pRL25C, P_{cypS}::*cypS-gfp*), P_{cypS} was amplified from *Anabaena* gDNA using primers #150/#151 and ligated into BamHI and EcoRI-digested pRL25C by Gibson assembly together with *cypS-gfp*, which was amplified from pTHS4 using primers #152/#153.

For pTHS57 (pRL25C, P_{ceaR}::*ceaR-gfp*), P_{ceaR} was amplified from *Anabaena* gDNA using primers #154/#155 and ligated into BamHI and EcoRI-digested pRL25C by Gibson assembly together with *ceaR-gfp*, which was amplified from pTHS3 using primers #156/#153.

For pTHS58 (pRL25C, P_{lfiA}::*lfiA-gfp*), P_{lfiA} was amplified from *Anabaena* gDNA using primers #157/#158 and ligated into BamHI and EcoRI-digested pRL25C by Gibson assembly together with *lfiA-gfp*, which was amplified from pTHS1 using primers #159/#153.

For pTHS59 (pRL25C, P_{lfiB}::*lfiB-gfp*), P_{lfiB} was amplified from *Anabaena* gDNA using primers #160/#161 and ligated into BamHI and EcoRI-digested pRL25C by Gibson assembly together with *lfiB-gfp*, which was amplified from pTHS2 using primers #162/#153.

For pTHS60 (pRL25C, P_{cypS}::*cypS-his*), P_{cypS} was amplified from *Anabaena* gDNA using primers #150/#151 and ligated into BamHI and EcoRI-digested pRL25C by Gibson assembly together with *cypS-his*, which was amplified from pTHS8 using primers #152/#163.

For pTHS61 (pRL25C, P_{ceaR}::*ceaR*), P_{ceaR}::*ceaR* was amplified from *Anabaena* gDNA using primers #154/#164 and ligated into BamHI and EcoRI-digested pRL25C by Gibson assembly.

For pTHS58 (pRL25C, $P_{lfiA/B}$::*lfiA-lfiB*), $P_{lfiA/B}$::*lfiA-lfiB* was amplified from *Anabaena* gDNA using primers #157/#165 and ligated into BamHI and EcoRI-digested pRL25C by Gibson assembly.

Anabaena mutant strain construction

All *Anabaena* mutant strains were generated using the pRL278-based double homologous recombination system employing the conditionally lethal *sacB* gene[119]. For this, 1500 bp upstream and downstream of the gene to be replaced were generated by PCR from *Anabaena* gDNA. Upstream and downstream regions of *cypS* and *ceaR*, were amplified using primers #121/#122 and #123/#124 or #125/#126 and #127/#128, respectively. Upstream region of *lfiA* was amplified using primers #129/#130 and downstream region of *lfiB* was amplified using primers #131/#132. The respective upstream and downstream homology regions flanking the CS.3 cassette (amplified with primer #119/#120 from pCSEL24) were then inserted into PCR-amplified pRL278 (using primer #117/#118) by Gibson assembly, yielding pTHS55, pTHS56 and pTHS57, respectively. *Anabaena* transformed with those plasmids was subjected to several rounds of re-streaking on new plates (about 5-8 rounds for each strain). To test for fully segregated clones, colony PCRs were performed. For this, *Anabaena* cells were resuspended in 10 µl sterile H_2O of which 1 µl was used for standard PCR with internal gene primers #3/#4, #5/#6 and #7/#10 for Δ*cypS*, Δ*ceaR* and Δ*lfiA*Δ*lfiB,* respectively. Correct placement of the CS.3 cassette was then further confirmed using primers CS.3 cassette primers with primers binding outside of the 5' and 3' flanks used for homologous recombination (#137/#118 and #117/#138 for Δ*cypS*, #135/#118 and #117/#136 for Δ*ceaR* and #133/#118 and #117/#134 for Δ*lfiA*Δ*lfiB*).

Growth curve analysis

For analysis of mutant viability, growth curves of *Anabaena* WT and Δ*ceaR* mutant strain were performed. For this, cells were grown in BG11 liquid medium, washed three times by centrifugation (6500 x *g*, RT, 3 min) in BG11 or $BG11_0$, adjusted to an OD_{750} of 0.1 and then grown in triplicates at standard growth conditions in 15 ml culture volumes. OD_{750} values were recorded once a day for 24 d.

Fluorescence microscopy

Bacterial strains grown in liquid culture were either directly applied to a microscope slide or previously immobilized on a 2% low-melting agarose in PBS (10 mM Na_2HPO_4, 140 mM NaCl, 2.7 mM KCl, 1.8 mM KH_2PO_4, pH 7.4) agarose pad and air dried before microscopic analysis. Epifluorescence was done using an Axio Imager.M2 light microscope (Carl Zeiss) equipped with Plan-Apochromat 63x/1.40 Oil M27 objective and the AxioCam MR R3 imaging device (Carl Zeiss). GFP, Alexa Fluor 488 and BODIPY™ FL Vancomycin (Van-FL) fluorescence was visualized using filter set 38 (Carl Zeiss; excitation: 470/40 nm band pass (BP) filter; emission: 525/50 nm BP). Chlorophyll auto-fluorescence was recorded using filter set 15 (Carl Zeiss; excitation: 546/12 nm BP; emission: 590 nm long pass). When applicable, cells were previously incubated in the dark at RT for about 5 min with 10 µg ml^{-1} DAPI (final concentration) to stain intracellular DNA. For visualization of DAPI fluorescence filter set 49 (Carl Zeiss; excitation: G 365 nm; emission: 455/50 nm) was employed. For confocal laser scanning microscopy, the LSM 880 Axio Imager 2 equipped with a C-Apochromat 63x/1.2 W Korr M27 objective and an Airyscan detector (Carl Zeiss) was used and visualization of GFP, eCFP and chlorophyll auto-fluorescence was done using Zen black smart setup settings. Also, to investigate putative alterations of the polysaccharide sheath of *Anabaena* mutants, cells were grown on $BG11_0$ agar plates, re-suspended in $BG11_0$ liquid medium and stained with 0.05% alcian blue (final concentration). Polysaccharide staining of *Anabaena* cells immobilized on an agarose pad was then observed with an Axiocam ERc 5s color camera (Carl Zeiss). *E. coli* BL21 (DE3) cells expressing C-terminally GFP-tagged protein candidates were were grown over night in LB and then diluted 1:40 in the same medium the following day. Cells were grown for 2 h at 37 °C, briefly acclimated to 20 °C for 10 min and induced with 0.05 mM IPTG at 20 °C. Protein localization of GFP-tagged proteins was then observed after indicated time points of cells immobilized on an agarose pad.

1052 Transmission electron microscopy and sacculi preparation

1053 For ultra-structure analysis, *Anabaena* filaments were fixed with 2.5% glutaraldehyde,
1054 immobilized in 2% agaorse, treated with 2% potassium permanganate and dehydrated through
1055 a graded ethanol series. The fixed cells were infiltrated by ethanol:EPON (2:1 to 1:2 ratio) and
1056 embedded in pure EPON. Ultrathin sections were prepared with a Leica UC6iUltramicrotome,
1057 transferred to formvar coated copper grids and post-stained with uranyl acetate and lead
1058 citrate[120]. Micrographs were recorded at a Philips Tecnai10 electron microscope at 80 kV.

1059 Peptidoglycan sacculi were isolated from filaments grown on BG11 agar plates by the method
1060 of Kühner *et al*.[121] with the following modifications: Cells were sonicated (Branson Sonifier 250;
1061 duty cycle 50%, output control 1, 2 min) prior to boiling in 0.1 M Tris-HCl pH 6.8 with 3% SDS.
1062 After incubation in a sonifier waterbath, the samples were incubated with α-Chymotrypsin (600
1063 µg ml^{-1}) at 37 °C over night in 50 mM Na_3PO_4 buffer pH 6.8. After inactivation of the enzyme,
1064 the sample was sonified again and loaded on a formvar/carbon film coated copper grid
1065 (Science Services GmbH, Munich) and stained with 1 % (w/v) uranyl acetate as described
1066 previously[122]. Images were taken with a Philips Tecnai10 electron microscope at 80 kV.

1067

1068 Calcein labelling and fluorescence recovery after photobleaching (FRAP) experiments

1069 *Anabaena* WT and mutant strains were either grown on BG11 plates and resuspended in BG11
1070 or directly taken from liquid cultures, washed several times in BG11, resuspended in 0.5 ml
1071 BG11 and incubated with 10 µl calcein-AM (1 mg ml^{-1} in DMSO). The cells were incubated in
1072 the dark at 30 °C for 1 hour and then subjected to four washing steps with 1 ml BG11.
1073 Subsequently, cells were resuspended in a small volume of BG11, spotted on BG11 agar
1074 plates (1 % w/v) and air dried. Samples were visualized by using an inverted confocal laser
1075 scanning microscope (Leica TCS SP5) with a x63 oil immersion objective (HCX PL APO 63x
1076 1.40-0.60 OIL CS). Fluorescence was excited at 488 nm and emission monitored by collecting
1077 across a window of 500 to 530 nm with a maximally opened pinhole (600 µm). FRAP
1078 experiments were carried out by an automated routine as previously described (Mullineaux *et*
1079 *al.* EMBO). After recording an initial image, selected cells were bleached by increasing the
1080 laser intensity by a factor of 5 for two subsequent scans and the fluorescence recovery followed
1081 in 0.5 s intervals for 30 s was recorded using the Leica LAS X software. Exchange coefficients
1082 (*E*) were then calculated according to Mullineaux *et al*. and Nieves-Morión *et al.*[43,101].

1083 BODIPY™ FL Vancomycin (Van-FL) staining

1084 Van-FL staining of BG11-grown filaments of the *Anabaena* WT and mutant strains was
1085 essentially performed as previously described by Lehner *et al*.[47] and Rudolf *et al*.[123]. Briefly,
1086 cells were resuspended in BG11 medium, washed once in BG11 by centrifugation (6500 x *g*,
1087 4 min, RT) and incubated with 5 µg ml^{-1} Van-FL (dissolved in methanol). Cells were incubated
1088 in the dark for 1 hour at 30 °C, washed three times with BG11 and immobilized on an agarose
1089 pad. Van-FL fluorescence signals were then visualized using epifluorescence microscopy with
1090 an excitation time of 130 ms. Arithmetic mean fluorescence intensities were then recorded
1091 from the septa between two cells with a measured area of 3.52 μm^2 using the histogram option
1092 of the Zen blue 2.3 software (Carl Zeiss).

1093

1094 Data analysis

1095 Cell length, volume and roundness were determined using the imaging software ImageJ. Cell
1096 volume was calculated based on the assumption of an elliptic cell shape of *Anabaena* cells
1097 using the Major Axis and Minor Axis values given by ImageJ and the formula for the volume of
1098 an ellipse ($V = \frac{4}{3}\pi abc$):

1099 • $V = \frac{4}{3}\pi\left(\left(\frac{Major\ Axis}{2}\right)^2 \frac{Minor\ Axis}{2}\right)$

1100 Distribution of DAPI fluorescence signals was done in ImageJ with the Plot Profile option along
1101 151 single cells with rectangle tool. The resulting grey values were arranged according to the
1102 maximum intensity focus and the width of the DAPI focal area was calculated as the range of
1103 DAPI staining around the maximum (± 10 grey value in arbitrary units).

1104

1105 Bacterial two-hybrid and beta galactosidase assays

1106 Chemically competent *E. coli* BTH101 cells were co-transformed with 5 ng of plasmids carrying
1107 the respective T18 and T25 translational fusion constructs, plated onto LB plates
1108 supplemented with 200 µg ml^{-1} X-gal, 0.5 mM IPTG, Amp, Km and grown at 30°C for 24-36 h.
1109 Interactions were quantified by beta-galactosidase assays from three independent colonies.
1110 For this aim, cultures were either grown over night at 30 °C or for two days at 20 °C in LB Amp,
1111 Km, 0.5 mM IPTG and beta-galactosidase activity was recorded as described in the
1112 manufacturer's instructions (Euromedex; BACTH System Kit Bacterial Adenylate Cyclase
1113 Two-Hybrid System Kit) in a 96 well plate according to Karimova, Davi and Ladant[103].

GFP-fragment reassembly assay

Chemically competent *E. coli* BL21 (DE3) were co-transformed with indicated plasmid combinations, plated on LB Amp, Km and grown over night at 37 °C. Liquid overnight cultures of single colonies of the respective plasmid-bearing *E. coli* strains were then diluted 1:40 in the same medium the following day. Cells were grown for 2 h at 37 °C, briefly acclimated to 20 °C for 10 min and protein expression was induced with 0.05 mM IPTG and 0.2% L-arabinose. Pictures of induced cultures grown at 20 °C were taken after 48 h of cells immobilized on an agarose pad.

Co-immunoprecipitation

About 20-30 ml of the respective *Anabaena* culture was pelleted by centrifugation (4800 x *g*, 10 min, RT), cells were washed twice by centrifugation (4800 x *g*, 10 min, RT) with 40 ml PBS and then resuspended in 1 ml lysis buffer (PBS-N: PBS supplemented with 1% NP-40) supplemented with protease inhibitor cocktail (PIC; cOmplete™, EDTA-free Protease Inhibitor Cocktail, Sigma-Aldrich). Cells were lysed using the VK05 lysis kit (Bertin) in a Precellys® 24 homogenizer (3 strokes for 30 seconds at 6500 rpm) and cell debris was pelleted by centrifugation (30 min, 21,100 x *g*, 4 °C). 50 µl µMACS anti-GFP MicroBeads (Miltenyi Biotec) was added to the resulting cell-free supernatant and incubated for 1 h at 4 °C with mild rotation. Afterwards, the sample was loaded onto µColumns (Miltenyl Biotec), washed two times with 1 ml lysis buffer and eluted in 50 µl elution Buffer (50 mM Tris HCl pH 6.8, 50 mM DTT, 1% SDS, 1 mM EDTA, 0.005% bromphenol blue, 10% glycerol; Miltenyl Biotec). Until further use, samples were stored at -80 °C.

Mass spectrometry analysis

Coomassie stained gel bands were excised and protein disulfide bonds were reduced with 10 mM dithiotreitol at 56 °C for 45 min and alkylated with 55 mM iodoacetamide at RT for 30 min in the dark. The gel bands were washed 50 mM ammonium bicarbonate and subsequently dehydrated with acetonitrile. 10 µl trypsin (5 ng μl^{-1} in 25 mM ammonium bicarbonate) were added and the gel bands were rehydrated for 5 min at 37 °C. Samples were digested over night at 37 °C. Prior to peptide extraction samples were acidified with 10% formic acid. After transferring the supernatant into a new Eppendorf tube, 5% formic acid was added to the gel bands and incubated for 10 min. Subsequently the samples were sonicated for 1 min in ice-cooled water and the supernatant was combined with the one from the step before. Two additional extraction steps with 60% acetonitrile/1% formic acid and 100% acetonitrile were

performed in the same manner. The combined supernatants were dried in the SpeedVac and the samples were reconstituted in 30 µL 3% acetonitrile/0.1% trifluoroacetic acid. LC-MS/MS analysis was performed using a Dionex U3000 nanoUHPLC coupled to a Q Exactive Plus mass spectrometer (both from Thermo Scientific). The LC-MS/MS parameters were as follows: Six microliter were injected and loaded on a trap column (Acclaim Pepmap 100 C18, 10 mm × 300 µm, 3 µm, 100 Å, Dionex) and washed for 3 min with 2% ACN/0.05% TFA at a flow-rate of 30 µL min^{-1}. separation was performed using an Acclaim PepMap 100 C18 analytical column (50 cm × 75 µm, 2 µm, 100 Å, Dionex) with a flow-rate of 300 nL/min and following eluents: A (0.05% FA) and B (80% ACN/0.04% FA); linear gradient 5-40% B in 60 min, 50-90% B in 5 min, 90% B for 10 min, 90-5% B in 1 min and equilibrating at 5% B for 11 min. Ionization was performed with 1.5 kV spray voltage applied on a non-coated PicoTip emitter (10 µm tip size, New Objective, Woburn, MA) with the source temperature set to 250°C. MS data were acquired from 5 to 85 min with MS full scans between 300 and 1,800 m/z at a resolution of 70,000 at m/z 200. The 10 most intense precursors with charge states ≥2+ were subjected to fragmentation with HCD with NCE of 27%; isolation width of 3 m/z; resolution, 17,500 at m/z 200. Dynamic exclusion for 30 s was applied with a precursor mass tolerance of 10 ppm. Lock mass correction was performed based on the polysiloxane contaminant signal of 445.120025 m/z. Additional wash runs were performed between samples from gel bands to reduce carry over while cytochrome C was used to monitor mass accuracy and LC quality control. The acquired MS/MS data were searched with the SequestHT algorithm against the entire reviewed Uniprot protein database of *Nostoc* sp. PCC 7120 including plasmids (6922 sequences in total). Static modifications applied were carbamidomethylation on cysteine residues, while oxidation on methionine residues was set as dynamic modification. Spectra were searched with full enzyme specificity. A MS mass tolerance of 10 ppm and a MS/MS tolerance of 0.02 Da was used. Proteins were identified with at least three unique peptides with a FDR confidence ≤ 0.01 (high).

Immunofluorescence

Immunolocalization of CypS-His and FtsZ in *Anabaena* was essentially performed as described by Ramos-León *et al*.[82]. For visualization of FtsZ, *Anabaena* WT and mutant strains were streaked from growth plates (BG11 and $BG11_0$ plates), resuspended in a small volume of distilled water and air-dried on Polysine® adhesion slides (Menzel) at RT followed by fixation and permeabilization with 70% ethanol for 30 min at -20 °C. Cells were allowed to air dry for 30 min at RT and then washed two times with PBST (PBS supplemented with 0.1% (v/v) Tween-20) for 2 min. Unspecific binding sites were blocked for 30 min at RT with blocking buffer (1x Roti®-ImmunoBlock in PBST; Carl Roth) and afterwards rabbit anti-FtsZ (Agrisera;

1:150 diluted) antibody in blocking buffer was added to the cells and incubated for 1.5 h at RT in a self-made humidity chamber followed by five washing steps with PBST. 7.5 µg ml^{-1} Alexa Fluor 488-conjugated goat anti-rabbit IgG (H+L) secondary antibody (Thermo Fischer Scientific) in blocking buffer was added to the cells and incubated for 1 h at RT in the dark in a self-made humidity chamber. Subsequently, cells were washed five times with PBST, air dried and mounted with ProLong™ Diamond Antifade Mountant (Thermo Fischer Scientific) overnight at 4 °C. Immunolocalization of FtsZ was then analyzed by epifluorescence microscopy. Similarly, *in vivo* localization of CypS-His expressed in *Anabaena* was evaluated by immunolocalization of $BG11_0$ grown liquid cultures, induced with 0.25 µM $CuSO_4$ for two days, and compared to *Anabaena* WT cells using mouse anti-His primary antibody (1:500 diluted; Thermo Fischer Scientific).

Spot assays

Spot assays were essentially performed as described by Dörrich *et al.*[124]. *Anabaena* WT and mutant strains were grown on BG11 growth plates, resuspended in BG11 liquid medium and adjusted to an OD_{750} of 0.4. Cells were then spotted in triplicates of 5 µl onto the respective growth plates containing either no additives (BG11 or $BG11_0$), 50 µg ml^{-1} Proteinase K or 100 µg ml^{-1} lysozyme in serial 1/10 dilutions and incubated under standard growth conditions until no further colonies arose in the highest dilution.

Protein purification and *in vitro* filamentation assays

For protein purification, *E. coli* BL21 (DE3) cells carrying His-tagged protein candidates were grown in overnight cultures at 37 °C and 250 rpm. The next day, overnight cultures were diluted 1:40 in the same medium and grown at 37 °C until they reached an OD_{600} of 0.5-0.6. Protein expression was induced with 0.5 mM IPTG for 3-4 h at 37 °C and 250 rpm. Afterwards, cell suspensions of 50 ml aliquots were harvested by centrifugation, washed once in PBS and stored at -80 °C until further use. For *in vitro* filamentation assays, cell pellets were resuspended in urea lysis buffer (ULB: 50 mM NaH_2PO_4, 300 mM NaCl, 25 mM imidazole, 6 M urea; pH 8.0) and lysed in a Precellys® 24 homogenizer (3x 6500 rpm for 30 s) using the 2 ml microorganism lysis kit (VK01; Bertin) or self-packed Precellys tubes with 0.1 mm glass beads. The resulting cell debris was pelleted by centrifugation at 21,000 x *g* (30 min, 4 °C) and the supernatant was incubated with 1 ml HisPur™ Ni-NTA resin (Thermo Fischer Scientific) for 1 h at 4°C in an overhead rotator. The resin was washed 5 times with 4x resin-bed volumes ULB and eluted in urea elution buffer (UEB: ULB supplemented with 225 mM imidazole). Total

protein concentration was measured using the Qubit® 3.0 Fluorometer (Thermo Fischer Scientific) and generally adjusted to 0.5-1.0 mg ml^{-1} before dialysis. Filament formation of purified proteins was induced by overnight dialysis against polymerization buffer (PLB: 50 mM PIPES, 100 mM KCl, pH 7.0; HLB: 25 mM HEPES, 150 mM NaCl, pH 7.4; or 25 mM HEPES pH 7.5) at 20 °C and 180 rpm with three bath changes using a Slide-A-Lyzer™ MINI Dialysis Device (10K MWCO, 0.5 ml or 2 ml; Thermo Fischer Scientific). Purified proteins were stained with an excess of NHS-Fluorescein (dissolved in DMSO; Thermo Fischer Scientific) and *in vitro* filamentation was analyzed by epifluorescence microscopy.

Data availability

All data generated or analyzed during this study are included in this published article (and its supplementary information files). The datasets generated during and/or analyzed during the current study are available from the corresponding authors on reasonable request.

Supplementary Table 2: Cyanobacterial strains used in this study

Strain	Genotype	Resistance Marker	Source
Anabaena sp. PCC 7120	WT		Pasteur culture collection of Cyanobacteria (PCC)
BLS1	*Anabaena* Δ*cypS*::CS.3	Sp, Sm	This study
BLS2	*Anabaena* (Δ*lfiA*Δ*lfiB*)::CS.3	Sp, Sm	This study
BLS3	*Anabaena* Δ*ceaR*::CS.3	Sp, Sm	This study

Sp = spectinomycin, Sm = streptomycin

Supplementary Table 3: *E. coli* strains used in this study

Strain	Genotype	Resistance	Source
DH5αMCR	F- *endA1 supE44 thi-1* λ^- *recA1 gyrA96 relA1 deoR* Δ(*lacZYA-argF*)U169 Φ80d*lacZ*ΔM15 *mcrA* Δ(*mrr* hsdRMS *mcrBC*)		Grant *et al.,*1990 ([125])
BL21 (DE3)	F^- *ompT gal dcm lon hsdS*$_B$($r_B^- m_B^-$) λ(DE3 [*lacI lacUV5-T7p07 ind1 sam7 nin5*]) [*malB*$^+$]$_{K-12}$(λ^S)		Studier *et al.,* 1986 ([126])
BTH101	F^-, *cya-99*, *araD139*, *galE15*, *galK16*, *rpsL1* (*Str*$_r$), *hsdR2, mcrA1*,*mcrB1*	Sm	Euromedex
XL1-blue	endA1 gyrA96(nal^R) thi-1 recA1 relA1 lac glnV44 F'[::Tn10 proAB$^+$ lacI^q Δ(*lacZ*)M15] *hsdR17*(r_K^- m_K^+)	Tet	Stratagene
HB101	F^- *mcrB mrr hsd*S20(r_B^- m_B^-) *rec*A13 *leuB*6 *ara*-14 *pro*A2 *lac*Y1 *gal*K2 *xyl*-5 mtl-1 rpsL20(Sm^R) glnV44 λ^-	Sm	Boyer & Roulland-Dessoix, 1969 ([127])

Tet = tetracycline

Supplementary Table 4: Plasmids used in this study

Name	Description	Resistance	Source
pET21a(+)	Bacterial vector for expressing N- terminal T7 and/or C-terminal His6-tagged proteins in *E. coli*	Amp	Novagen
pRL25C	Shuttle cosmid vector for cyanobacteria and *E. coli*	Km, Nm	Wolk *et al.,* 1988 ([117])
pRL623	Methylation plasmid	Cm	Wolk *et al.,* 1988 ([117])
pRL443	Conjugation plasmid	Amp	Wolk *et al.,* 1988 ([117])
pRL278	Suicide vector used for homologous recombination in cyanobacteria; contains *sacB* for positive selection of double recombination events	Km, Nm	Wolk *et al.,* 1988 ([117])
pKNT25	P_{lac}::-*T25*	Km	Euromedex
pKT25	P_{lac}::*T25*-	Km	Euromedex
pUT18	P_{lac}::-*T18*	Amp	Euromedex
pUT18C	P_{lac}::*T18*-	Amp	Euromedex
pKT25-zip	pKT25; P_{lac}::*T25-zip*	Km, Nm	Euromedex
pUT18C-zip	pUT18C, P_{lac}::*T18-zip*	Amp	Euromedex

pET11a-link-NGFP	IPTG-inducible expression vector for translational fusion of target gene with a N-terminal *gfp* fragment in *E. coli*	Amp	Wilson *et al.,* 2004 ([99])
pMRBAD-link-CGFP	L-arabinose-inducible expression vector for translational fusion of target gene with a C-terminal *gfp* fragment in *E. coli*	Km	Wilson *et al.,* 2004 ([99])
pAM5084	P_{trc}::*ecfp-kaiC*	Amp	Cohen *et al.,* 2014 ([128])
pCSEL24	Integrates into the *nucA-nuiA* region of *Anabaena*	Amp, Sm, Sp	Olmedo-Verd *et al.,* 2006 ([129])
pJET1.2-P*petE-gfp*	pJET1.2 vector containing P_{petE}::*gfp*[a)]	Amp	Stucken *et al.,* 2012 ([118])
pTHS1	pRL25C, P_{petE}::*lfiA-gfp*	Km, Nm	This study
pTHS2	pRL25C, P_{petE}::*lfiB-gfp*	Km, Nm	This study
pTHS3	pRL25C, P_{petE}::*ceaR-gfp*	Km, Nm	This study
pTHS4	pRL25C, P_{petE}::*cypS-gfp*	Km, Nm	This study
pTHS5	pRL25C, P_{petE}::*trunc-ceaR-gfp* (truncated *ceaR* without the N-terminal transmembrane domain; first 156 base pairs removed)	Km, Nm	This study
pTHS6	pRL25C, P_{petE}::*cypS-his*	Km, Nm	This study
pTHS7	pRL25C, P_{petE}::*lfiA*-ec*fp*[b)], P_{petE}::*lfiB-gfp*	Km, Nm	This study
pTHS8	pET21a(+),P_{T7}::*cypS-his*	Amp	This study
pTHS9	pET21a(+), P_{T7}::*lfiA-his*	Amp	This study
pTHS10	pET21a(+), P_{T7}::*lfiB-his*	Amp	This study
pTHS11	pET21a(+), P_{T7}::*ceaR-his*	Amp	This study
pTHS12	pET21a(+); P_{T7}::*cypS-gfp*	Amp	This study
pTHS13	pET21a(+), P_{T7}::*ceaR-gfp*	Amp	This study
pTHS14	pET11a-link-NGFP, P_{T7}::*ngfp-lfiA*	Amp	This study
pTHS15	pET11a-link-NGFP, P_{T7}::*lfiA-ngfp*	Amp	This study
pTHS16	pMRBAD-link-CGFP, P_{ara}::*lfiB-cgfp*	Km	This study
pTHS17	pKNT25, P_{lac}::*cypS-T25*	Km, Nm	This study
pTHS18	pKT25, P_{lac}::*T25-cypS*	Km, Nm	This study
pTHS19	pUT18, P_{lac}::*cypS-T18*	Amp	This study
pTHS20	pUT18C, P_{lac}::*T18-cypS*	Amp	This study
pTHS21	pKNT25, P_{lac}::*lfiA-T25*	Km, Nm	This study
pTHS22	pKT25, P_{lac}::*T25-lfiA*	Km, Nm	This study
pTHS23	pUT18, P_{lac}::*lfiA-T18*	Amp	This study
pTHS24	pUT18C, P_{lac}::*T18-lfiA*	Amp	This study
pTHS25	pKNT25, P_{lac}::*lfiB-T25*	Km, Nm	This study
pTHS26	pKT25, P_{lac}::*T25-lfiB*	Km, Nm	This study
pTHS27	pUT18, P_{lac}::*lfiB-T18*	Amp	This study
pTHS28	pUT18C, P_{lac}::*T18-lfiB*	Amp	This study
pTHS29	pKNT25, P_{lac}::*ceaR-T25*	Km, Nm	This study
pTHS30	pKT25, P_{lac}::*T25-ceaR*	Km, Nm	This study
pTHS31	pUT18, P_{lac}::*ceaR-T18*	Amp	This study

pTHS32	pUT18C, P_{lac}::*T18-ceaR*	Amp	This study
pTHS33	pKNT25, P_{lac}::*sepJ-T25*	Km, Nm	This study
pTHS34	pKT25, P_{lac}::*T25-sepJ*	Km, Nm	This study
pTHS35	pUT18, P_{lac}::*sepJ-T18*	Amp	This study
pTHS36	pUT18C, P_{lac}::*T18-sepJ*	Amp	This study
pTHS37	pKNT25, P_{lac}::*ftsZ-T25*	Km, Nm	This study
pTHS38	pKT25, P_{lac}::*T25-ftsZ*	Km, Nm	This study
pTHS39	pUT18, P_{lac}::*ftsZ-T18*	Amp	This study
pTHS40	pUT18C, P_{lac}::*T18-ftsZ*	Amp	This study
pTHS41	pKNT25, P_{lac}::*mreB-T25*	Km, Nm	This study
pTHS42	pKT25, P_{lac}::*T25-mreB*	Km, Nm	This study
pTHS43	pUT18, P_{lac}::*mreB-T18*	Amp	This study
pTHS44	pUT18C, P_{lac}::*T18-mreB*	Amp	This study
pTHS45	pKNT25, P_{lac}::*fraC-T25*	Km, Nm	This study
pTHS46	pKT25, P_{lac}::*T25-fraC*	Km, Nm	This study
pTHS47	pUT18, P_{lac}::*fraC-T18*	Amp	This study
pTHS48	pUT18C, P_{lac}::*T18-fraC*	Amp	This study
pTHS49	pKNT25, P_{lac}::*fraD-T25*	Km, Nm	This study
pTHS50	pKT25, P_{lac}::*T25-fraD*	Km, Nm	This study
pTHS51	pUT18, P_{lac}::*fraD-T18*	Amp	This study
pTHS52	pUT18C, P_{lac}::*T18-fraD*	Amp	This study
pTHS53	pRL278 containing 1500 bp upstream and downstream of *cypS* flanking the CS.3 cassette	Nm, Km, Sm, Sp	This study
pTHS54	pRL278 containing 1500 bp upstream and downstream of *ceaR* flanking the CS.3 cassette	Nm, Km, Sm, Sp	This study
pTHS55	pRL278, containing 1500 bp upstream of *lfiA* and 1500 bp downstream of *lfiB* flanking the CS.3 cassette	Nm, Km, Sm, Sp	This study
pTHS56	pRL25C, P_{cypS}::*cypS-gfp*	Nm, Km,	This study
pTHS57	pRL25C, P_{ceaR}::*ceaR-gfp*	Nm, Km,	This study
pTHS58	pRL25C, P_{lfiA}::*lfiA-gfp*	Nm, Km,	This study
pTHS59	pRL25C, P_{lfiB}::*lfiB-gfp*	Nm, Km,	This study
pTHS60	pRL25C, P_{cypS}::*cypS-his*	Nm, Km,	This study
pTHS61	pRL25C, P_{ceaR}::*ceaR*	Nm, Km,	This study
pTHS62	pRL25C, $P_{lfiA/B}$::*lfiA-lfiB*	Nm, Km,	This study

Km = kanamycin, Nm = neomycin, Amp = ampicillin; Cm = chloramphenicol

- a) Modified gfpmut3.1[118] in which the internal NdeI site was removed by replacing CAT by the synonymous CAC codon. The GFP is N-terminally preceded by 12 alanine and serine residues. Abbreviated: *gfp*.
- b) eCFP from Cohen *et al.* (2014)[128] was adjusted for C-terminal translational fusion instead of N-terminal fusion. For this, a N-terminal Myc sequences followed by a seven amino acid linker (GSGSGSG) and an additional stop codon at the C-terminus were added.

1243 **Supplementary Table 5: Oligonucleotides used in this study**

#	Given name	Sequence (5' - > 3')
1	rnpB_intern_A	TGCTGGATAACGTCCAGTGC
2	rnpB_intern_B	GGTTTACCGAGCCAGTACCTC
3	Nos295_intern_A	CAAAGTCAGGCGATGAGTGA
4	Nos295_intern_B	GGAACCGCATTACCAGAAGT
5	Nos842_intern_A	TCGGGCAGAAATTACCCAGT
6	Nos842_intern_B	TGCCATTCTTCAGGCAAAGC
7	Nos903_intern_A	TCAGCTAGACGTAAAGAGTGGC
8	Nos903_intern_B	TAATTCTGCTGGGAATGCAGC
9	Nos904_intern_A	TGGAATTAGCGAAGGGGTGG
10	Nos904_intern_B	TGTTCATAGCCATCTGTTGCCA
11	petE_903_Fwd	GAGATTATCAAAAAGGATCCCAGTACTCAGAATTTTTTGCTGAGGTACT
12	petE_903_Rev	TTGAGTGCAACTGTCGTCATGGCGTTCTCCTAACCTGTAGTTTTATTTTT
13	pRL25-Nos903_Fwd	CTACAGGTTAGGAGAACGCCATGACGACAGTTGCACTCAAAGATAG
14	pRL25-Nos903_Rev	GCACTAGCAGATGCACTAGCTTTAGCCGTAGAACTATCAAAAGCTCTCATTGC
15	GFP_903_Fwd	TTGATAGTTCTACGGCTAAAGCTAGTGCATCTGCTAGTGCTAGT
16	GFP_903_Rev	CTTTCGTCTTCAAGAATTCTTTATTTGTATAGTTCATCCATGCCATGTGTAATCC
17	pRL25c-903_V_F	TGGATGAACTATACAAATAAAGAATTCTTGAAGACGAAAGGGCC
18	pRL25c-903_V_R	GCAAAAAATTCTGAGTACTGGGATCCTTTTTGATAATCTCATGACCAAAATCC
19	Nos904-2A	CTACAGGTTAGGAGAACGCCATGGCAGTCAAAAAGTTAACAGACAAAAAC
20	Nos904_2B	GCACTAGCAGATGCACTAGCTTTATTTTTCACTTGACTTTTTGCCTGTTCTAAAGC
21	Nos842_2A	TACAGGTTAGGAGAACGCCATGCAACAAGTCATAGTAAGTAATCGATT
22	Nos842_2B	CACTAGCAGATGCACTAGCGGATGCGTATCTAGCTATTAGATGTTC
23	pRL25c_NEB_Fwd	GCTAGTGCATCTGCTAGTGCTAGTG
24	pRL25c_NEB_Rev	GGCGTTCTCCTAACCTGTAGTTTTATTTTTCT
25	Nos295His_2A	TACAGGTTAGGAGAACGCCATGCTGTATTTAGCAGAAGTACAAAAG
26	Nos295His_2B	CCTTTCGTCTTCAAGAATTCTTCAGTGGTGGTGGTGGTG
27	MBP7_1A	AGAATTCTTGAAGACGAAAGGGCC
28	petE_2A	ACTACCGCATTAAAGCTTATCAGTACTCAGAATTTTTTGCTGAGGTAC
29	Nos903_2B	TTCGCTGATAAGCTTCTGTTCTTTAGCCGTAGAACTATCAAAAGCTCTC
30	Linker_eCFP_3A	GGCTCTGGATCGGGTTCAGGAATGGTGAGCAAGGGCGAG
31	eCFP_3B	CTGCTGCTTACTTGTACAGCTCGTCCATGCC

32	MYC_Linker_3A2	GAACAGAAGCTTATCAGCGAAGAAGATCTGGGCTCTGGATCGGGTTCAG
33	eCFP_3B2	TCATGTTTGACAGCTTATCATTTACTTGTACAGCTCGTCCATGCC
34	petE_BamHI_2A	TTGGTCATGAGATTATCAAAAAGCAGTACTCAGAATTTTTTGCTGAGG
35	GFP_BamHI_2B	ATTGATTTAAAACTTCATTTTTAATTTAAAAGTTATTTGTATAGTTCATCCATGCCATGTG
36	Nos295_NdeI_Fwd	GCTACATATGCTGTATTTAGCAGAAGTACAAA
37	Nos295_XhoI_wo_R	GCTACTCGAGAGATGCCAACAACTCAGG
38	Nos295_SacI_wo_R	GCTAGAGCTCAGATGCCAACAACTCAGG
39	Nos903_NdeI_F	GCTACATATGACGACAGTTGCACTCA
40	Nos903_XhoI_R_w/o	GCTACTCGAGTTTAGCCGTAGAACTATCAAAAGC
41	Nos904_NdeI_F	GCTACATATGGCAGTCAAAAAGTTAACAGAC
42	Nos904_XhoI_wo_R	GCTACTCGAGTTTATTTTTCACTTGACTTTTTGCCT
43	Nos842_NdeI_F	GCTACATATGCAACAAGTCATAGTAAGTAATCG
44	Nos842_XhoI_wo_R	GCTACTCGAGGGATGCGTATCTAGCTATTAGATG
45	Nos903_pET_2A	GTTTAACTTTAAGAAGGAGATATACATATGACGACAGTTGCACTCAAAG
46	Nos904_pET_2A	GTTTAACTTTAAGAAGGAGATATACATATGGCAGTCAAAAAGTTAACAGAC
47	Nos842_pET_2A	GTTTAACTTTAAGAAGGAGATATACATATGCAACAAGTCATAGTAAGTAATCG
48	GFP_pET21a_2B	AGTGGTGGTGGTGGTGGTGTTTGTATAGTTCATCCATGCCATGTGTAATC
49	pET21a_1A	CACCACCACCACCACCAC
50	pET21a_1B	ATGTATATCTCCTTCTTAAAGTTAAACAAAATTATTTCTAGAGG
51	903_split_A	AAGGTGGCTCTGGCTCTGGCTCGAGCATGACGACAGTTGCACTCAAAG
52	903_split_B	CGGGCTTTGTTAGCAGCCGTTATTTAGCCGTAGAACTATCAAAAGCTCTC
53	903_split_A2	TTAACTTTAAGAAGGAGATATACATATGACGACAGTTGCACTCAAAG
54	903_split_B2	CCATGGTGATGGTGGTGATGAGATGCACTAGCTTTAGCCGTAGAACTATCAAAAGCTCT
55	904_split_A	TTTAACTTTAAGAAGGAGATATACCATGGCAGTCAAAAAGTTAACAGACA
56	904_split_B	TTACCGCTTCCACCCGACGTTTTATTTTTCACTTGACTTTTTGCCTGTTC
57	N-term_1A	GAGGATCCCCGGGTACC
58	N-term_1B	TAGAGTCGACCTGCAGGCA
59	pKT25_1A	CCCCGGGTACCTAAGTAAGTAAG
60	pKT25_1B	ATCCTCTAGAGTCGACCCTGC
61	pUT18C_1A	CCGAGCTCGAATTCATCGAT
62	pUT18C_1B	TACCCGGGGATCCTCTAGAGT
63	MB_5A	TGCCTGCAGGTCGACTCTAATGCTGTATTTAGCAGAAGTACAAAAG
64	MB_5B	TCGGTACCCGGGGATCCTCAGATGCCAACAACTCAGGC
65	MB_6A	AGGGTCGACTCTAGAGGATATGCTGTATTTAGCAGAAGTACAAAAGC
66	MB_6B	CTTACTTAGGTACCCGGGGAGATGCCAACAACTCAGGC
67	MB_8A	TCTAGAGGATCCCCGGGTAATGCTGTATTTAGCAGAAGTACAAAAG

68	MB_8B	TCGATGAATTCGAGCTCGGAGATGCCAACAACTCAGGC
69	MB_17A	TGCCTGCAGGTCGACTCTAATGACGACAGTTGCACTCAAAG
70	MB_17B	TCGGTACCCGGGGATCCTCTTTAGCCGTAGAACTATCAAAAGCTCTC
71	MB_18A	AGGGTCGACTCTAGAGGATATGACGACAGTTGCACTCAAAG
72	MB_18B	CTTACTTAGGTACCCGGGGTTTAGCCGTAGAACTATCAAAAGCTCTC
73	MB_20A	TCTAGAGGATCCCCGGGTAATGACGACAGTTGCACTCAAAG
74	MB_20B	TCGATGAATTCGAGCTCGGTTTAGCCGTAGAACTATCAAAAGCTCTC
75	MB_21A	TGCCTGCAGGTCGACTCTAATGGCAGTCAAAAAGTTAACAGACAA
76	MB_21B	TCGGTACCCGGGGATCCTCTTTATTTTTCACTTGACTTTTTGCCTGTTC
77	MB_22A	AGGGTCGACTCTAGAGGATATGGCAGTCAAAAAGTTAACAGACAA
78	MB_22B	CTTACTTAGGTACCCGGGGTTTATTTTTCACTTGACTTTTTGCCTGTTC
79	MB_24A	TCTAGAGGATCCCCGGGTAATGGCAGTCAAAAAGTTAACAGACAA
80	MB_24B	TCGATGAATTCGAGCTCGGTTTATTTTTCACTTGACTTTTTGCCTGTTC
81	MB_25A	TGCCTGCAGGTCGACTCTAATGCAACAAGTCATAGTAAGTAATCGAT
82	MB_25B	TCGGTACCCGGGGATCCTCGGATGCGTATCTAGCTATTAGATGTTC
83	MB_26A	AGGGTCGACTCTAGAGGATATGCAACAAGTCATAGTAAGTAATCGAT
84	MB_26B	CTTACTTAGGTACCCGGGGGGATGCGTATCTAGCTATTAGATGTTC
85	MB_28A	TCTAGAGGATCCCCGGGTAATGCAACAAGTCATAGTAAGTAATCGAT
86	MB_28B	TCGATGAATTCGAGCTCGGGGATGCGTATCTAGCTATTAGATGTTC
87	MB_41A	TGCCTGCAGGTCGACTCTAATGGGGCGATTTGAGAAGC
88	MB_41B	TCGGTACCCGGGGATCCTCACCTTCTGCATTGGCAGG
89	MB_42A	AGGGTCGACTCTAGAGGATATGGGGCGATTTGAGAAGC
90	MB_42B	CTTACTTAGGTACCCGGGGACCTTCTGCATTGGCAGG
91	MB_44A	TCTAGAGGATCCCCGGGTAATGGGGCGATTTGAGAAGC
92	MB_44B	TCGATGAATTCGAGCTCGGACCTTCTGCATTGGCAGG
93	MB_49A	ATGCCTGCAGGTCGACTCTAATGACACTTGATAATAACCAAGAGCTTACC
94	MB_49B	CTCGGTACCCGGGGATCCTCATTTTTGGGTGGTCGCCGTC
95	MB_50A	CAGGGTCGACTCTAGAGGATATGACACTTGATAATAACCAAGAGCTTACC
96	MB_50B	TACTTACTTAGGTACCCGGGGATTTTTGGGTGGTCGCCGTC
97	MB_52A	CTCTAGAGGATCCCCGGGTAATGACACTTGATAATAACCAAGAGCTTACC
98	MB_52B	TATATCGATGAATTCGAGCTCGGATTTTTGGGTGGTCGCCGTC
99	MB_53A	ATGCCTGCAGGTCGACTCTAATGGGGCTTTTTAGGAACTTTCG
100	MB_53B	CTCGGTACCCGGGGATCCTCCATATTTCGAGATCGTCCGCTAAAAAC
101	MB_54A	CAGGGTCGACTCTAGAGGATATGGGGCTTTTTAGGAACTTTCG
102	MB_54B	TACTTACTTAGGTACCCGGGGCATATTTCGAGATCGTCCGCTAAAAAC
103	MB_56A	CTCTAGAGGATCCCCGGGTAATGGGGCTTTTTAGGAACTTTCG
104	MB_56B	TATATCGATGAATTCGAGCTCGGCATATTTCGAGATCGTCCGCTAAAAAC
105	MB_69A	ATGCCTGCAGGTCGACTCTAATGTTTGAAGATTTGACTATACCCAGG
106	MB_69B	CTCGGTACCCGGGGATCCTCCCTATTACGTATCAATAAAATAATAGTTATAGCGGTG
107	MB_70A	CAGGGTCGACTCTAGAGGATATGTTTGAAGATTTGACTATACCCAGG

108	MB_70B	TACTTACTTAGGTACCCGGGGCCTATTACGTATCAATAAAATAATAGTTATAGCGGTG
109	MB_72A	CTCTAGAGGATCCCCGGGTAATGTTTGAAGATTTGACTATACCCAGG
110	MB_72B	ATATCGATGAATTCGAGCTCGGCCTATTACGTATCAATAAAATAATAGTTATAGCGGTG
111	MB_73A	ATGCCTGCAGGTCGACTCTAGTGAATTTATTATTTAAAGACCTTTTCGGAATATT
112	MB_73B	CTCGGTACCCGGGGATCCTCCTGCTGCGGTGGCGCTG
113	MB_74A	GGGTCGACTCTAGAGGATGTGAATTTATTATTTAAAGACCTTTTCGGAAT
114	MB_74B	TACTTACTTAGGTACCCGGGGCTGCTGCGGTGGCGCTG
115	MB_76A	CTAGAGGATCCCCGGGTAGTGAATTTATTATTTAAAGACCTTTTCGGAAT
116	MB_76B	TATATCGATGAATTCGAGCTCGGCTGCTGCGGTGGCGCTG
117	pRL271_Fwd	GAGCTCGCGAAAGCTTGCATG
118	pRL271_Rev	CTCGAGATCTAGATATCGAATTTCTGCCAT
119	CS.3_Fwd	GATCCGTGCACAGCACCTTG
120	CS.3_Rev	TTATTTGCCGACTACCTTGGTGATCT
121	295KO_2A	ATTCGATATCTAGATCTCGAGACTCAACATAATCATCGGTATATACCGAAAT
122	295KO_2B	CAAGGTGCTGTGCACGGATCACCGTTCTTCCTCTTGTGTACTTGA
123	295KO_4A	CCAAGGTAGTCGGCAAATAACAATTCAAAATTCAAAATTCAAAATATTTAGGACTTACG
124	295KO_4B	ATGCAAGCTTTCGCGAGCTCTGTAAATTTCTCACTAAGTGATGGATCAACACT
125	842KO_2A	ATTCGATATCTAGATCTCGAGATGGATAATCCAGCAATGTCGGC
126	842KO_2B	AAGGTGCTGTGCACGGATCATTGCTGATTTTTAGCGTAGTTAAGCTTT
127	842KO_4A	CAAGGTAGTCGGCAAATAAAATTTAATATCCCTAGCTCATCGTAAAATTTTTATAAAAATATG
128	842KO_4B	ATGCAAGCTTTCGCGAGCTCTTTAAAACTAGAACTATGAACTAGCTCGCTAAAC
129	903KO_2A	ATTCGATATCTAGATCTCGAGAAGCAACGGCAACGCC
130	903KO_2B	AAGGTGCTGTGCACGGATCATTTCAACTCCCTTGATTAGATAATGATTAATCGAG
131	904KO_4A	CAAGGTAGTCGGCAAATAAAATACAAATAATAAAAATAAATAAAAAGACGTAACGAAAATTACG
132	904KO_4B	TGCAAGCTTTCGCGAGCTCGTAGTGGGTTTCGCACAAGCTATC
133	903KO_Seq_A	TGCGAATTCCAGTAGGTCTTGGTAA
134	904KO_Seq_B	GGTGGCGCAGAAGTATTTTTG
135	842KO_Seq_A	TCAACAGTCAACAGTCAATAGTGAAGG
136	842KO_Seq_B	TTCATCTACACCGATATCTTGACCC
137	295KO_Seq_A	GCCATCCTAGCTCTGATTTGATC
138	295KO_Seq_B	CAGGGTTATCGGTAAGGAATCG
139	Fragment1.FOR	GATTTCGAACCCGGGGTACCACCTGTAGAGAAGAGTCCCTGAATATCAA
140	Fragment1.REV	TTTTTCGTATTTTCCCTCATTGAATTAATCTCCTACTTGACTTTATGAGTTGGGA
141	Fragment4.FOR	TGGATGAACTATACAAATAAACCGGTGTTTGGATTGTCGG
142	Fragment4.REV	CCCTGCAGGTCGAGGAATTCGCTGTCGAAGTTGAACATCAGTAAGC
143	Nos903_pIGA_2A	TAAAGTCAAGTAGGAGATTAATTCAATGACGACAGTTGCACTCAAAG
144	Fragment3.FOR	ATTTAATGACTGCCTTAGTCGCTAGTGCATCTGCTAGTGCTAGT

145	Fragment3.REV	CCGACAATCCAAACACCGGTTTATTTGTATAGTTCATCCATGCCATGTGTAATCC
146	Vector.FOR	TGATGTTCAACTTCGACAGCGAATTCCTCGACCTGCAGGG
147	Vector.REV	AGGGACTCTTCTCTACAGGTGGTACCCCGGGTTCGAAATCG
148	842_petE_F	CTACAGGTTAGGAGAACGCCATGGATAAGCGACGGAGGAAT
149	petE_842_R	CTCCGTCGCTTATCCATGGCGTTCTCCTAACCTGTAGTTTTATTTTTCT
150	p295_25C_long_A	TTTTGGTCATGAGATTATCAAAAAGATTGACGCAGCATGGC
151	pNos295_Rev	ACCGTTCTTCCTCTTGTGTACT
152	Nos295_pNos295_A	CACAAGAGGAAGAACGGTGTGCTGTATTTAGCAGAAGTACAAAAG
153	GFP_25C_R	AGGCCCTTTCGTCTTCAAGTTATTTGTATAGTTCATCCATGCCATGTGT
154	p842_25C_long_A	TTTTGGTCATGAGATTATCAAAAAGTCTCTCTATCCCCAAGTACAATTTCTCC
155	pNos842_2B	CTTGTTGCATATTGCTGATTTTTAGCG
156	Nos842_pNos842_3A	AATCAGCAATATGCAACAAGTCATAGTAAGTAATCGATTTATTTTAG
157	p903_25C_long_A	TTTTGGTCATGAGATTATCAAAAAGACCCGACACTCTTGAGG
158	pNos903_2B	ACTGTCGTCATATTTCAACTCCCTTG
159	Nos903_pNos903_3A	GGAGTTGAAATATGACGACAGTTGCACTCAAAG
160	pNos904_25C_F	ATTTTGGTCATGAGATTATCAAAAAGAGAAATATCAGCTAGACGTAAAGAGTGG
161	pNos904_2B	TGACTGCCATAAAAACCTCTATTTATTGC
162	Nos904_pNos904_3A	AGAGGTTTTTATGGCAGTCAAAAAGTTAACAGACAAAAAC
163	295_His_25C_R	GGCCCTTTCGTCTTCAAGTTAGTGGTGATGGTGATGATGAGATGC
164	Nos842_25C_B	GAGGCCCTTTCGTCTTCAAGTCAGGATGCGTATCTAGCTATTAGATG
165	Nos904_25C_Ba	GGCCCTTTCGTCTTCAAGTTATTTATTTTTCACTTGACTTTTTGCCTGT

Employed enzymatic cut sites are underlined.

References

1. Shapiro, J. A. Thinking about bacterial populations as multicellular organisms. *Annu. Rev. Microbiol.* **52**, 81–104 (1998).

2. Lyons, N. A. & Kolter, R. On the evolution of bacterial multicellularity. *Curr. Opin. Microbiol.* **24**, 21–28 (2015).

3. Claessen, D., Rozen, D. E., Kuipers, O. P., Søgaard-Andersen, L. & Van Wezel, G. P. Bacterial solutions to multicellularity: A tale of biofilms, filaments and fruiting bodies. *Nat. Rev. Microbiol.* **12**, 115–124 (2014).

4. Smith, W. P. J. *et al.* Cell morphology drives spatial patterning in microbial communities. *Proc. Natl. Acad. Sci.* **114**, E280–E286 (2017).

5. Lin, T.-Y., Santos, T. M. A., Kontur, W. S., Donohue, T. J. & Weibel, D. B. A Cardiolipin-Deficient Mutant of Rhodobacter sphaeroides Has an Altered Cell Shape and Is Impaired in Biofilm Formation. *J. Bacteriol.* **197**, 3446–3455 (2015).

6. Lam, H. *et al.* D-amino acids govern stationary phase cell wall remodeling in bacteria. *Science* **325**, 1552–1555 (2009).

7. Kolodkin-Gal, I. *et al.* D-amino acids trigger biofilm disassembly. *Science* **328**, 627–629 (2010).

8. Typas, A. *et al.* Regulation of peptidoglycan synthesis by outer-membrane proteins. *Cell* **143**, 1097–1109 (2010).

9. Reichenbach, H. The ecology of the myxobacteria. *Environ. Microbiol.* **1**, 15–21 (1999).

10. Flärdh, K., Richards, D. M., Hempel, A. M., Howard, M. & Buttner, M. J. Regulation of apical growth and hyphal branching in Streptomyces. *Curr. Opin. Microbiol.* **15**, 737–743 (2012).

11. Flores, E. & Herrero, A. Compartmentalized function through cell differentiation in filamentous cyanobacteria. *Nat. Rev. Microbiol.* **8**, 39–50 (2010).

12. Rossetti, V. & Bagheri, H. C. Advantages of the division of labour for the long-term population dynamics of cyanobacteria at different latitudes. *Proceedings. Biol. Sci.* **279**, 3457–3466 (2012).

13. Fuchs, E. & Weber, K. INTERMEDIATE FILAMENTS: Structure, Dynamics, Function and Disease. *Annu. Rev. Biochem.* **63**, 345–382 (1994).

14. Köster, S., Weitz, D. A., Goldman, R. D., Aebi, U. & Herrmann, H. Intermediate filament mechanics in vitro and in the cell: From coiled coils to filaments, fibers and networks. *Curr. Opin. Cell Biol.* **32**, 82–91 (2015).

15. Ausmees, N., Kuhn, J. R. & Jacobs-Wagner, C. The bacterial cytoskeleton: An intermediate filament-like function in cell shape. *Cell* **115**, 705–713 (2003).

16. Fuchino, K. *et al.* Dynamic gradients of an intermediate filament-like cytoskeleton are recruited by a polarity landmark during apical growth. *Proceedings of the National Academy of Sciences* **110**, E1889–E1897 (2013).

17. Holmes, N. A. *et al.* Coiled-coil protein Scy is a key component of a multiprotein assembly controlling polarized growth in Streptomyces. *Proceedings of the National Academy of Sciences* **110**, E397–E406 (2013).

18. Fenton, A. K., Hobley, L., Butan, C., Subramaniam, S. & Sockett, R. E. A coiled-coil-repeat protein 'Ccrp' in Bdellovibrio bacteriovorus prevents cellular indentation, but is not essential for vibroid cell morphology. *FEMS Microbiology Letters* **313**, 89–95 (2010).

19. Waidner, B. *et al.* A novel system of cytoskeletal elements in the human pathogen Helicobacter pylori. *PLoS Pathogens* **5**, (2009).

20. Ent, F. van den, Amos, L. A. & Löwe, J. Prokrayotic origin of the actin cytoskeleton. *Nature* **413**, 39–44 (2001).

21. de Boer, P., Crossley, R. & Rothfield, L. The essential bacterial cell-division protein FtsZ is a GTPase. *Nature* **359**, 254–256 (1992).

22. Lin, L. & Thanbichler, M. Nucleotide-independent cytoskeletal scaffolds in bacteria. *Cytoskeleton* **70**, 409–423 (2013).

23. Kaiser, D. & Crosby, C. Cell movement and its coordination in swarms of Myxococcus xanthus. *Cell Motil.* **3**, 227–245 (1983).

24. Yang, R. *et al.* AglZ Is a Filament-Forming Coiled-Coil Protein Required for Adventurous Gliding Motility of Myxococcus xanthus. *J. Bacteriol.* **186**, 6168–6178 (2004).

25. Nan, B., Mauriello, E. M. F., Sun, I. H., Wong, A. & Zusman, D. R. A multi-protein complex from Myxococcus xanthus required for bacterial gliding motility. *Mol. Microbiol.* **76**, 1539–1554 (2010).

26. Nan, B. *et al.* Myxobacteria gliding motility requires cytoskeleton rotation powered by proton motive force. *Proc. Natl. Acad. Sci.* **108**, 2498–2503 (2011).

27. Mauriello, E. M. F. *et al.* Bacterial motility complexes require the actin-like protein, MreB and the Ras homologue, MglA. *EMBO J.* **29**, 315–326 (2010).

28. Schumacher, D. & Søgaard-Andersen, L. Regulation of Cell Polarity in Motility and Cell Division in Myxococcus xanthus. *Annu. Rev. Microbiol. Regul.* **71**, 61–78 (2017).

29. Letek, M. *et al.* DivIVA is required for polar growth in the MreB-lacking rod-shaped actinomycete Corynebacterium glutamicum. *J. Bacteriol.* **190**, 3283–3292 (2008).

30. Puffal, J., García-Heredia, A., Rahlwes, K. C., Siegrist, M. S. & Morita, Y. S. Spatial control of cell envelope biosynthesis in mycobacteria. *Pathog. Dis.* **76**, fty027 (2018).

31. Surovtsev, I. V & Jacobs-Wagner, C. Subcellular organization: a critical feature of bacterial cell replication. *Cell* **172**, 1271–1293 (2018).

32. Bagchi, S., Tomenius, H., Belova, L. M. & Ausmees, N. Intermediate filament-like proteins in bacteria and a cytoskeletal function in Streptomyces. *Mol. Microbiol.* **70**, 1037–1050 (2008).

33. Hempel, A. M., Wang, S., Letek, M., Gil, J. A. & Flärdh, K. Assemblies of DivIVA mark sites for hyphal branching and can establish new zones of cell wall growth in Streptomyces coelicolor. *J. Bacteriol.* **190**, 7579–7583 (2008).

34. Wagstaff, J. & Löwe, J. Prokaryotic cytoskeletons: protein filaments organizing small cells. *Nat. Rev. Microbiol.* (2018). doi:10.1038/nrmicro.2017.153

35. Schwedock, J., McCormick, J. R., Angert, E. R., Nodwell, J. R. & Losick, R. Assembly of the cell division protein FtsZ into ladder-like structures in the aerial hyphae of Streptomyces coelicolor. *Mol. Microbiol.* **25**, 847–858 (1997).

36. Rippka, R., Stanier, R. Y., Deruelles, J., Herdman, M. & Waterbury, J. B. Generic

Assignments, Strain Histories and Properties of Pure Cultures of Cyanobacteria. *Microbiology* **111**, 1–61 (1979).

37. Herrero, A., Stavans, J. & Flores, E. The multicellular nature of filamentous heterocyst-forming cyanobacteria. *FEMS Microbiol. Rev.* **40**, 831–854 (2016).

38. Zhang, C.-C. C., Hugenin, S., Friry, A., Huguenin, S. & Friry, A. Analysis of genes encoding the cell division protein FtsZ and a glutathione synthetase homologue in the cyanobacterium Anabaena sp. PCC 7120. *Res. Microbiol.* **146**, 445–455 (1995).

39. Hu, B., Yang, G., Zhao, W., Zhang, Y. & Zhao, J. MreB is important for cell shape but not for chromosome segregation of the filamentous cyanobacterium Anabaena sp. PCC 7120. *Mol. Microbiol.* **63**, 1640–1652 (2007).

40. Burnat, M., Schleiff, E. & Flores, E. Cell envelope components influencing filament length in the heterocyst-forming cyanobacterium Anabaena sp. strain PCC 7120. *J. Bacteriol.* **196**, 4026–4035 (2014).

41. Cho, H., Uehara, T. & Bernhardt, T. G. Beta-lactam antibiotics induce a lethal malfunctioning of the bacterial cell wall synthesis machinery. *Cell* **159**, 1310–1311 (2014).

42. Fenton, A. K., Mortaji, L. El, Lau, D. T. C., Rudner, D. Z. & Bernhardt, T. G. CozE is a member of the MreCD complex that directs cell elongation in Streptococcus pneumoniae. *Nat. Microbiol.* **2**, 1–9 (2016).

43. Mullineaux, C. W. *et al.* Mechanism of intercellular molecular exchange in heterocyst-forming cyanobacteria. *EMBO J.* **27**, 1299–1308 (2008).

44. Wilk, L. *et al.* Outer membrane continuity and septosome formation between vegetative cells in the filaments of Anabaena sp. PCC 7120. *Cell. Microbiol.* **13**, 1744–1754 (2011).

45. Weiss, G. L., Kieninger, A.-K., Maldener, I., Forchhammer, K. & Pilhofer, M. Structure and function of a bacterial gap junction analog. *bioRxiv* 462465 (2018). doi:10.1101/462465

46. Flores, E. *et al.* Septum-localized protein required for filament integrity and diazotrophy in the heterocyst-forming cyanobacterium Anabaena sp. strain PCC 7120. *J. Bacteriol.* **189**, 3884–3890 (2007).

47. Lehner, J. *et al.* Prokaryotic multicellularity: A nanopore array for bacterial cell communication. *FASEB J.* **27**, 2293–2300 (2013).

48. Nayar, A. S., Yamaura, H., Rajagopalan, R., Risser, D. D. & Callahan, S. M. FraG is necessary for filament integrity and heterocyst maturation in the cyanobacterium Anabaena sp. strain PCC 7120. *Microbiology* **153**, 601–607 (2007).

49. Merino-Puerto, V. *et al.* FraC/FraD-dependent intercellular molecular exchange in the filaments of a heterocyst-forming cyanobacterium, Anabaena sp. *Mol. Microbiol.* **82**, 87–98 (2011).

50. Merino-Puerto, V., Mariscal, V., Mullineaux, C. W., Herrero, A. & Flores, E. Fra proteins influencing filament integrity, diazotrophy and localization of septal protein SepJ in the heterocyst-forming cyanobacterium Anabaena sp. *Mol. Microbiol.* **75**, 1159–1170 (2010).

51. Herrmann, H. & Aebi, U. Intermediate Filaments: Molecular Structure, Assembly Mechanism, and Integration Into Functionally Distinct Intracellular Scaffolds. *Annu. Rev. Biochem.* **73**, 749–789 (2004).

52. Specht, M., Schätzle, S., Graumann, P. L. & Waidner, B. Helicobacter pylori Possesses Four Coiled-Coil-Rich Proteins That Form Extended Filamentous Structures and Control Cell Shape and Motility. *J. Bacteriol.* **193**, 4523–4530 (2011).

53. Herrmann, H., Bär, H., Kreplak, L., Strelkov, S. V. & Aebi, U. Intermediate filaments: From cell architecture to nanomechanics. *Nat. Rev. Mol. Cell Biol.* **8**, 562–573 (2007).

54. Kelemen, G. H. Intermediate Filaments Supporting Cell Shape and Growth in Bacteria BT - Prokaryotic Cytoskeletons: Filamentous Protein Polymers Active in the Cytoplasm of Bacterial and Archaeal Cells. in (eds. Löwe, J. & Amos, L. A.) 161–211 (Springer International Publishing, 2017). doi:10.1007/978-3-319-53047-5_6

55. Camberg, J. L., Hoskins, J. R. & Wickner, S. ClpXP protease degrades the cytoskeletal protein, FtsZ, and modulates FtsZ polymer dynamics. *Proc Natl Acad Sci U S A* **106**, 10614–10619 (2009).

56. Charbon, G., Cabeen, M. T. & Jacobs-Wagner, C. Bacterial intermediate filaments: In vivo assembly, organization, and dynamics of crescentin. *Genes and Development* **23**, 1131–1144 (2009).

57. Weissenbach, J. *et al.* Evolution of Chaperonin Gene Duplication in Stigonematalean Cyanobacteria (Subsection V). *Genome Biol. Evol.* **9**, 241–252 (2017).

58. Elhai, J., Vepritskiy, A., Muro-Pastor, A. M., Flores, E. & Wolk, C. P. Reduction of conjugal transfer efficiency by three restriction activities of Anabaena sp. strain PCC 7120. *J. Bacteriol.* **179**, 1998–2005 (1997).

59. Sakr, S., Thyssen, M., Denis, M. & Zhang, C. C. Relationship among several key cell cycle events in the developmental cyanobacterium Anabaena sp. strain PCC 7120. *J. Bacteriol.* **188**, 5958–5965 (2006).

60. Sakr, S., Jeanjean, R., Zhang, C.-C. & Arcondeguy, T. Inhibition of cell division suppresses heterocyst development in Anabaena sp. strain PCC 7120. *J. Bacteriol.* **188**, 1396–1404 (2006).

61. Solovyev, V. & Salamov, A. Automatic Annotation of Microbial Genomes and Metagenomic Sequences. in *Metagenomics and its Applications in Agriculture, Biomedicine and Environmental Studies* (ed. Robert W. Li, pp) 61–78 (Nova Science Publishers, Inc., 2011).

62. Buikema, W. J. & Haselkorn, R. Expression of the Anabaena hetR gene from a copper-regulated promoter leads to heterocyst differentiation under repressing conditions. *Proc. Natl. Acad. Sci.* **98**, 2729–2734 (2001).

63. Callahan, S. M. & Buikema, W. J. The role of HetN in maintenance of the heterocyst pattern in Anabaena sp. PCC 7120. *Mol. Microbiol.* **40**, 941–950 (2001).

64. Cabeen, M. T. & Jacobs-Wagner, C. Bacterial cell shape. *Nat. Rev. Microbiol.* **3**, 601–610 (2005).

65. Rojas, E. R. & Huang, K. C. Regulation of microbial growth by turgor pressure. *Curr. Opin. Microbiol.* **42**, 62–70 (2018).

66. Swulius, M. T. & Jensen, G. J. The helical mreb cytoskeleton in Escherichia coli MC1000/pLE7 is an artifact of the N-terminal yellow fluorescent protein tag. *J. Bacteriol.* **194**, 6382–6386 (2012).

67. Wang, Y. *et al.* Coiled-coil networking shapes cell molecular machinery. *Mol. Biol. Cell* **23**, 3911–3922 (2012).

68. Mason, J. M. & Arndt, K. M. Coiled coil domains: Stability, specificity, and biological implications. *ChemBioChem* **5**, 170–176 (2004).

69. Lupas, A. N. & Gruber, M. B. T.-A. in P. C. The Structure of α-Helical Coiled Coils. in *Fibrous Proteins: Coiled-Coils, Collagen and Elastomers* **70**, 37–38 (Academic Press, 2005).

70. Newman, J. R. S., Wolf, E. & Kim, P. S. A computationally directed screen identifying interacting coiled coils from Saccharomyces cerevisiae. *Proc. Natl. Acad. Sci.* **97**, 13203–13208 (2002).

71. Litowski, J. R. & Hodges, R. S. Designing Heterodimeric Two-stranded α-Helical Coiled-coils. *J. Biol. Chem.* **277**, 37272–37279 (2002).

72. Vinson, C. R., Hai, T. & Boyd, S. M. Dimerization specificity of the leucine zipper-containing bZIP motif on DNA binding: Prediction and rational design. *Genes Dev.* **7**, 1047–1058 (1993).

73. Shea, E. K. O., Rutkowski, R., Iii, W. F. S. & Kim, P. S. Preferential Heterodimer Formation by Isolated Leucine Zippers from Fos and Jun. *Science (80-.).* **245**, 646–648 (1989).

74. Mier, P., Alanis-Lobato, G. & Andrade-Navarro, M. A. Protein-protein interactions can be predicted using coiled coil co-evolution patterns. *J. Theor. Biol.* **412**, 198–203 (2017).

75. Hai, T., Liu, F., Coukos, W. J. & Green, M. R. Transcription factor ATF cDNA clones: An extensive family of leucine zipper proteins able to selectively form DNA-binding heterodimers. *Genes Dev.* **3**, 2083–2090 (1989).

76. Strauss, H. M. & Keller, S. Pharmacological Interference with Protein – Protein Interactions Mediated by Coiled-Coil Motifs. *Handb. Exp. Pharmacol.* 13125–13125 (2008). doi:10.1007/978-3-540-72843-6_19

77. Cabeen, M. T. & Jacobs-Wagner, C. The Bacterial Cytoskeleton. **44**, 365–392 (2010).

78. Kerff, F., Terrak, M., Charlier, P., Sauvage, E. & Ayala, J. A. The penicillin-binding proteins: structure and role in peptidoglycan biosynthesis. *FEMS Microbiol. Rev.* **32**, 234–258 (2008).

79. van Teeseling, M. C. F., de Pedro, M. A. & Cava, F. Determinants of bacterial morphology: From fundamentals to possibilities for antimicrobial targeting. *Front. Microbiol.* **8**, 1–18 (2017).

80. Lutkenhaus, J. The ParA/MinD family puts things in their place. *Trends Microbiol.* **20**, 411–418 (2012).

81. Leipe, D. D., Wolf, Y. I., Koonin, E. V & Aravind, L. Classification and evolution of P-loop GTPases and related ATPases. *J. Mol. Biol.* **317**, 41–72 (2002).

82. Ramos-León, F., Mariscal, V., Frías, J. E., Flores, E. & Herrero, A. Divisome-dependent subcellular localization of cell-cell joining protein SepJ in the filamentous cyanobacterium Anabaena. *Mol. Microbiol.* **96**, 566–580 (2015).

83. Heins, S. & Aebi, U. Making heads and tails of intermediate filament assembly, dynamics and networks. *Curr. Opin. Cell Biol.* **6**, 25–33 (1994).

84. Herrmann, H. *et al.* Structure and assembly properties of the intermediate filament protein vimentin: The role of its head, rod and tail domains. *J. Mol. Biol.* **264**, 933–953 (1996).

85. England, P. *et al.* The Scc Spirochetal Coiled-Coil Protein Forms Helix-Like Filaments and Binds to Nucleic Acids Generating Nucleoprotein Structures. *J. Bacteriol.* **188**, 469–476 (2005).

86. Ingerson-Mahar, M., Briegel, A., Werner, J. N., Jensen, G. J. & Gitai, Z. The metabolic enzyme CTP synthase forms cytoskeletal filaments. *Nature Cell Biology* **12**, 739–746 (2010).

87. Cabeen, M. T. *et al.* Bacterial cell curvature through mechanical control of cell growth. *The EMBO Journal* **28**, 1208–1219 (2009).

88. Shieh, Y.-W. *et al.* Operon structure and cotranslational subunit association direct protein assembly in bacteria. *Science (80-.).* **350**, 678 LP – 680 (2015).

89. Jones, L. J. F., Carballido-López, R. & Errington, J. Control of cell shape in bacteria: Helical, actin-like filaments in Bacillus subtilis. *Cell* **104**, 913–922 (2001).

90. Alberts, B. *et al. Molecular Biology of the Cell*. (Garland Science, 2014).

91. Herrmann, H. & Aebi, U. Intermediate filaments and their associates: Multi-talented structural elements specifying cytoarchitecture and cytodynamics. *Curr. Opin. Cell Biol.* **12**, 79–90 (2000).

92. Leung, C. L., Green, K. J. & Liem, R. K. H. Plakins: A family of versatile cytolinker proteins. *Trends Cell Biol.* **12**, 37–45 (2002).

93. Zhang, R., Zhang, C., Zhao, Q. & Li, D. Spectrin: Structure, function and disease. *Sci. China Life Sci.* **56**, 1076–1085 (2013).

94. Typas, A., Banzhaf, M., Gross, C. A. & Vollmer, W. From the regulation of peptidoglycan synthesis to bacterial growth and morphology. *Nat. Rev. Microbiol.* **10**, 123–136 (2012).

95. Persat, A. *et al.* The mechanical world of bacteria. *Cell* **161**, 988–997 (2015).

96. Park, A., Jeong, H.-H., Lee, J., Kim, K. P. & Lee, C.-S. Effect of shear stress on the formation of bacterial biofilm in a microfluidic channel. *BioChip J.* **5**, 236–241 (2011).

97. Young, K. D. The selective value of bacterial shape. *Microbiol. Mol. Biol. Rev.* **70**, 660–703 (2006).

98. Lupas, A., Van Dyke, M. & Stock, J. Predicting coiled coils from protein sequences. *Science* **252**, 1162–1164 (1991).

99. Wilson, C. G. M., Magliery, T. J. & Regan, L. Detecting protein-protein interactions with GFP-fragment reassembly. *Nat. Methods* **1**, 255–262 (2004).

100. Yang, Y. *et al.* Phenotypic variation caused by variation in the relative copy number of pDU1-based plasmids expressing the GAF domain of Pkn41 or Pkn42 in Anabaena sp. PCC 7120. *Res. Microbiol.* **164**, 127–135 (2013).

101. Nieves-Morión, M. *et al.* Specific Glucoside Transporters Influence Septal Structure and Function in the Filamentous, Heterocyst-Forming Cyanobacterium Anabaena sp. Strain PCC 7120. *J. Bacteriol.* **199**, e00876-16 (2017).

102. Bornikoel, J. *et al.* Role of Two Cell Wall Amidases in Septal Junction and Nanopore Formation in the Multicellular Cyanobacterium Anabaena sp. PCC 7120. *Front. Cell. Infect. Microbiol.* **7**, 386 (2017).

103. Karimova, G., Davi, M. & Ladant, D. The β-lactam resistance protein Blr, a small membrane polypeptide, is a component of the Escherichia coli cell division machinery.

J. Bacteriol. **194**, 5576–5588 (2012).

104. Roy, A., Yang, J. & Zhang, Y. COFACTOR: An accurate comparative algorithm for structure-based protein function annotation. *Nucleic Acids Res.* **40**, 471–477 (2012).

105. Zhang, Y. I-TASSER: Fully automated protein structure prediction in CASP8. *Proteins Struct. Funct. Bioinforma.* **77**, 100–113 (2009).

106. Yang, J. & Zhang, Y. I-TASSER server: New development for protein structure and function predictions. *Nucleic Acids Res.* **43**, W174–W181 (2015).

107. Lutkenhaus, J. Another Cytoskeleton in the Closet. *Cell* **115**, 648–650 (2003).

108. Jin, S. K. & Sun, S. X. Morphology of Caulobacter crescentus and the mechanical role of crescentin. *Biophysical Journal* **96**, (2009).

109. Cabeen, M. T., Herrmann, H. & Jacobs-Wagner, C. The domain organization of the bacterial intermediate filament-like protein crescentin is important for assembly and function. *Cytoskeleton* **68**, 205–219 (2011).

110. Dagan, T. *et al.* Genomes of stigonematalean cyanobacteria (subsection V) and the evolution of oxygenic photosynthesis from prokaryotes to plastids. *Genome Biol. Evol.* **5**, 31–44 (2013).

111. Tria, F. D. K., Landan, G. & Dagan, T. Phylogenetic rooting using minimal ancestor deviation. *Nat. Ecol. Evol.* **1**, 0193 (2017).

112. Altschul, S. F., Gish, W., Miller, W., Myers, E. W. & Lipman, D. J. Basic local alignment search tool. *J. Mol. Biol.* **215**, 403–410 (1990).

113. Rice, P., Longden, I. & Bleasby, A. EMBOSS: the European Molecular Biology Open Software Suite. *Trends Genet.* **16**, 276–7 (2000).

114. Letunic, I. & Bork, P. Interactive tree of life (iTOL) v3: an online tool for the display and annotation of phylogenetic and other trees. *Nucleic Acids Res.* **44**, W242–W245 (2016).

115. Sambrook, J. & Green, M. R. *Molecular Cloning: A Laboratory Manual*. (Cold Spring Harbor Laboratory Press, 2012).

116. Ungerer, J. & Pakrasi, H. B. Cpf1 Is A Versatile Tool for CRISPR Genome Editing Across Diverse Species of Cyanobacteria. *Sci. Rep.* **6**, 1–9 (2016).

117. Wolk, C. P. *et al.* Isolation and complementation of mutants of Anabaena sp. strain PCC 7120 unable to grow aerobically on dinitrogen. *J. Bacteriol.* **170**, 1239–1244 (1988).

118. Stucken, K., Ilhan, J., Roettger, M., Dagan, T. & Martin, W. F. Transformation and conjugal transfer of foreign genes into the filamentous multicellular cyanobacteria (subsection V) Fischerella and Chlorogloeopsis. *Curr. Microbiol.* **65**, 552–560 (2012).

119. Cai, Y. & Wolk, C. P. Use of a conditionally lethal gene in Anabaena sp. strain PCC 7120 to select for double recombinats and to entrap insertion sequnces. *J. Bacteriol.* **172**, 3138–3145 (1990).

120. Fiedler, G., Arnold, M., Hannus, S. & Maldener, I. The DevBCA exporter is essential for envelope formation in heterocysts of the cyanobacterium Anabaena sp. strain PCC 7120. *Mol. Microbiol.* **27**, 1193–1202 (1998).

121. Kühner, D., Stahl, M., Demircioglu, D. D. & Bertsche, U. From cells to muropeptide structures in 24 h: Peptidoglycan mapping by UPLC-MS . (2014).

122. Lehner, J. *et al.* The morphogene AmiC2 is pivotal for multicellular development in the cyanobacterium Nostoc punctiforme. *Mol. Microbiol.* **79**, 1655–1669 (2011).

123. Rudolf, M. *et al.* The Peptidoglycan-Binding Protein SjcF1 Influences Septal Junction Function and Channel Formation in the Filamentous Cyanobacterium Anabaena *MBio* **6**, e00376-15 (2015).

124. Dörrich, A. K., Mitschke, J., Siadat, O. & Wilde, A. Deletion of the Synechocystis sp. PCC 6803 kaiAB1C1 gene cluster causes impaired cell growth under light???dark conditions. *Microbiol. (United Kingdom)* **160**, 2538–2550 (2014).

125. Grant, S. G., Jessee, J., Bloom, F. R. & Hanahan, D. Differential plasmid rescue from transgenic mouse DNAs into Escherichia coli methylation-restriction mutants. *Proc. Natl. Acad. Sci.* **87**, 4645–4649 (1990).

126. Studier, F. W. & Moffatt, B. A. Use of bacteriophage T7 RNA polymerase to direct selective high-level expression of cloned genes. *J. Mol. Biol.* **189**, 113–130 (1986).

127. Boyer, H. & Roulland-Dessoix, D. A complementation analysis of the restrcition and modification of DNA in Escherichia coli. *J. Mol. Biol.* **41**, 459–472 (1969).

128. Cohen, S. E. *et al.* Dynamic localization of the cyanobacterial circadian clock proteins. *Curr. Biol.* **24**, 1836–1844 (2014).

129. Olmedo-Verd, E., Muro-Pastor, A. M., Flores, E. & Herrero, A. Localized induction of the ntcA regulatory gene in developing heterocysts of Anabaena sp. strain PCC 7120. *J. Bacteriol.* **188**, 6694–6699 (2006).